GABRIELĖ ŠARAPAJEVAITĖ

SUSTAINABLE SYNTHESIS AND PROPERTIES OF CuS AND APPLICATION OF ITS COMPOSITES FOR DEGRADATION OF ORGANIC COMPOUNDS

DOCTORAL DISSERTATION

Kaunas
2024

KAUNAS UNIVERSITY OF TECHNOLOGY

GABRIELĖ ŠARAPAJEVAITĖ

SUSTAINABLE SYNTHESIS AND PROPERTIES OF CuS AND APPLICATION OF ITS COMPOSITES FOR DEGRADATION OF ORGANIC COMPOUNDS

Doctoral dissertation
Technological Sciences, Chemical Engineering (T 005)

2024, Kaunas

This doctoral dissertation was prepared at Kaunas University of Technology, Faculty of Chemical Technology, Department of Silicate Technology during the period of 2020–2024. The studies were supported by the Research Council of Lithuania.
Dissertation was prepared based on the agreement signed on 12 July 2021 with University of Bologna for double doctorate.

Scientific Supervisors:
Prof. Dr. Kęstutis BALTAKYS (Kaunas University of Technology, Technological Sciences, Chemical Engineering, T 005);
Assoc. Prof. Dr. Paola FABBRI (University of Bologna, Italy, Material Science and Technology).

Edited by English language editor Dr. Armandas Rumšas (Publishing House *Technologija*), Lithuanian language editor Aurelija Gražina Rukšaitė (Publishing House *Technologija).*

The public defence of the dissertation will be held at 11 a.m. on 19 June 2024 at the public meeting of the Dissertation Defence Board of Chemical Engineering Science Field in Rectorate Hall at Kaunas University of Technology.

Address: K. Donelaičio 73-402, LT-44249 Kaunas, Lithuania.
Phone (+370) 608 28 527; email doktorantura@ktu.lt

The doctoral dissertation was sent out on 17 May 2024.
The doctoral dissertation is available on the internet at http://ktu.edu, at the library of Kaunas University of Technology (Gedimino 50, LT-44239 Kaunas, Lithuania) and at the library of University of Bologna (Via Zamboni, 33/35 – 40126, Bologna, Italy).

KAUNO TECHNOLOGIJOS UNIVERSITETAS

GABRIELĖ ŠARAPAJEVAITĖ

TVARI CuS SINTEZĖ, SAVYBĖS IR JO KOMPOZITŲ TAIKYMAS ORGANINIAMS JUNGINIAMS SKAIDYTI

Daktaro disertacija
Technologijos mokslai, chemijos inžinerija (T 005)

2024, Kaunas

Disertacija rengta 2020–2024 metais Kauno technologijos universiteto Cheminės technologijos fakultete, Silikatų technologijos katedroje. Mokslinius tyrimus rėmė Lietuvos mokslo taryba.
Disertacija parengta pagal 2021 m. liepos 12 d. pasirašytą sutartį su Bolonijos universitetu dėl dvigubo laipsnio doktorantūros.

Moksliniai vadovai:
prof. dr. Kęstutis BALTAKYS (Kauno technologijos universitetas, technologijos mokslai, chemijos inžinerija, T 005);
doc. dr. Paola FABBRI (Bolonijos universitetas, Italija, medžiagų mokslas ir technologijos).

Redagavo: anglų kalbos redaktorius dr. Armandas Rumšas (leidykla „Technologija“), lietuvių kalbos redaktorė Aurelija Gražina Rukšaitė (leidykla „Technologija“).

Chemijos inžinerijos mokslo krypties disertacijos gynimo taryba:
doc. dr. Irmantas BARAUSKAS (Kauno technologijos universitetas, technologijos mokslai, chemijos inžinerija, T 005) – **pirmininkas**;
doc. dr. Martino COLONNA (Bolonijos universitetas, Italija, technologijos mokslai, medžiagų inžinerija, T 008);
doc. dr. Dario FRASCARI, (Bolonijos universitetas, Italija, technologijos mokslai, chemijos inžinerija, T 005);
prof. dr. Eugenijus VALATKA (Kauno technologijos universitetas, technologijos mokslai, chemijos inžinerija, T 005).

Disertacija bus ginama viešame Chemijos inžinerijos mokslo krypties disertacijos gynimo tarybos posėdyje 2024 m. birželio 19 d. 11 val. Kauno technologijos universiteto Rektorato salėje.

Adresas: K. Donelaičio g. 73-402, LT-44249 Kaunas, Lietuva.
Tel. (+370) 608 28 527; el. paštas doktorantura@ktu.lt

Disertacija išsiųsta 2024 m. gegužės 17 d.
Su disertacija galima susipažinti interneto svetainėje http://ktu.edu, Kauno technologijos universiteto bibliotekoje (Gedimino g. 50, LT-44239 Kaunas, Lietuva) ir Bolonijos universiteto bibliotekoje (Via Zamboni, 33/35 – 40126, Bolonija, Italija).

ALMA MATER STUDIORUM
UNIVERSITÀ DI BOLOGNA

in cotutela con Kaunas University of Technology

DOTTORATO DI RICERCA IN

Civil, Chemical, Environmental and Materials Engineering

Ciclo XXXVI

Settore Concorsuale: 09/D1 Scienza e tecnologia dei materiali

Settore Scientifico Disciplinare: ING-IND/22 Scienza e tecnologia dei materiali

SUSTAINABLE SYNTHESIS AND PROPERTIES OF CuS AND APPLICATION OF ITS COMPOSITES FOR DEGRADATION OF ORGANIC COMPOUNDS

Presentata da: Gabrielė Šarapajevaitė

Coordinatore Dottorato

Prof. Dr. Alessandro Tugnoli

Supervisore

Prof. Dr. Paola Fabbri

Esame finale anno 2024

TABLE OF CONTENTS

LIST OF TABLES

LIST OF FIGURES

LIST OF ABBREVIATIONS

AOP – advanced oxidation process;
CBD – chemical bath deposition;
CRM – critical raw materials;
Cu_xS_y – copper sulfides;
CVD – chemical vapour deposition;
DE – degradation efficiency;
DIOX – 1,4-dioxane;
DRS – diffuse reflectance spectroscopy;
DSC – differential scanning calorimetry;
EC – European Commission;
EDA – ethylendiamine;
EDX – energy dispersive X-ray;
Eg – band gap;
EtOH – ethyl alcohol;
FE-SEM – field emission scanning electron microscopy;
MB – methylene blue;
MFC – micro fibrillated cellulose;
PHBV – poly(3-hydroxybutyrate-co-3-hydroxyvalerate);
PVD – physical vapour deposition;
ROS – reactive oxygen species;
SDG – sustainable development goals;
SEM – scanning electron microscopy;
STA – simultaneous thermal analysis;
TC – tetracycline hydrochloride;
TEM – transmission electron microscopy;
TG – thermogravimetry;
TIPS – thermally induced phase separation;
UN – United Nations;
UV – ultraviolet light;
UV-Vis – ultraviolet and visible light;
WCA – water contact angle;
XRD – X-ray diffraction;
XRF – X-ray fluorescence;
TEM – transmission electron microscopy;
WCA – water contact angle.

INDICES IN THE X-RAY DIFFRACTION PATTERNS

* – $Cu_{1.81}S$;
+ – Cu_2S;
a – anhydrite;
b – bonattite;
c – covellite;
d – digenite;
d*– digenite high;
h – chalcocyanite;
n – anilite;
Q – quartz;
r – roxbyite;
S – sulfur.

INTRODUCTION

The data reported during the last decade pertaining to the analysis of the trends of waste material neutralisation clearly indicates a concerning situation regarding waste treatment. Studies reveal findings proving the presence of various sulfur containing non-valuable compounds or materials in the environment – whether in the solid or in the gaseous state. The occurrence of the presently mentioned compounds in aerobic conditions causes the formation of hazardous substances negatively affecting the environment and human health.

Moreover, the continuously rising demands of humanity for both familiar and novel comforts result in a higher quantity of consumed fossil raw material, which inherently leads to the enhanced negative anthropogenic influence on the environment. As the earth resources are limited and since the industrial effect presumably exerts an irreversible negative impact, solutions towards sustainable raw material management must be established. In addition, the implementation of circular economy, particularly the use of waste compounds as secondary raw materials, is one of the solutions towards reducing the amount of generated non-valuable products and the quantity of fossil raw material.

It is also worth noting that, with the rising needs of finding new effective technological solutions in many environmentally important areas, the search for compounds with the enhanced functional characteristics is still far from the being completed. In this context, the research reporting the industrial waste neutralisation approach by producing valuable promising compounds is severely needed.

Transition metal chalcogenides, in particular copper sulfides (Cu_xS_y), are considered as a low-cost, physiochemically stable and non-toxic material possessing the properties depending on synthesized size and shape. Cu_xS_y possesses desirable properties for p-type semiconductors, such as a high theoretical specific charge capacity, high concentrations of free charge carriers, and the perfect ability to absorb light. These properties lead to the application of the latter material in the fields of photocatalysis, energy storage, or green hydrogen production. The ability of Cu_xS_y to generate free charge carriers by absorbing the irradiation of visible light is harvested in applying Cu_xS_y for the advanced oxidation process and the degradation of dyes or antibiotics. In particular, the presently mentioned organic molecules are widely known waste water pollutants whose presence in the water cycle enhances the unexpected acceleration of antimicrobial resistance; they also exert toxic influence on plants and animals.

While numerous techniques for synthesizing CuS have been proposed by researchers, the quest for an industry-applicable approach to produce compounds with superior characteristics is far from over. Additionally, the synthesis of many high-value products relies on fossil-based reagents, thereby contributing to a lack of sustainability and disregarding the *Sustainable Development Goals*. Considering the sustainability point of view, the possibility to synthesize high value compounds, such as copper sulfides, by using waste material as reactive components, is a desirable technological proposal. In addition, it is essential to validate the functional properties of secondary raw material based products. It is also of importance to note that the

exploitation of nano-sized material in a large scale should also correspond to the sustainability point of view.

Moreover, the possible application areas of Cu_xS_y may cover conditions in a higher-than-ambient temperature, for example for use in photovoltaic or electronic devices. During the temperature treatment of the material, the variation of the constituents' crystal lattice may occur, significantly impacting the size of nanoparticles. Given that the nanoparticle size plays a crucial role in determining the electrochemical and optical properties of copper sulfide, it becomes essential to investigate both the thermal stability and recrystallization phenomena.

Aim of the dissertation

To develop a sustainable approach of CuS synthesis by using waste of sulfuric acid production and to produce CuS–PHBV biocomposite applicable for degradation of organic molecules.

Objectives of the dissertation

1. To investigate the influence of the composition of sulfuric acid production waste and conditions of hydrothermal treatment on the formation of CuS.
2. To investigate the morphology and photocatalytic properties of the synthesized samples and the thermal decomposition of synthetic CuS in the air environment.
3. To produce biocomposites from the synthesized CuS and poly(3-hydroxybutyrate-co-3-hydroxyvalerate) in different structures and to determine their capabilities to degrade organic molecules.

Statements presented for the defence

1. It has been proven that sulfuric acid production waste is suitable to be used as a secondary raw material of sulfur for sustainable synthesis of CuS, which is characteristic of photocatalytic and other functional properties.
2. The biocomposites of synthetic CuS and poly(3-hydroxybutyrate-co-3-hydroxyvalerate) degrade tetracycline up to 100% during 3 h of visible light irradiation.

Scientific novelty of the research

1. Thermally stable (25–300 °C) CuS obtained in the system of S–CuO–H_2O under hydrothermal conditions during 0.5–4 h at temperatures between 145 and 180 °C possess the crystallite size of 27–40 nm and the band gap of 1.72–1.81 eV.
2. It has been determined for the first time that CuS–PHBV biocomposite is eligible to degrade tetracycline and methylene blue and can be reused for 5 times.

Practical significance of the scientific research

A sustainable method of CuS synthesis from a mixture of secondary raw material of sulfur and copper oxide has been proposed. It has been established that the synthesized samples have a constant chemical composition and thermal stability up to 300 °C. Synthetic CuS was used for the production of a CuS–PHBV biocomposite in a different structure. Moreover, the presently mentioned product can be applied for

the decomposition of organic pollutants and their mixtures in wastewater, by cyclically decomposing not only single compounds, but also mixtures of organic compounds (tetracycline – methylene blue).

Approval and publication of the research results

The results obtained in the course of the research of PhD studies have been published in 4 scientific publications cited in the *Clarivate Analytics Web of Science* data base: *Waste and Biomass Valorization*, *Journal of Thermal Analysis and Calorimetry*, *Materials and Advanced Sustainable Systems.*

The results have also been presented in 6 scientific international conferences: *6th Central and Eastern European Conference on Thermal Analysis and Calorimetry* (CEEC-TAC6) and *15th Mediterranean Conference on Calorimetry and Thermal Analysis* (Medicta2021), *Chemistry and Chemical Technology 2022* (CCT2022), *Merck Young Chemists' Symposium 2022* (MYCS2022), *International Conference-School Advanced Materials and Technologies* (AMT2023), *Workshop on Polymers and Biopolymers for Sustainable Life and Applications 2023* (MoDeSt2023), *Baltic University Symposium 2023* (BUP2023).

Contribution of the author and co-authors

Ms. Gabrielė Šarapajevaitė carried out the synthesis of copper sulfide from the secondary raw material of sulfur. The author also investigated the morphological and photocatalytic properties of the synthesized samples and carried out the thermal stability investigation of CuS. The above mentioned research steps were performed in KTU under supervision of Prof. Dr. Kęstutis Baltakys who advised on experimental proceedings, such as material synthesis, the investigation of thermal stability, and who also revised the manuscripts of scientific publications.

Furthermore, Ms. G. Šarapajevaitė fabricated the composites and carried out the experiments of photodegradation; she also performed data processing. The production of the composites and the investigation of their photocatalytic properties was carried out at the University of Bologna under the supervision of Prof. Paola Fabbri who was supporting the student during her staying at UNIBO. Dr. Micaela Degli Esposti advised on the experimental peculiarities of the fabrication of composites and revised the manuscripts of scientific publications. Dr. Davide Morselli supported the preparation of composites, the characterisation of samples as well as the degradation experiments involving the fabricated composites; he also revised the manuscripts of scientific publications.

Structure and content of the dissertation

The dissertation consists of an introduction, a literature review presenting the importance of circular economy implementation in the industry and the properties of copper sulfides as well as their synthesis methods and application. Furthermore, the subsequent sections present the materials and methods applied in the course of the research of PhD studies, the obtained results and conclusions. The list of references contains 144 bibliographic sources. The results are discussed in 134 pages featuring 20 tables, 38 figures and 8 appendices.

1. LITERATURE REVIEW

1.1. Circular Economy in Industry

Over the last two decades, numerous reports have presented substantial data proving a continuously worsening impact of anthropogenic processes on the environment. For this reason, the *European Commission* (EC) together with the *United Nations* (UN) have been making maximum effort to facilitate the development of solutions aimed at ensuring a more sustainable future for our world.

For example, one of the EC priorities during 2019–2024 was to implement the European Green Deal which aims to overcome the challenges of climate change and environmental degradation [1]. According to this development model, the new strategy of progress is formulated which is based on the development of new technology, sustainable solutions, and disruptive innovations [2]. Based on an industrial strategy suggested by the *Green Deal*, the primary objective is to exploit the substantial potential within worldwide markets for low-emission technologies, sustainable products and services, with the aim of attaining climate neutrality by 2050 [1].

Furthermore, with the objective to address many global issues, UN named 17 *Sustainable Development Goals* (SDG) [3] (Fig. 1.1). In particular, the 12th goal is set to ensure the sustainable patterns of consumption and production. To achieve the presently mentioned goal, the UN named several targets. For example, the second target (Target 12.2) aims to achieve sustainable management and efficient use of natural resources by 2030 [4]. The fifth target (Target 12.5) seeks to reduce waste generation through prevention, reduction, recycling and reuse; it also refers to 2030 [4].

Fig. 1.1. Sustainable development goals [5]

The monitoring of the progress towards achieving the 12th SDG is implemented by the observing the specific indicators [4]. For example, the advance to reach Target 12.2 is evaluated by global domestic material consumption, which is a parameter representing the amount of raw materials to be directly used for production processes [4]. Unfortunately, over the past 20 years, this parameter has increased by 66% and is also set to further increase, which indicates a continuously growing trend of material extraction [6,7]. The material footprint is one more indicator representing the total amount of extracted raw materials to meet the final consumption demands [4]. During the last 20 years, the global material footprint has increased by 70%, which also shows a continuously growing amount of extracted raw material to meet the consumption needs [4]. Consequently, both of the latter indicators represent not only the rising trend of material demand or an increased amount of extracted material, but also the rising quantities of generated waste as well as the expanded negative impact of the processed materials to the environment. Unfortunately, the statistics, reporting waste generation through years have presented the steady or rising trend in most European countries. For example, over the past 20 years, the amount of hazardous waste in Lithuania has increased from 26.2 kg/capita to 91.33 kg/capita [4]. It was estimated that, by following this tendency, the waste generation would increase by 70% [8].

In addition, the above mentioned data is a clear indication that the current *status quo* of waste material treatment has to change fundamentally. For example, to address the issues of resource consumption and waste generation, the circular economy in the industry has to be implemented [9]. One of the goals in the circular economy is to reduce the amount of the generated waste, which can be achieved by recycling non-valuable products [9]. In this case the waste becomes a secondary raw material, and, consequently, not only the quantity of waste is decreased, but also the amount of extracted resources [9]. In particular, over the last 10 years, the circular material use in EU has only increased by 0.8%, thus reaching the current value of 11.8% [9,10]. Moreover, 95.5 million t/year of hazardous waste was generated last year in the EU, and only 38.5% of it was either recycled or backfilled [6]. Therefore, there is a great potential for further processing development of recycling non-value material.

It is important to note that the material recycling problem also serves as a solution regarding the issue of sustainable supply of *Critical Raw Materials* (CRM) in EU [11]. Over the last decades the heavy dependency on non-member states in terms of important raw materials has been detected in EU [11]. To solve this issue, the EC is promoting the exploitation of a sustainable source by implementing circularity and utilizing waste as a resource of CRM [11].

It is of importance to highlight that, by treating waste as a secondary raw material, the employed processing approach gives opportunity to extract the value or beneficial properties of the material, thus valorising the waste. Therefore, the possibility arises to utilise non-value by-products by employing them as resources to produce high value products, for example, compounds called advanced materials. In addition, reuse of waste not only mitigates the environmental impact, but also creates ways to build innovation together with the enhanced cost-effectiveness.

One of the strategic goals of the EC in implementing the European Industrial Strategy is the production of semiconductor materials [12]. Semiconductor

microchips are crucial in the production of various everyday devices and services, including automobiles, airplanes, medical equipment, smartphones, computers, and networks. Nevertheless, there is limited production capacity of semiconductors as well as a high entering cost, which restricts Europe's ability to exploit the opportunities in the area of semiconductor production [12]. Furthermore, EC also seeks to implement the concept of sustainable products by aiming to produce energy- and resource-efficient products which would be produced from sustainable resources [8]. Considering the negative impact of production on the environment, valorisation of waste is a possible solution to produce high value materials with the enhanced properties, such as semiconductors, which would also be achieved in a cost-effective way.

To address the delicate issues concerning the environmental point of view, Lithuania proposed the *National Plan of Advance 2021–2030* [2]. During the last decade, wide opportunities opened up to for the development of circular technologies, sustainable products and services in global markets. It is of importance to note that the circular economy also has significant potential for opening up new business activities and jobs. In order to achieve the goals of the green concept, new technologies, sustainable solutions, and disruptive innovations are particularly important. For these reasons, some of the strategic goals set by the government of Lithuania are to develop the innovation-driven sustainable economy based on knowledge and advanced technologies, and to enhance the international competitiveness of the country [2].

Some of other national strategic goals are to ensure good environmental quality and sustainable use of natural resources, to preserve biological diversity and to mitigate Lithuania's impact on the climate change along with enhancing resilience to its effects [2]. For these reasons, the industry is motivated to transit towards circular economy-based technologic solutions by using secondary raw materials and environmentally friendly innovations.

Furthermore, the Ministry of the Economy and Innovation of the Republic of Lithuania has proposed the concept of *smart specialisation* [13]. Specifically, the latter notion is aimed to strengthen the capabilities of scientific research and innovation and to develop new technologies, consequently enhancing the competitiveness and position of the country globally. One of the priorities in this area is the development of new processes, materials and technologies, for example, by creating advanced materials and construction, or by designing technologies of versatile products, production, and operation of processes [13]. It is also worth noting that, according to the concept of smart specialisation, the innovative production is oriented towards fabricating materials possibly generating high added value.

In addition, Lithuanian Government institutions suggested several measures focused on the development of high value technologies and materials along with supporting research aimed at addressing environmental issues. Moreover, the concept of circular economy in industry opens up a way to find solutions not only intended to reduce the amount of the generated waste, but also to decrease the amount of extracted raw material. Therefore, the implementation of circular economy is a necessary

condition to neutralise the negative man-made effect of resources processing on the environment.

1.2. Concerns Regarding Sulfur-Based Waste

Some of the manufacturing sectors generate industrial waste possessing sulfur in their composition, which may also appear in the gaseous or liquid state.

One of the sectors producing sulfurous by-products is oil refining. Unprocessed oil may contain 1 to 3% of organic sulfur compounds, which, during oil processing, are released to the atmosphere in the form of SO_2 [14]. According to various sources, natural gases may contain 0–90% of sulfur, liquefied petroleum gas may contain 0.05–14% of sulfur, and biofuels may contain up to 30% of hydrogen sulfide [15,16]. The latter compound is removed from the hydrocarbon mixture by employing the Claus process, which follows hydrogen sulfide oxidation to produce sulfur dioxide and then the reaction of SO_2 proceeds with the remaining H_2S in a catalytic reaction to precipitate elemental sulfur [14,17]. However, according to NASA estimations, the oil and gas refining and combustion sector is responsible for 21% of anthropogenic SO_2 emission [18].

The coal industry is another possible source of gaseous sulfur waste, since the raw material of coal may contain up to 14% of S [15]. In the latter rock, sulfur is contained in various compounds, such as pyrite, sulfates, and organic sulfur compounds. Thus, the removal of impurities from coal can result in sludge, containing pyritic, aliphatic and aromatic sulfur compounds, sulfoxides, and sulfones [19]. In order to reduce the emission of SO_x into the atmosphere and to avoid catalyst pollution or equipment corrosion, hydrodesulfurisation is applied for sulfur removal. Nevertheless, studies have presented data revealing the rise of SO_2 concentration in the atmosphere in coal-based urban regions showing 36% contribution of anthropogenic SO_2 emissions by coal combustion for power generation and industries [18,20].

Hydrodesulfurisation is also applied to remove sulfur compounds, such as alkyl thiols from bitumen fuel, which leads to one more sulfur-containing waste stored in the landfill [21].

Another type of waste containing sulfur is gypsum which is formed during the production of hydrofluoric acid. Production of 1 t of HF generates about 4 t of $CaSO_4$ [22]. Moreover, the latter waste is also generated during the wet process of phosphoric acid production, but it contains phosphorus impurities, the so-called phosphogypsum.

Producing 1 t of phosphoric acid results in approximately 4-to-5 t of phosphogypsum [23]. Studies indicate that over 200 million tons of phosphogypsum are generated annually [14]. Due to the origin of phosphoric acid raw materials, the possibilities for processing or utilising phosphogypsum are very limited. According to data from 2019, only 15% of this waste was used worldwide in fertilisers, the agricultural sector, and the cement industry [23]. Therefore, large quantities of phosphogypsum are stored in specialised landfills, or disposed of in oceans [14].

Moreover, due to the reaction of sulfur with oxygen and water in the course of ore mining and metal processing, thiosulfates and sulfuric acid are formed, which are

considered as production residues contaminated with sulfides in hydrometallurgy. In addition, the latter waste material is referred to as acidic mine drainage [24].

In the production of sulfuric acid, gaseous waste compounds are also generated, which leads to approximately 100 million tons of SO_2 entering the atmosphere each year [25]. Due to insufficient SO_2 oxidation, inefficient SO_3 absorption, and the pressure of sulfuric acid/oleum vapour formed, sulfuric gases or sulfuric acid vapours can be released into the environment, albeit in small quantities [22].

It is worth noting that the sulfurous solid state waste is typically stored in specified landfills. Nevertheless, the presence of the above mentioned compounds in aerobic conditions may negatively affect the environment due to natural bacterial oxidation to sulfur dioxide, which leads to the changes of soil pH, corrosion, and acidic rain formation [15,26]. Furthermore, the occurrence of SO_2 and H_2S in the environment may lead to reaction(s) with other substance(s) occurring in the environment, such as H_2O or O_2, consequently forming hazardous compounds, such as sulfuric acid or formed fine sulfate-based particles [18].

1.3. Properties of Copper Sulfides (Cu_xS_y)

Binary copper sulfides (Cu_xS_y) exist in various stoichiometric compositions, although only eight compounds exist in the thermodynamically stable dominant crystal phase in terms of the Cu content: low-chalcocite, high-chalcocite, cubic-chalcocite, djurleite, digenite, anilite, roxybite, and covellite (Table 1.1) [27].

Table 1.1. Stoichiometries of binary copper sulfides

Mineral name	Composition	S packing	Crystal system
Low-chalcocite	Cu_2S	hcp	monoclinic
High-chalcocite	Cu_2S	hcp	hexagonal
Cubic-chalcocite	Cu_2S	fcc	cubic
Djurleite	$Cu_{31}S_{16}$ $Cu_{1.97}S$	hcp	monoclinic
Digenite	Cu_9S_5 $Cu_{1.8}S$	fcc	cubic
Anilite	Cu_7S_4 $Cu_{1.75}S$	fcc	orthorhombic
Roxybite	$Cu_{58}S_{32}$ $Cu_{1.81}S$	hcp	triclinic
Covellite	CuS	hcp	hexagonal

Moreover, some of the other, less researched, compounds are also possible in the bulk material, such as geerite ($Cu_{1.6}S$), spionkopite ($Cu_{1.39}S$), yarrowite ($Cu_{1.12}S$) and villamanitite (CuS_2). All of the copper sulfides are characterised by different crystal structures of sulfur, such as hexagonal closest packing (hcp) or face-centred cubic (fcc), with Cu atoms occupying various interstitial sites (Table 1.1) [27].

Due to copper vacancies in the crystal lattice, copper sulfides are considered as a p-type semiconductor. The concentration of the vacancies (holes) depends on stoichiometry and increases with the number of Cu vacancies, i.e., it decreases as the x value in Cu_xS_y compound lessens. The sulfide anions are considered as a solid frame of the molecules, whereas Cu^{2+} atoms are mobile cations showing superionic behaviour [27].

Compared to other transition metal chalcogenides, copper sulfides are considered to be abundant and low-cost compounds possessing the properties depending on the synthesized size and shape. For example, many researchers have reported on fabricating Cu_xS_y in different shapes in sizes of 0D as nanoparticles, 1D as nanorods, nanowires and nanotubes, 2D as nanoplates and 3D as flowers and hollow architectures [28,29].

Despite the achieved morphology, Cu_xS_y possesses desirable properties for p-type semiconductors, such as high theoretical specific charge capacity (337–560 mAh/g) and high electronic conductivity (~10^{-3} S/m) [29]. Moreover, outstanding discharge characteristics together with potential high carrier concentrations, low thermal conductivity, low solubility in most electrolytes and appropriate direct band gaps for solar light absorption are also characteristic to copper sulfides [27,29–34]. It is important to note that the presently discussed electrochemical properties are strongly affected by the structure and morphology of the material [29].

The photocatalytic properties of Cu_xS_y are also widely exploited. In general, photocatalysis is a catalytic reaction which is initiated by the wavelength of the electromagnetic wave, typically varying in the wavelength of ultraviolet light (UV) and the visible light range. In order to exploit a semiconductor in a catalytic reaction, the material must have an energy gap between its valence and conduction bands, which also called the band gap (E_g). This energy gap allows electrons to transition from the valence band to the conduction band when excited by light irradiation at the appropriate wavelength. Therefore, the band gap of a semiconductor determines the amount of energy, and, consequently, the wavelength of irradiation which excites the electron leading to the participation of the material in the catalytic reaction.

Due to the physicochemical stability, optical/magnetic properties and a lower cytotoxicity of Cu_xS, the material is widely employed as a narrow band gap photocatalyst [35]. Typically, the band gap varies from 1.2 to 2 eV, which allows to harvest the irradiation visible light to initiate the photocatalytic reaction [35]. It has been reported that Cu_xS_y synthesized in 1D shows extensively enhanced photocatalytic properties due to its electrochemical characteristics [36].

1.4. Synthesis Methods of Copper Sulfides

The functional properties, as described in Section 1.3, reveal many possible application ways to exploit the functionalities of copper sulfides in the field of

advanced materials [35,37]. Considering the rising demand for materials to be used in high tech material assembly, over the past 20 years, the attention of researchers towards the approaches of synthesizing such materials has been increasing. Especially, the attention has been paid to the development of novel, facile, low-cost, and low toxicity approaches towards fabrication, by which the structure and shape together with the respective properties of the target synthesis products are altered.

According to Coughlan *et al.*, *colloidal synthesis* is definitely the most commonly applied method to fabricate transition metal nanoparticles due to many possible advantages such as the regulation of the size, shape and crystal phase of the products, possibility to achieve high-order crystallinity and well as monodispersed nanoparticles and the ability of high dispersion in organic solvents [27]. Colloidal synthesis is performed with standard *Schlenk* equipment which consists of a three-neck, round bottom flask connected to a condenser and a Schlenk line to provide an oxygen-free environment [27]. In general, this approach involves several stages: 1) nucleation from the initially homogenous solution; 2) growth of the performed nuclei; 3) isolation of particles from the reaction mixture; 4) post-synthetic washing treatments to remove unreacted precursors and ligands from the solution of products [27].

One of the techniques in the colloidal synthesis method is called *hot-injection.* Due to the earlier mentioned processing steps, the latter approach creates conditions for producing monodisperse, high-quality transition metal nanocrystals from the mixture of organic solvents and capping agents [33,38]. The procedure involves the sudden addition of cold (room temperature) reactants into a hot mixture of organic compounds, which results in a sudden burst of nucleation followed by growth of nuclei in the presence of surfactant under optimum reaction conditions [33]. Since the nucleation and growth stages take place at different times, the hot-injection method enables a high degree of size and shape control during the synthesis [27]. Various researchers state that the temperature of the reaction is the main factor in terms of determining the size and shape of nanocrystals. In order to synthesize particles up to 20 nm in size, the precursors are preheated up to 180–220 °C [33]. Moreover, the thermodynamic theory states that the sum of the volume and surface energy is critical for the growth of a nanomaterial [38]. The influence of the volume energy, which is released when monomers of the solution are incorporated into growing nuclei, depends on the chemical potential of solution monomers and the time of evolution. Meanwhile, the surface energy is determined as the energy which is consumed to create new solid solution interfaces and is influenced by crystal geometry and the presence of surfactants [38]. Due to these reasons, the selection of a solvent and surfactants is fundamentally important for the achievement of the target products.

In addition, the latter technique has been successfully employed for the fabrication of copper sulfides nano and micro particles in dots, nano wires, nano fibers, nano disks, lettuce-like, etc. shapes [33,38–41]. Furthermore, fossil-based liquid mediums such as dodecanethiol, oleylamine, trioctylphosphine oxi and oleic acid have been applied widely as reaction precursors [40–43].

It is important to emphasize that the latter method allows shaping the properties of materials by synthesizing compounds in nanoscale; therefore, indisputable

advantages on material synthesis are provided by this method. For these reasons, due to the input in developing the hot-injection synthesis method, Bawendi and colleagues were awarded the Nobel Prize in Chemistry in 2023 [44].

The *mechanochemical method* is also a commonly applied approach of nanomaterial synthesis nowadays. In general, mechanochemistry is a branch of chemistry which specifies on physicochemical and chemical transformations caused by mechanical energy during the process [45,46]. The simplicity and efficacy of the method allows employing copper and sulfur resources in the non-ion state without using capping agents or precursors of organic origin. In addition, no by-product or waste component is produced, and therefore the separation step is no longer needed. According to Guo *et al*., due to the decreased number of technological stages and the simplicity of the process, mechanochemical synthesis is considered to be an environmentally friendly method compared to the traditional technological procedures [46]. Furthermore, the reactivity of a material synthesized by this approach is higher because of the new surfaces, point defects and dislocations, as well as polymorphic transformations in the crystalline structure [45]. In addition, multiple reports have stated that mechanochemical synthesizing of copper sulfide yields agglomerated micro-sized grains [47–52]. Nevertheless, it is worth noting that the synthesis of transition metal sulfides by this approach usually takes up to several hours; therefore, a lot of energy is required for this process.

The third widely employed method to produce copper sulfides is the *template-based technique* which is applied to fabricate hollow or porous structures directly on a substrate [27]. In general, the ongoing processes can be divided into three steps: 1) preparation of the template; 2) direct synthesis of the target product on the prepared template; 3) removal of the template to obtain hollow structures (if needed) [27,38]. The thickness and size of the products depend on the reaction conditions, such as the deposition time, and the concentration of metal ions in the solution. The applied templates can be a rigid material, such as glass, stainless steel, or polivynylpyrrolidone which is used as the matrix to deposit the products linked by the covalent bond [43]. Soft templates containing ligands, surfactants and polymers are also applied as a matrix which is formed due to compound aggregation [27,43].

There are several ways of deposing target products on the matrix. Electrochemical deposition or anodization is a well know low-cost technique to produce nanostructures directly on a substrate [33,38]. In this approach, the electric field is created between the cathode and the anode leading to a specific ion deposition on either the anode or the cathode through a redox reaction [43]. Another approach is the *Chemical Bath Deposition* (CBD), whereby the film is deposited on the template in a solution of transition metal ions and a sulfur source. This approach is considered as a facile and inexpensive one, which is performed in low temperatures on various substrates, and which has already been used for the fabrication of Cu_xS_y [53–55].

Some of the most commonly used methods to depose transition metal sulfides are *Physical Vapour Deposition* (PVD) and *Chemical Vapour Deposition* (CVD). Both of them mainly involve the conversion of reactant from liquid phase to vapour by the physical (specifically, high temperature vacuum for PVD) or the chemical (specifically, a chemical reaction for CVD) method, which is followed by vapour

transportation to the substrate, and then the formation of a film by condensation [56,57]. According to this method, CuS particles get formed in a hierarchically grown hollow structure or in clear spherical morphology distributed throughout the film [58–60]. However, the drawbacks of the latter methods are the reaction performance in vacuum, and, usually, the demand for complex equipment.

Another broadly exploited approach towards synthesizing copper sulfides is *hydrothermal or solvothermal treatment,* which through the last few years due to process advantages, such as low production cost, easy processing, and eco-friendliness, became one the most commonly used methods [35,36,61]. According to *Demazeau*, solvothermal process is performed in a presence of a solvent, whereas hydrothermal synthesis is carried out in an aqueous solution [62]. Either way, both processes are carried out in a specialized closed reaction vessel, called an autoclave, which usually consists of the inner teflon liner and the outer stainless steel shell, assembled together to withstand a high temperature and pressure environment during specific duration [27]. Hydrothermal/solvothermal synthesis is performed in a high temperature (typically higher than the solvent's boiling temperature) and pressure, in order to speed up the process and perform the reaction without catalysts. Consequently, the high interfacial energy between the substrate and the liquid is overcome, which allows achieving the desirable morphology of the products [27,56,62]. It is worth noting that the pressure of the reaction in most cases is self-generated and depends on the experimental conditions, such as the temperature, the vessel filling percentage, the properties of the solvent, the concentration of salts, and the properties of the generated gases [27].

Typically, following the principles of the hydrothermal/solvothermal technique, organometallic compounds and metal chloride salts are employed as the copper ion source. Meanwhile, thiourea, sodium sulfide, carbon disulfide, thioacetmide, and sulfur powder have been applied as a sulfur precursor [27]. The selection of the solvent is very important for the quality of the products since the medium regulates the reactivity of the precursors, as well as the solubility and diffusion behaviour [27]. The most commonly used solvents for solvothermal fabrication are ethylendiamine (EDA), ethylene glycol, and ethanol. In addition, hydrothermal/solvothermal synthesis have already been performed to fabricate copper sulfides in the shape of nanospheres, nanocages, nanospheres, nanoflowers, nanorods, nanosheets, nanoflakes, etc. [28,61,63–65].

Although the investigation of approaches towards the synthesis copper sulfides already extends across several decades, among the diverse developed methodologies to control the morphology of the products, researchers are still facing issues, such as the long synthesis duration and high energy consumption [66–70]. Moreover, many researchers have synthesized copper sulfides on a very small scale and with yields of the target product being quite low, which is inherently unsuitable for the envisioned scale-up [69]. Consequently, the production of a high value material covers high processing costs.

It is of importance to note that majority of the above presented approaches towards fabricating Cu_xS_y employ soluble reagents which release Cu (e.g., $CuCl_2$, $CuSO_4$, $Cu(NO)_3$) and S (e.g., Na_2S, $Na_2S_2O_3$, CH_4N_2S, $SC(NH_2)_2$) in the ion state

[31,40–42,63,71,72]. Furthermore, most of the earlier mentioned techniques to produce copper sulfides are carried out in organic reagents as a reaction medium, such as oleyl amine, hydrazine hydrate, or a fossil-based medium, e.g., polyvinylpyrrolidone or toluene [38,69]. Although the latter material is used as organic based capping agents and surfactants in order to selectively control the growth rates of crystal planes and consequently obtain non-agglomerated nanomaterial in the target size and shape, it is also worth noting that the above discussed processing conditions are environmentally unsustainable and even hazardous for humans [31,61]. Nevertheless, so far, only a few studies have reported a Cu_xS_y synthesis procedure in the aqueous medium without surface stabilisers or by employing cheap and earth-abundant reagents, for instance, insoluble copper oxide or sulfur sources [67].

1.5. Prospects of Copper Sulfide Application

Application focusing on electrochemical properties

Copper sulfides are known to possess superior electrochemical characteristics, such as good electrical conductivity, high theoretical charge capacity, and perfect discharge characteristics [34]. It is also worth noting that the above outlined electrochemical properties firmly depend on the morphology of the synthesized material, which is possible to be altered depending on the synthesis conditions [34,73]. For example, a material synthesized in sheets, flakes, or in the plate form has a high surface-to-volume aspect ratio, and is more mechanically flexible compared to nanoparticles in the 1D shape. Therefore, a material in 2D characteristically possesses better charge transport properties and a higher electrochemical charge storage efficiency [34]. In addition, the possible application areas to exploit the superior electrochemical properties of copper sulfides are strongly affected by the synthesis conditions and the achieved morphology.

Due to the tunable electronic charge properties as well as the enhanced mechanical and thermal stability, CuS is considered to be a promising candidate for application in energy storage. Its high power density and long life cycles also make copper sulfide a promising candidate for storing energy in supercapacitors. In particular, copper sulfide has revealed a great potential to be employed as a pseudocaptive material in supercapacitors [34,55,73–75].

Moreover, with the objective to enhance the energy storage capabilities of researchable batteries, regardless of the achieved morphology, copper sulfide is employed as an electrode-composing material [29]. In particular, the material has been tested for novel batteries as lithium ion, sodium ion and magnesium ion [76–80].

It is also worth noting that, due to the perfect ability to absorb light, CuS can be applied to solar cells as a light-absorbing layer [33]. Moreover, its high chemical and thermal stability, together with its high optical transparency and excellent hole transporting properties, such as mobility and conductivity, render copper sulfide into a promising candidate as a hole transporting material for perovskite-based solar cells [81].

Application focusing on photocatalytic properties

By exploiting its photocatalytic properties, CuS is employed for the degradation of potential environmental hazards, for example, various organic molecules, such as dyes and antibiotics [35,82]. The photodegradation reaction, which is also referred to as the *Advanced Oxidation Process* (AOP), starts by irradiation of the wavelength corresponding to the band gap energy of the photocatalyst in order to excite the jump of an electron (e^-) from the valance band to the conductive band (1.1). The jump also creates a positive charge, which is called a *hole* (h^+) (1.1).

1) Generation of free charge carriers:

$$CuS + h\nu \rightarrow h^+ (CuS) + e^- (CuS) \quad (1.1)$$

Once the free charge carriers have been generated and separated from the catalyst surface, the generation of reactive radical species begins (1.2–1.7). Reactive hydroxyl radicals are produced by holes reacting with water molecules (1.2). To enhance the rate of hydroxyl radical production, typically, hydrogen peroxide can be employed due to its property to be a better electron acceptor (1.3) [42].

2) Generation of hydroxyl radical:

$$h^+ (CuS) + H_2O \rightarrow H^+ + \cdot OH \quad (1.2)$$

$$e^- (CuS) + H_2O_2 \rightarrow \cdot OH + OH^- \quad (1.3)$$

$$h^+ (CuS) + OH^- \rightarrow \cdot OH \quad (1.4)$$

3) Generation of other reactive free radical species:

$$e^- (CuS) + O_2 \rightarrow \cdot O_2^- \quad (1.5)$$

$$H^+ + O_2^- \rightarrow \cdot OOH \quad (1.6)$$

$$2H^+ + 2 \cdot O_2^- \rightarrow \cdot O_2 + H_2O_2 \quad (1.7)$$

In addition, the generated active radicals, such as superoxide and hydroxyl radicals, superoxide anion, a further attack on the organic molecules takes place, and, consequently, they are degraded to non-toxic compounds such as water, carbon dioxide, and insoluble salts (1.8) [33,83].

4) Degradation of organic molecules:

$$\text{Organic molecule} + \cdot R \rightarrow CO_2 + H_2O + \text{insoluble salts} \quad (1.8)$$

where $\cdot R$ – $\cdot OH$, $\cdot OOH$, $h^+ (CuS)$, $e^- (CuS)$, $\cdot O_2$, $\cdot O_2^-$.

Typically, the photocatalytic properties of CuS are evaluated by the degradation of dyes, such as methylene blue, methylene orange, rhodamine B under UV or visible light irradiation [50,51,84,85]. Nevertheless, other types of organic molecules can also be photodegraded, for example, antibiotics, e.g., tetracycline, doxycycline, penicillin G, or sulfamethoxazole [82,86–88].

It is important to emphasise that the above mentioned organic molecules are widely known waste water pollutants, since the currently applied conventional

remediation methods in terms of antibiotic degradation are ineffective [89]. In particular, up to 70% of industrial wastewater in the developing countries is untreated, and approximately 80% of wastewater containing dyes is released to the water cycle without remediation [90,91]. In addition, the above mentioned pollutants can be easily detected in the surface waters, such as rivers, lakes and even drinking water [89,90,92]. For example, up to 4.2 μg/L of tetracycline and 200 μg/L of amoxicillin was detected in the surface waters, 2.34 μg/L of ofloxacin was found in effluents leaving hospitals [89]. In particular, due to the ongoing presence of antimicrobial substances in the environment, the unexpected acceleration of antimicrobial resistance has emerged as a significant concern for healthcare systems on a global scale [92–94]. Furthermore, the presence of dye molecules in the water cycle leads to the toxic influence on plants, animals and humans because of carcinogen and mutagenic properties of undegraded molecules of dyes [91].

To remove antimicrobial and toxic compounds from waste water, AOP is considered as one the most promising techniques [95,96]. Moreover, AOP, by virtue of exploiting the photocatalytic properties of CuS, has been used to degrade other problematic waste water pollutants of the organic origin, such as petroleum refinery wastewater pollutants, pharmaceuticals, and pesticides [60,97].

Nevertheless, AOP as a possible wastewater remediation process is still not constructed well enough to be implemented on a large scale. Yet, many researchers have investigated the degradation of organic molecules by applying CuS in a powder form [86,87,98,99]. Consequently, an effective separation step of nanosized photocatalysts from a pollutant stream is needed, which further complicates the process [89]. It is also important to note that many reported approaches towards producing an effective photocatalyst use fossil-based reagents. Moreover, fossil-based reagents are processed in high energy requiring conditions (e.g., a long synthesis duration, a small scale) [87,98]. Therefore, more sustainable solutions have to be developed for the waste water remediation purposes by AOP [89].

One of the solutions to solve the above mentioned issues is to incorporate or depose the photocatalytic material on a stable matrix. For example, a previous study suggested the incorporation of a semiconductor into a composite material by using fossil-based matrices (like N,N′-dimethylacrylamide and graphitic carbon nitride) to aid in the removal of photocatalysts from wastewater [98,100]. Nevertheless, the research reporting sustainable application approaches to exploit photocatalysts in the degradation of organic molecules on the industrial scale is still scarce.

Another way to exploit the photocatalytic properties of CuS is to degrade other possibly hazardous species, specifically, bacteria [101,102]. In this case, the light generated reactive radicals, which are also called *Reactive Oxygen Species* (ROS), further attack bacteria or their cell membrane. As a result, the membrane of bacteria is destroyed, thus causing leakage inside the substance and inactivating bacterial DNA, leading to the death of bacteria [101]. Consequently, bacteria such as *Escherichia coli*, or *Staphylococcus aureus* have been degraded by Cu_xS_y nanoparticles, such as CuS microspheres, CuS nanoclasters or even bulk copper sulfide [51,63,103,104].

Considering the currently rising need for alternative sustainable energy sources, for example, green hydrogen, the ability of CuS to generate electron-hole pairs under visible light irradiation has been also employed in producing green hydrogen by water splitting [42,105]. In this case, excited charge carriers react with protons or water molecules by producing hydrogen [37]. It is worth mentioning that, in order to enhance photocatalyst properties, for example, to prolong the lifetime of photogenerated charge carriers, to enhance their separation from the surface, CuS can also be used as a catalyst in forming heterojunction [106]. In addition, a copper sulfide based composite photocatalyst has been successfully employed for green hydrogen evolution by producing up to 1.041 mmol/g/h under visible light irradiation [107].
In addition, copper sulfide possesses promising electrochemical properties which are important in energy-related applications, such as novel solar cells, super capacitors, and rechargeable batteries. Furthermore, the property to generate free charge carriers by the excitement of visible light can be exploited for waste water treatment, generation of green hydrogen, or for antibacterial purposes. Therefore, copper sulfide is an important compound in the currently environmentally problematics areas.

****

The implementation and establishment of circular economy, especially through the utilization of waste compounds as secondary raw materials, stands as a solution to decrease the production of non-valuable products, as well as to reduce the reliance on fossil raw materials. Additionally, considering the growing demand for innovative technological solutions in various environmentally critical domains, the exploration of compounds with enhanced functional characteristics remains an ongoing process. Furthermore, there is a pressing need for research to focus on neutralising industrial waste by generating valuable and promising compounds. Copper sulfides are recognised as cost-effective, physicochemically stable and non-toxic material with properties influenced by their synthesized size and shape. Cu_xS_y exhibits favourable characteristics for p-type semiconductors, including a high theoretical specific charge capacity, high concentrations of free charge carriers and excellent light absorption capabilities. Copper sulfides also possess superior characteristics which are important in the application initiated by photocatalysis or in the area related to energy storage. By exploiting these properties, many currently crucial environmentally related issues are possibly addressed, such as organic molecule degradation in the wastewater, green hydrogen production, or assembly of enhanced energy storage devices. Although researchers have suggested many techniques to synthesized CuS, the search for an approach to produce compounds with superior characteristics which would be applicable across the industry is still far from being completed. Furthermore, many high value products are synthesized from fossil based reagents, which leads to a lack of sustainability, and SDGs get ignored. On the other hand, the exploitation of the functional properties of CuS in a large scale to address the currently important sustainability issues has not yet been reported in the literature. It is also worth noting that the reports presenting the application of sustainable raw materials to fabricate copper sulfides with valid functional properties are even more scarce. For these reasons, finding a sustainable approach to produce copper sulfide as well as to

investigate its promising properties on a large scale is relevant. Furthermore, the data regarding thermal stability and recrystallisation are not only constrained; the data also display discrepancies across various sources, which suggests that thermal decomposition and stability are influenced by the synthesis approach and conditions. Lastly, utilising a photocatalyst in bulk powder form for the industrial degradation of organic molecules comes with various economic drawbacks. Notably, an additional technological step is needed to efficiently separate the powdered material from the flow of organic molecules, thereby leading to an increase in the processing costs. Hence, in order to investigate a more industry-applicable approach involving the incorporation of a synthesized powder photocatalyst into an easily removable solid matrix is an important asset to be addressed.

2. MATERIALS AND METHODS

2.1. Materials

Waste of sulfuric acid production

Industrial sulfur waste, which was used as a secondary raw material of sulfur, is a by-product of sulfuric acid production at the chemical plant *AB Lifosa* (Kedainiai, Lithuania). This waste is formed while melting raw elemental sulfur of 99.98% content of S. Impurities are separated from the melt by filtration, collected, and then dried.

Other conventional materials

- Elemental reference sulfur (99.99%, *AB Lifosa*, Lithuania);
- Copper oxide (CuO, 99%, *Reachem*, Slovakia);
- Poly(3-hydroxybutyrate-*co*-3-hydroxyvalerate) (PHBV), (custom grade, M_n 209.300 g/mol, M_w 586.000 g/mol, 20 mol% 3HV unit) was purchased from *Merck*, USA. Before the experiments, PHBV was purified by firstly solubilising the polymer in chloroform, then filtering through celite, and precipitating in cold methanol;
- Dry micro fibrillated cellulose (MFC), which was produced by the method reported in [108];
- Chloroform ($CHCl_3$, HPLC grade), 1,4-dioxane (DIOX, ≥99.0%), ethyl alcohol (EtOH, ≥99.8%), hydrogen peroxide (H_2O_2, 30%), methylene blue (MB, $C_{16}H_{18}ClN_3S \cdot 3H_2O$), and tetracycline hydrochloride (TC, $C_{22}H_{24}N_2O_8 \cdot HCl$, analytical standard) were purchased from the *Merck Group*, USA.

2.2. Experimental

2.2.1. Mixture preparation for hydrothermal synthesis

The industrial sulfur waste (secondary raw material of sulfur), which was obtained from the industry in the alloy lump shape, was pulverised in the ball mill for 70 min. 5 kg of sulfur waste was milled in a capacity of 6.6 l, and filled with 21% of ball shape feed material with an average diameter of 42 mm. After that, 30 g of powder was milled in a 150 mL vibrating cup (*Pulverisette 9*, *Fritsch*, Italy) filled in by 53% of a single milling body (a solid cylinder, diameter = 55 mm) at 600 rpm for 2 min.

The primary mixtures of synthesis were prepared by mixing milled sulfur waste as a sulfur source with copper oxide with a molar ratio of S and CuO equal to 1.5:1. Firstly, both materials were homogenised for 1 h in a homogeniser (*Turbula Type T2F*, *Willy A Bachofen AG*, Switzerland) at 34 rpm. Then, 10 g of the mixture was milled in a 50 mL planetary mill *Pulverisette 9* for 1 or 5 min at 600 rpm speed.

For validation reasons, another batch of primary mixture was prepared under the same experimental conditions, although by using the conventional sulfur – that is, reference elemental sulfur – as a sulfurizing agent.

2.2.2. Hydrothermal synthesis

Hydrothermal synthesis was carried out in a 150 mL stainless steel autoclave (*Series 4560*, *Parr Instruments*, USA). The synthesis was carried out in stirred suspensions (50 rpm) by mixing 5 g of the primary mixture with 50 mL of water. The experiments were carried out at a temperature of 145–180 °C for 0.5–4 h; isothermal treatment was performed (Table 2.1). The temperature was reached by applying an hourly rate of increase of 100 °C. Following the isothermal treatment, the reaction vessel was cooled down to room temperature naturally. The resulting sample suspension was then filtered, and the black precipitate was dried under an air atmosphere at a temperature of 104 °C for 12 hours. Then, the dried solid material was ground, sieved through a 100 μm sieve, and analysed by instrumental analysis.

Table 2.1. Experimental conditions of synthesis

Sulfurizing agent	Duration, h	Temperature, °C	Abbreviation
Sulfur waste	0.5	145	Sw0.5h145C
		180	Sw0.5h180C
	4		Sw4h180C
Reference sulfur	0.5	145	Sr0.5h145C
		180	Sr0.5h180C
	4		Sr4h180C

After the hydrothermal treatment, the percentage distribution of sulfur and the copper mass was calculated, while taking into account that the molar ratio of S and CuO was 1.5 in each hydrothermally treated mixture: in the sulfur waste origin mixture, the supplied mass of S to the system was 1.776 g, along with 2.354 g of Cu; whereas, in the sulfur reference based mixture, there was 1.881 g of S, and 2.494 g of Cu. The content of S and Cu in the solid phase was calculated while considering that only CuS constituted the powder product. The mass loss of both S and Cu was estimated according to the calculated loss of the Cu mass in the system. Furthermore, the percentage distribution of components in the liquid was estimated from the data of XRF (X-ray fluorescence) analysis.

During hydrothermal treatment, the temperature, the generated pressure in the autoclave, and the supplied amount of heat by the heater was measured, while collecting the data every 30 s throughout the whole process. For comparison reasons, the hydrothermal treatment was performed without a primary mixture under the same processing conditions, and this experiment shall be referred below as ‘empty’. The experiments were performed 3 times, and the average values shall be presented in the figures.

2.2.3. Investigation of thermal stability

The thermal stability investigation of the synthesized samples was conducted by using a tabular furnace (*RT 50/250/11*, *Nabertherm*, Germany). Each synthesized sample, weighing 0.5 g, was thermally treated in an air environment at temperatures of 250, 300, 400, 450, and 500 °C. The temperature was increased at a rate of 10

°C/min. Once the desired temperature had been reached, the sample was promptly removed from the furnace and cooled in a desiccator. The thermally treated products were then analysed by using the DSC (i.e., *differential scanning calorimetry*) and XRD (i.e., *X-ray diffraction*) techniques. Specifically, the change of the crystallite size of the target synthesis product – CuS (covellite) (PDF 04-006-9635) – was determined in each heated sample. For this reason, the main diffraction peaks characteristic of hexagonal covellite were investigated (Table 2.2). The crystallite size was estimated at each of the main peaks, by repeating the measurement 3 times and calculating according to Scherrer's Equation (2.1).

$$Dhkl = \frac{K\lambda}{Bhkl cos\theta} \tag{2.1}$$

Where: *Dhkl* – crystallite size in the direction perpendicular to lattice planes, nm;
hkl – Miller indices;
K – numerical crystallite-shape factor, i.e., 0.94;
λ – the wavelength of the X-rays, nm;
Bhkl – the full width at half maximum of the X-ray diffraction peak, radians;
θ – Bragg angle, radians.

The standard deviation values are presented in Appendix 1; they were calculated according to Formula 2.2:

$$St.dev. = \sqrt{\frac{\sum_{i=1}^{N}(\bar{X} - X_i)^2}{N-1}} \tag{2.2}$$

Where: N – the number of experiments;
$\bar{X}$ – the average value of experiments;
X_i – the results of a single experiment.

Table 2.2. Investigated peaks of hexagonal CuS

***d*, nm**	**2*θ*, °**	**Left angle, °**	**Right angle, °**	**hkl**
0.305	29.25	28.760	29.760	102
0.282	31.757	30.677	32.391	103
0.273	32.820	32.391	33.227	006
0.190	47.889	47.076	48.728	110
0.174	52.669	52.154	53.419	108

2.2.4. Photocatalytic properties of synthesized samples

The photocatalytic properties of powder synthesized samples were evaluated by degrading methylene blue under irradiation of visible light. In the course of these experiments, only Sw0.5h180C and Sr0.5h180C samples were investigated. 15 mg of the synthesized photocatalyst was mixed with 100 mL of aqueous MB solution (20 mg/L) and 4 mL of H_2O_2. Before illumination, the mixture was magnetically stirred in the dark for 10 min at room temperature to reach the adsorption-desorption

equilibrium, and then the suspension was illuminated with visible light (a 23W LED light bulb, 183 W/m^2 light intensity). The light source was placed 10 cm above the solution, giving irradiation to 28 cm^2 of the surface area. 5 ml of the experimental suspension was taken at specified intervals during the irradiation, and then centrifuged for 5 minutes to separate the particles of the photocatalyst. Then, the UV-Vis (ultraviolet and visible) spectrum of the resulting MB solution was measured by using a UV-vis spectrophotometer (*PerkinElmer Lambda 25*, USA). Specifically, the intensity of the MB characteristic absorption peak centred at 664 nm was measured in order to determine the concentration of MB. The *Degradation Efficiency* (DE) was calculated by the following Equation 2.3:

$$DE = \left(1 - \frac{A_t}{A_0}\right) \cdot 100\% \tag{2.3}$$

Where: A_t – absorbance value of MB at a specific timepoint;
A_0 – the initial absorbance value of MB before the start of irradiation.

The irradiation process lasted 180 min. For comparison reasons, additional tests were conducted in the absence of light, both with and without photocatalysts, as well as with and without hydrogen peroxide. The degradation rate was calculated according to the pseudo-first-order kinetics model (see Formula 2.4). The reaction rate constant was determined by analysing the linear part of the kinetic curves of the initial reaction within the first 20 min of the experiment.

$$ln\left(\frac{c_t}{c_0}\right) = -kt \tag{2.4}$$

Where: c_t – the concentration of MB at a specific timepoint, mg/L;
c_0 – the initial concentration of MB before irradiation, mg/L;
k – the reaction rate constant, min^{-1};
t – time interval, min.

2.2.5. Fabrication of composites

The composites were formed in porous and film architectures. For the formation of composites, only Sw0.5h180C and Sr0.5h180C samples were used. In order to decrease the complexity of the text, in the research step of composites formation, Sw0.5h180C and Sr0.5h180°C samples shall be further referred as *CuSw* and *CuSr*, respectively.

The porous structure was fabricated by dispersing 15 wt.% of Sw0.5h180C/ Sw0.5h180C sample to a solution of PHBV and DIOX (1.08 g of the polymer to 30 mL of the solvent). To ensure thorough mixing, the dispersion was stirred, and dip-sonication was employed for 3 h in 95 °C temperature with reflux conditions. The dip-sonication was carried out by using an ultrasonic processor (*UP50H*, *Hielsher*, Germany) equipped with a sonotrode *MS2* operating at 50 W and 30 kHz. After the dispersion step, the porous structure of the composite was achieved by using the *Thermally Induced Phase Separation* (TIPS) technique. Initially, the dispersed hot suspension was poured into a circular aluminium mould measuring 55 mm in diameter

and 10 mm in height. The mould was then kept at a temperature of –18 °C for 18 h to freeze. Subsequently, the frozen sample was removed from the mould and immersed in an ethanol bath which was also maintained at –18 °C to extract DIOX from the composite structure. The ethanol bath was refreshed every 24 h for a total of 2 times. Afterwards, the resulting porous structure was rinsed with distilled water by using an ultrasound bath and dried in an oven at 50 °C for 24 h.

To enhance the hydrophilicity of the samples, 5 wt.% of MFC (relative to the polymer) was added to the dispersion before sonication. The incorporation of MFC was aimed to improve the wettability of the composite.

Furthermore, composite films were prepared through solvent casting by using the same formulation as for the porous materials but employing chloroform as the solvent. Specifically, CuS and MFC were dispersed together for 3 hours by using dip-sonication combined with magnetic stirring at a temperature of 50 °C. The resulting mixture was then cast in a Petri dish with an 11 cm diameter and left to dry at room temperature overnight. All the compositions of the fabricated CuS–PHBV composites are reported in Table 2.3.

Table 2.3. Formulations of CuS–PHBV composites

Sample structure	The origin of sulfur in photocatalyst	Hydrophilicity modifier filler	Sample code
Porous	Reference	-	CuSr/Po
	Waste	-	CuSw/Po
	Reference	MFC	CuSr/MFC/Po
	Waste	MFC	CuSw/MFC/Po
	-	-	PHBV/Po
Film	Reference	-	CuSr/Fi
	Waste	-	CuSw/Fi
	Reference	MFC	CuSr/MFC/Fi
	Waste	MFC	CuSw/MFC/Fi
	-	-	PHBV/Fi

2.2.6. Investigation of photodegradation of organic molecules by CuS–PHBV composites

The composites in porous and film architectures were investigated to determine the photodegrading properties of the prepared samples. For these experiments, tetracycline was chosen as the model organic molecule. The experiments were performed in a 4 mL quartz cuvette in stirred solutions under irradiation of visible light (λ >420 nm, *Philips PL-S*, 900 lm, 2986 W/m^2 light intensity). 3 mL of TC solution (50 mg/L) was mixed with 60 μm of H_2O_2. The porous composite sample was cut in a cube form with the dimensions of 1x1x1 cm and then immersed in the experimental solution. The average mass of each sample was approximately 0.04 g. Meanwhile, the film composite sample was prepared in an area of 1 cm^2, cut into 8 equal pieces, and immersed into the TC solution. The average mass of each film

sample was 0.01 g. To establish adsorption-desorption equilibrium, the samples were kept in the dark for 10 min before initiating the irradiation process. The experimental solution was then exposed to visible light irradiation, whose source was positioned 4 cm above the solution's surface in 1 cm^2 size, with the solution height equalling 3 cm. At specific time points of irradiation, the concentration of the organic molecule was determined by measuring the UV-Vis absorption peak at 351 nm, which is characteristic of TC. For these measurements a UV-Vis spectrophotometer (*V-650*, *Jasco*, Japan) was used. The degradation efficiency was determined, and the reaction rate constant was calculated according to the pseudo-first-order kinetics model by analysing the linear part of the kinetic curve during the first 15 min of the experiment (see Sections 2.3–2.4).

To investigate the reusability of the composites, only CuSw/MFC/Po and CuSw/Fi samples were analysed. After the initial photodegradation experiment, the composites were air-dried at room temperature and then reused for four subsequent batches of fresh pollutant solution.

Furthermore, simultaneous degradation of multiple organic molecules by the prepared composites was assessed. Specifically, the mixture was prepared with a concentration of 100 mg/L for TC and 10 mg/L for MB. The photodegradation experiments followed the same procedure and conditions as described above. The concentration of MB was determined by measuring the intensity of the MB characteristic absorption peak which was centred at 664 nm.

For comparative analysis, blank tests were conducted to evaluate the photodegradation of TC and TC/MB solutions without any photocatalyst. Neat polymer samples were also investigated.

Moreover, each photodegradation experiment was repeated three times to ensure the accuracy and reliability of the obtained results. The average values are presented in the figures, whereas the standard deviations are presented in appendices (see Appendices 2–5). In determining the reaction rate constant, the values were obtained by fitting the linear part of the pseudo first order kinetic model with the high correlation coefficient (R^2), and the obtained values are reported in appendices (see Appendices 6–8).

2.3. Characterisation Methods

X-ray diffraction analysis

X-ray Diffraction Analysis (XRD) was used to determine the phase composition of the samples. The powder samples were investigated with a *D8 Advance* diffractometer (*Bruker AXS*, Karlsruhe, Germany) equipped with a CuKα X-ray tube operated at 40 kV and 45 mA. The diffraction patterns were obtained in a Bragg-Brentano geometry by using a fast counting detector, specifically, the *Bruker LynxEye*, based on the silicon strip technology. The selected scanning range was 2θ = 3–68 °, which was obtained by 6 °/min shifting. The XRD software *Diffract.Eva* was used to calculate the crystallite size and the intensity of the component diffraction peaks.

To determine the compound composition of the composites, the measurements were carried out by using a diffractometer (*Empyrean*, *Malvern Panalytical*,

Netherlands), equipped with a 4 kW CuKα X-ray tube (λ = 1.5418 Å) and a *PIXcel3D* area detector. The measurements were conducted at 40 kV and 30 mA. The scanning range for the analysis was 2θ = 20–70°, which was obtained by 0.22 °/s scanning speed at a 0.01° step size. For data processing, the XRD software *HighScore 5.1a* from *Malvern Panalytical* was employed.

X-ray fluorescence analysis

X-ray Fluorescence Analysis (XRF) was applied to identify the chemical composition of the sulfur waste and hydrothermal synthesis samples in a liquid medium. The analysis was performed on a high performance wavelength dispersive XRF spectrometer (*S8 Tiger*, *Bruker*, USA) equipped with a Rh tube with the energy of up to 60 eV. Powder samples were formed in a 40 mm tablet and then measured. Liquid samples were measured in a 3 cm plastic holder using the *Millar* film of 3.6 μm thickness. All the measurements were performed in the helium atmosphere, and the data were analysed with *SPECTRAPlus QUANT EXPRESS* standardless software.

The average values and standard deviations presented in the results were calculated based on three measurements.

Thermal analysis

Simultaneous Thermal Analysis (STA), which simultaneously conducts *Differential Scanning Calorimetry* (DSC) and *Thermogravimetry* (TG), was used to investigate the thermal stability and phase transformations of the investigated sulfur waste. STA was performed on a thermal analyser (*PT1000*, *Linseis*, Germany) employing ceramic sample handlers and Pt crucibles. The measurements were conducted by using an air atmosphere, with a heating rate of 10 °C/min in the temperature range of 30–300 °C.

DSC was used to measure the amount of the released heat in the investigation of thermal stability of the synthesized solid samples. A thermal analyser (*DSC 214 Polyma*, *Netzsch*, Germany) was used with the following parameters: the temperature was raised at a rate of 10 °C/min, the investigated temperature range was 25–600 °C, and an empty aluminium Al crucible served as the reference. The atmosphere in the furnace was nitrogen with a flow rate of 20 mL/min. The experiments were carried out in closed crucibles with the E type thermocouple.

Particle size distribution

The particle size distribution of the primary mixtures was determined by employing the fractionation equipment (*L3P Sonic Sifter Separator*, *Advantech*, USA). A vertical impulse-type kick wave was transmitted to a set of sieves (with sizes of 425, 212, 106, 80, and 63 μm) every 4 s to reorient and break apart any agglomerated particles. The sieving procedure lasted for 5 min, with a frequency of 60 Hz.

The particle size distribution of the solid synthesized products was assessed by using a particle size analyser (*1090 LD*, *CILAS*, France) according to the laser diffraction methodology. The experiments were performed in the water medium with

the content of ground particles ranging from 12 to 15% within sensitivity varying from 0.04 to 500 μm. Each measurement took approx. 60 s.

UV-Vis diffuse reflectance spectroscopy

The optical properties of the synthesized solid material were evaluated by UV-vis *Diffuse Reflectance Spectroscopy* (DRS), which was conducted by using a UV-vis-NIR spectrophotometer (*V-650*, *Jasco*, Japan). The measurements were performed within the wavelength range of 200 to 900 nm. Before performing the measurements, the spectrophotometer was calibrated with the $BaSO_4$ reference. The band gap of the synthesis products was estimated by applying the Kubelka-Munk theory Equations (2.5–2.7) [109,110].

$$R = \frac{R_{sample}}{R_{standard}} \tag{2.5}$$

$$F(R) = \frac{(1-R)^2}{2R} \tag{2.6}$$

$$F(R) = \frac{A\left(1-E_g\right)^n}{h\upsilon} \tag{2.7}$$

Where: R – the reflectance of sample;

E_g – the optical band gap energy, eV;

$h\upsilon$ – the light energy, eV;

A – the proportional constant;

n – a value depending on the nature of electronic transition, e.g., for direct transition, n = ½; for forbidden direct transition, n = 3/2; for indirect transition, n = 2; for forbidden indirect transition, n = 3.

Scanning electron microscopy with energy dispersive X-ray analysis

Scanning Electron Microscopy with Energy Dispersive X-ray analysis (SEM-EDX) was employed to determine the morphology and chemical composition of the waste origin synthesized powder samples. For this reason, a scanning electron microscope (*Helios Nanolab 650*, *FEI Company*, USA) equipped with an EDX spectrometer (*X-Max*, *Oxford Instruments*, UK) was used within 3 kV of the accelerating voltage. The element composition obtained by EDX spectra was estimated by performing 3 measurements, within the highest standard deviation value of 3.7%.

To study the formation of the porous structure and the distribution of the filler in the polymer matrix, *Field Emission Scanning Electron Microscopy* (FE-SEM) was employed by using a scanning electron microscope (*Mira3*, *Tescan*, Czechia). To prepare cross sections of the film composites for the investigation, the samples were cryo-fractured in liquid nitrogen. Afterwards, all the samples were attached to an aluminium stub by using a conductive carbon tab and coated with approximately 10 nm of gold by employing the electro-deposition method. The examination of the cross-section and top view images of the films was carried out by applying an accelerating voltage of 20 kV along with a backscattered electron detector. For the

analysis of the porous composites, the low vacuum mode was applied with an accelerating voltage of 10 kV.

Transmission electron microscopy

Solid synthesis products were examined with a transmission electron microscope (TEM) (*Tecnai G2 F20X-TWIN*, *FEI Company*, USA) by using an accelerating voltage of 200 kV.

Measurement of water contact angle

The measurement of the static *Water Contact Angle* (WCA) of the prepared composites was performed by using a contact angle goniometer (*DSA30*, *Kruss Scientific*, Germany) which was equipped with a digital camera. To measure the WCA value, 4 μL of Milli-Q water droplets was placed on the surface of the composite samples. The average values and the standard deviations presented in the results were calculated based on five measurements.

2.4. Thermodynamic Modelling

For the thermodynamic calculations of the hypothetical reaction parameters, the method of absolute entropies was employed [111–113]. According to this method, the change of the reaction standard free Gibbs energy $\Delta_r G_T^0$ was calculated with Equation 2.8:

$$\Delta_r G_T^0 = \Delta_r H_T^0 - T\Delta_r S_T^0 \tag{2.8}$$

Where: $\Delta_r H_{298}^{0,f}$, and $\Delta_r S_{298}^{0,f}$ – the change/alteration/variation of the reaction enthalpy and entropy at temperature *T*.

The standard molar thermodynamic properties values used at 25 °C and 1 bar are given in Table 2.4 [114–116].

Table 2.4. Standard molar thermodynamic properties at 25 °C and 1 bar *

Component	$\Delta H_{298}^{0,f}$ (kJ/mol)	$\Delta S_{298}^{0,f}$ (J/(mol·K)	ΔC_p (J/mol·K)
H^+ (aq)	0	0	0
H_2O (l)	–285.8	70.0	75.3
S (l)	1.4	35.2	23.6
SO_2 (aq)	–323.8	159.5	195.0
H_2S (g)	–20.6	205.8	34.2
HS^- (aq)	–17.6	62.8	NG
Cu^{2+} (aq)	64.8	–99.6	NG
CuO (s)	–157.3	42.6	42.3
CuS (s)	–79.5	120.9	76.3

* aq – aqueous; l – liquid; g – gas; s – solid; NG – non-given

2.5. Reaction Modelling with Aspen HYSIS

The modelling and simulation of sulfuric gaseous compounds formation was performed by using *Aspen HYSIS V12* modelling program. Modelling estimations were obtained by employing the Peng-Robinson fluid package for the conversion reaction. Moreover, the real initial quantities of elemental sulfur and water as well as the actual hydrothermal treatment conditions, such as the temperature and pressure, were simulated.

3. RESULTS AND DISCUSSION

3.1. Properties of Primary S–CuO Mixture

Characterisation of secondary raw material of sulfur

The secondary raw material of sulfur obtained from sulfuric acid production was investigated with the XRD and XRF analysis methods together with STA to identify the phase and elemental composition the material (Fig. 3.1, Table 3.1). According to the XRD and XRF analysis, the main component of sulfur waste was elemental sulfur (PDF 00-024-0733, *d*-spacing = 0.385; 0.344; 0.321 nm) in a rhombic structure, which constituted 86% of the material sample (Fig. 3.1A, Table 3.1). The sulfur waste was also composed of quartz (PDF 00-046-1045, *d*-spacing = 0.425; 0.333 nm) and anhydrite (PDF 00-037-1496, *d*-spacing = 0.350 nm) (Fig. 3.1A). XRF analysis also showed traces of iron, potassium, aluminium, and magnesium, whose presence is due to the origin of fossil elemental sulfur (Table 3.1). It is worth noting that the content of the latter elements in the waste is in a relatively low amount, and no apparent diffraction maximums or an amorphous phase consisting of the presently mentioned elements was observed.

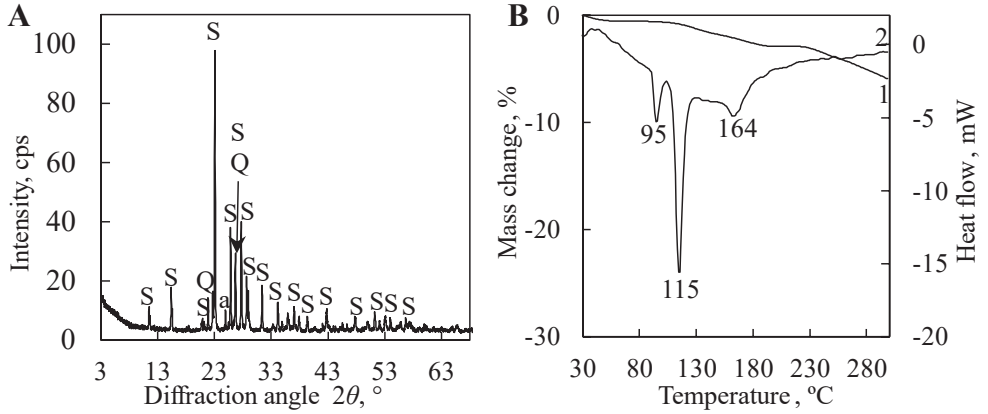

Fig. 3.1. XRD pattern of sulfur waste (A). Indices: S – sulfur; a – anhydrite; Q – quartz. STA curves of sulfur waste (B). 1 – mass loss; 2 – heat flow

Table 3.1. Elemental composition of sulfur waste

Element	S	Ca	Fe	Si	K	Al	Mg	Other
Concentration, %	86.3	6.9	4.0	2.3	0.153	0.142	0.115	0.09

According to the STA analysis of sulfur waste, three exothermic effects were identified in a range of 30–300 °C (Fig. 3.1B). The first endothermic reaction in which 11 J/g of heat was released appeared at 95 °C due to the rhombic α-S recrystallisation to monoclinic β-S. By increasing the temperature up to 115 °C, the melting of monoclinic sulfur occurred, which went along with an endothermic effect of 62 J/g of heat. The third endothermic effect within 20 J/g of the released heat occurred at 164

°C due to the formation of long spiral chains μ-S [117,118]. The beginning of the second endothermic effect at 109 °C was followed by the decrease of the mass loss until 195 °C, in which 2.88% of sulfur was lost. Afterwards, sulfur did not react until 221 °C, since the mass in the sample remained the same. By raising the temperature up to 300 °C, the mass continuously decreased by losing 3.03% (Fig. 3.1B).

Preparation conditions of primary mixture

The preparation of the material for hydrothermal synthesis was investigated by evaluating the particle size distribution. Three different mixtures were prepared under the following conditions: homogenisation, homogenisation followed by 1 min of milling, and homogenisation followed by 5 min of milling. According to the obtained results, the biggest amount of the smallest fraction was reached in the sample which was only homogenised, since 60.1% of the mixture contained particles which were smaller than 106 μm (the smallest fraction), 22.0% of the sample constituted 106–212 μm-sized particles, and 17.9% of the particles were larger than 212 μm (which thus was the largest fraction) (Fig. 3.2). A slight increase in the particle size was observed in the sample which was further milled for 1 min because 54.8% of the latter sample was smaller than 106 μm, 23.0% was within the size frame of 106–212 μm, and 22.2% of the particles was larger than 212 μm (Fig. 3.2). By further increasing the duration of milling up to 5 min, the amount of the largest fraction further increased by 8 percent (Fig. 3.2). The rise of the particle size during milling is attributed to the coalescence of the material due to the fine particles agglomeration during the operation.

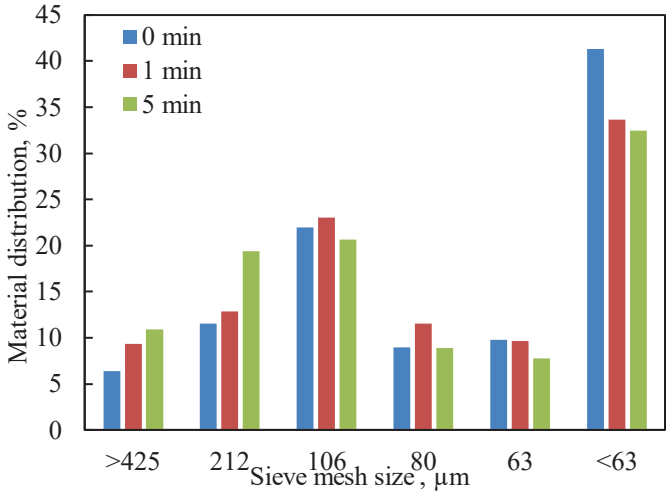

Fig. 3.2. Particle size distribution of the primary mixture with sulfur waste depending on the duration of milling

XRD analysis was further employed to investigate the phase composition of the primary mixtures. The results showed that the sample which was prepared during 1 h of homogenisation consisted of the compounds originating from mixed components: sulfur, quartz, and tenorite (CuO, PDF 04-007-0518, *d*-spacing = 0.253, 0.233, 0.187 nm) (Fig. 3.3). Moreover, it was noted that the samples after 1 and 5 min of milling

had the same compound composition as the homogenised sample (Fig. 3.3). Therefore, no new components were formed during the milling.

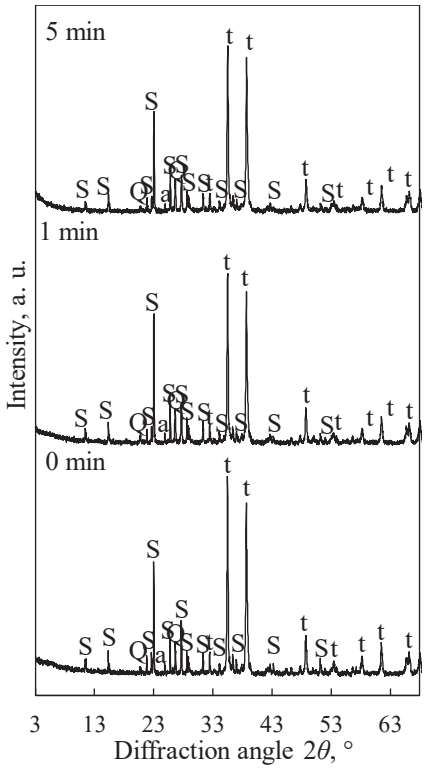

Fig. 3.3. XRD patterns of the primary mixture prepared by different durations of milling. Indices: S – sulfur; t – tenorite; Q – quartz

In addition, by comparing different approaches towards primary mixture preparation, the difference in the particle size of the samples was not significant, since the smallest fraction was larger by 5% in the sample which was milled for 1 min compared to the particle size of the homogenised sample. Nevertheless, it is important to note that, during the material treatment by milling, the crystal defects in the sample were possibly created, which led to a higher amount of reactive surfaces, and, consequently, which led to an increase of the reactivity of the material [119]. Taking this into account, the mixture prepared by homogenisation and further milled for 1 min was selected for the following hydrothermal treatment.

By summarising the obtained results, the proposed preparation conditions of the primary mixture for hydrothermal treatment are 1 h homogenisation of the sulfurizing agent and copper oxide followed by milling for 1 min at 600 rpm.

Acknowledgements:

Reprinted/Adapted with permission from *Springer Nature*: *Waste and Biomass Valorization* / Purification of Sulfur Waste under Hydrothermal Conditions / G. Sarapajevaite, K. Baltakys. 12:3407-3416. 2021. https://doi.org/10.1007/s12649-020-01206-y; license No. 5756421139083

3.2. Thermodynamic Estimations of Reaction Mechanism

Before treating the primary mixtures under hydrothermal conditions, thermodynamic calculations were conducted to trace the possible pathway of copper sulfide formation from elemental sulfur and copper oxide in a water medium. According to the estimations of free Gibbs energy, the solid sulfur particles firstly melted, and then liquid sulfur reacted with water molecules to produce soluble hydrogen sulfide gas and sulfur dioxide (Equation 3.1). It has been reported in the literature that the particular reaction, known as the reverse Claus reaction, is possible in temperatures below 200 °C [120,121]. Subsequently, the produced hydrogen sulfide reacted with copper oxide particles to form copper sulfide (Equation 3.2). Meanwhile, sulfur dioxide reacted with water through disproportion reactions, leading to the production of hydrogen cations (Equations 3.3 and 3.6). These hydrogen cations then participated in further reactions with liquid sulfur and copper oxide (Equations 3.4 and 3.5) [110].

The hydrothermally synthesized H^+ was employed in the reaction with CuO, which resulted in the formation of copper cations (Equation 3.5). These copper cations then reacted with HS^-, a product of the second disproportion reaction, to yield the desired synthesis product – CuS (Equation 3.7). Based on this proposed mechanism, the sample solution consisted of H_2O, SO_4H^-, H^+, as well as – possibly – unreacted compounds, such as H_2S, SO_2, HSO_3^-, and HS^-. Importantly, the estimated free Gibbs energy values for Equations 3.4, 3.2, and 3.7 were significantly below zero, thus confirming the high reliability of the suggested mechanism (Fig. 3.4).

$$3S\ (l) + 2H_2O\ (l) \rightarrow 2SO_2\ (aq) + H_2S\ (g) \quad (3.1)$$

$$CuO\ (s) + H_2S\ (g) \rightarrow CuS\ (s) + H_2O\ (l) \quad (3.2)$$

$$SO_2\ (aq) + H_2O\ (l) \leftrightarrow H_2SO_3\ (aq) \leftrightarrow H^+\ (aq) + HSO_3^-\ (aq) \quad (3.3)$$

$$S\ (l) + 2H^+\ (aq) \rightarrow H_2S\ (g) \quad (3.4)$$

$$CuO\ (s) + H^+\ (aq) \rightarrow Cu^{2+}\ (aq) + H_2O\ (l) \quad (3.5)$$

$$S\ (s) + HSO_3^-\ (aq) + H_2O\ (l) \leftrightarrow S_2O_3H^-\ (aq) + H_2O\ (l) \leftrightarrow HS^-\ (aq) + SO_4H^-\ (aq) \quad (3.6)$$

$$Cu^{2+}\ (aq) + HS^-\ (aq) \rightarrow CuS\ (s) + H^+\ (aq) \quad (3.7)$$

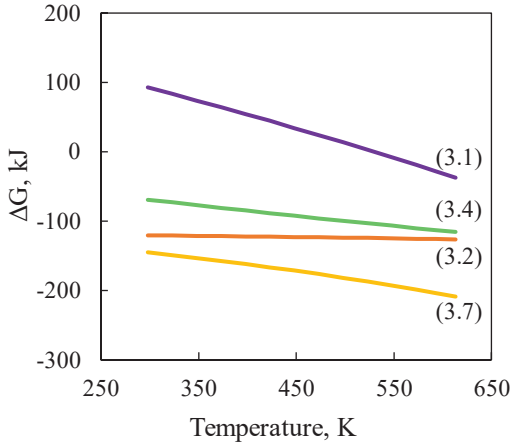

Fig. 3.4. Dependence of Gibbs free energy on temperature

In addition, during the hydrothermal treatment, elemental sulfur possibly served as the raw material for the formation of soluble sulfur compounds. The resulting anions and cations then engaged in further reactions with copper oxide, leading to the generation of copper sulfide particles.

3.3. Characterisation of the Synthesis Products

Mineralogical composition of powder product

After the mixture of CuO and sulfur raw material was hydrothermally treated, the phase composition of the synthesized powder samples was examined. It was observed that a hexagonal CuS phase – covellite (PDF 04-006-9635) – was synthesized in 0.5 h of hydrothermal treatment at 145 °C when using both sulfur waste and the reference sulfur (Fig. 3.5). Moreover, those samples which were produced in 180 °C in 0.5 or 4 h also consisted of covellite (Fig. 3.5). Furthermore, the impurities originating from sulfur waste, such as quartz and anhydrite, remained unreacted in all the samples under various hydrothermal synthesis conditions (Fig. 3.5A). It is also worth noting that elemental sulfur was identified in Sw0.5h145C sample, thus showing that synthesis at a temperature of 145 °C for 0.5 h is not sufficient for the primary components to react completely (Fig. 3.5A). Meanwhile, all the samples obtained from the reference sulfur treated under different experimental conditions contained unreacted sulfur (Fig. 3.5B). Sample Sr0.5h145C also consisted of unreacted tenorite (Fig. 3.5B).

Since the samples of the origin of sulfur waste exhibited diffraction peaks of CuO and S of a higher intensity compared to the reference origin samples, a slower formation of CuS crystals in the reference sample took place. The latter phenomenon is attributed to the differences in the reactivity of sulfurizing agents caused by the diverse mechanical preparation of sulfurizing agents during the industrial treatment of the material.

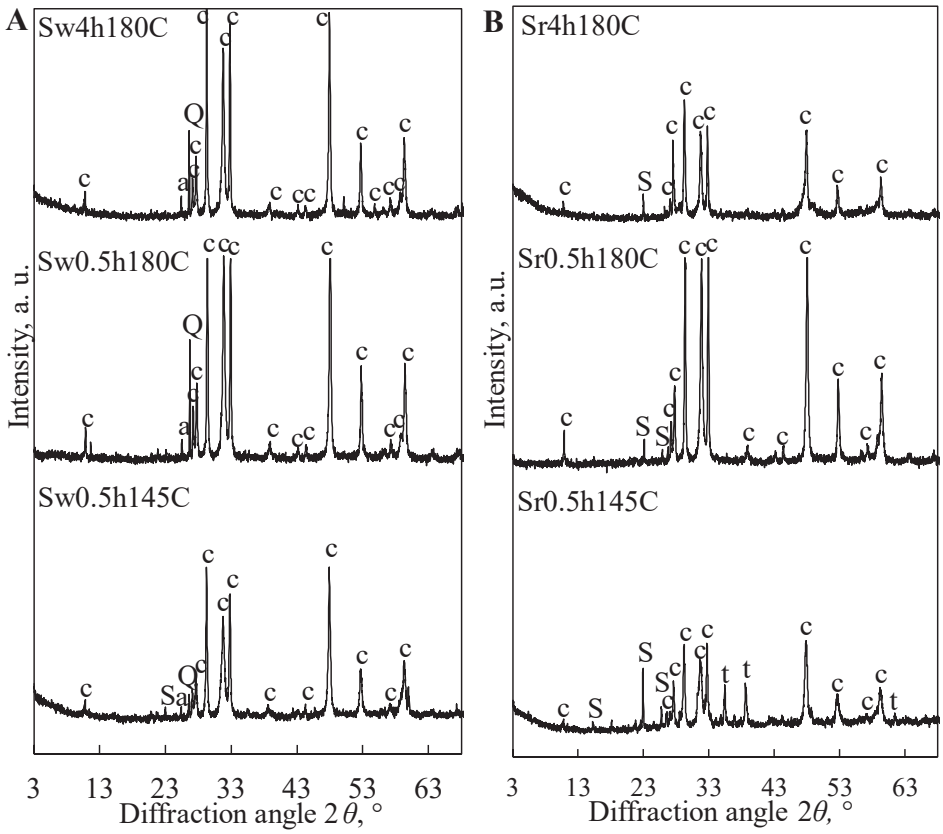

Fig. 3.5. XRD patterns of synthesis samples originating from sulfur waste (A); and sulfur reference (B). Indices: c – covellite; S – sulfur; Q – quartz; t – tenorite; a – anhydrite

Furthermore, it was also noticed that the intensity of covellite diffraction maximums differed depending on the type of the sulfurizing agent and the duration of hydrothermal treatment. The intensity of the main diffraction maximums of covellite in the sulfur waste-based samples differed by 3–8% depending on the synthesis duration (see Table 3.2).

Table 3.2. Intensity of the diffraction maximums characteristic to covellite in synthesized samples

Sample	***d*, nm**				
	0.305	**0.282**	**0.273**	**0.190**	**0.174**
	Intensity, cps				
Sw0.5h180C	2597	1997	2179	2531	804
Sw4h180C	2521	2065	2272	2631	866
Sr0.5h180C	1976	1835	2062	1834	704
Sr4h180C	1347	973	1075	982	343

Meanwhile, the crystallinity of covellite obtained from elemental sulfur was influenced by the duration of synthesis since the peak intensities of CuS obtained in 0.5 h of treatment was higher by 32–51% compared to the covellite obtained in 4 h (Table 3.2). Besides, by analysing the influence of the sulfurizing agent on crystallinity, it was determined that the diffraction maximums were higher in the waste based sample by 8–28% when the synthesis took 0.5 h, and by 47–63% for 4 h synthesis compared to the samples obtained from elemental sulfur (see Table 3.2). Therefore, the origin of the sulfurizing agent had an influence on the crystallinity of the target synthesis product, i.e., covellite.

It is also worth mentioning that, during the production of sulfuric acid, sulfur waste was collected after melting elemental raw sulfur; therefore, the material underwent thermal pre-treatment, which was followed by waste aggregating to the alloy form during the cooling. Moreover, to get the waste material in a powder form, which is suitable for hydrothermal synthesis, sulfur waste was treated mechanically with a ball mill before it was further mechanically activated with a planetary mill. Meanwhile, elemental sulfur as a sulfurizing agent only underwent the treatment of a planetary mill. In addition, the different mechanical and thermal pre-treatment of the sulfurizing agent led to different reactivity of the material during the hydrothermal treatment, which led to a different mineralogic composition and crystallinity of covellite. Therefore, the sulfurizing agent influenced the formation of the desired synthesis product, i.e., covellite.

Furthermore, the investigation was conducted on the particle size of the bulk synthesized material. It was found that the majority of the samples consisted of particles smaller than 100 μm (Fig. 3.6). However, the prevailing particle size in the samples was less than 30 μm, as 53.7–70.1% of the bulk material consisted of the presently mentioned value (Fig. 3.6). Additionally, particles smaller than 1 μm accounted for 5.9–9.9% of the samples (Fig. 3.6).

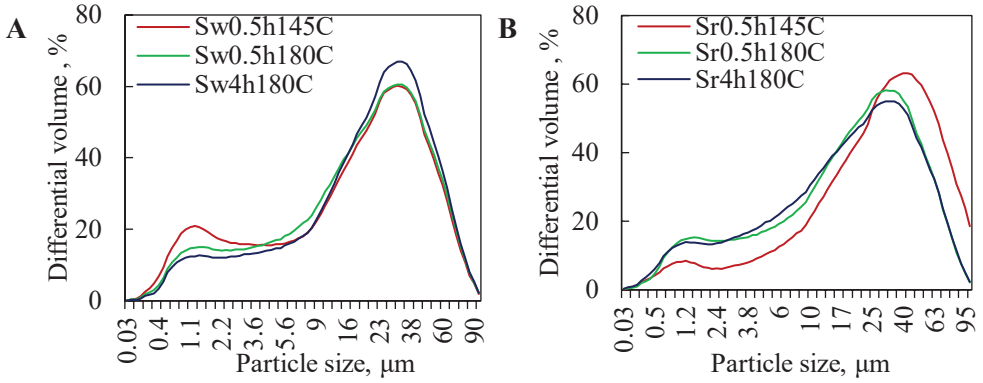

Fig. 3.6. Particle size distribution of synthesized samples originating from sulfur waste (A); and sulfur reference (B)

It is of importance to note that the largest particle size was observed in sample Sr0.5h145C (Fig. 3.6B). This characteristic of the sample can be attributed to the highest content of unreacted sulfur, which was revealed by XRD analysis (Fig. 3.5).

During the cooling phase of hydrothermal treatment, the molten unreacted sulfur solidified into particles, which, presumably, were in larger than the synthesized products, thus leading to an increase in the average particle size.

The treatment conditions, such as the processing medium and the drying conditions, commonly influence the particle size of bulk material. On the contrary, the crystallite size, which is a parameter related to the functional properties of a semiconductor material, is affected differently. It was noticed that the samples synthesized at 145 °C in 0.5 h of hydrothermal treatment exhibited the smallest crystallite size (Table 3.3). The average crystallite size of covellite in the waste and reference samples was 33 nm and 27 nm, respectively (Table 3.3, Appendix 1).

Table 3.3. Crystallite size of covellite in synthesized samples

Synthesis conditions	**Sample of sulfur waste**	**Sample of sulfur reference**
	Range of crystallite size (min–max), nm	
0.5 h 145 °C	19.9–42.7	18.3–42.3
0.5 h 180 °C	27.3–49.0	25.8–50.3
4 h 180 °C	28.7–50.6	27.8–53.0

An increase of the hydrothermal treatment temperature to 180 °C resulted in a 6 nm increase in the crystallite size of covellite for the waste sample and an 8 nm increase for the reference sample (Table 3.3). This indicates that the growth of CuS crystals accelerated with higher reaction temperatures. However, the duration of the synthesis was found to make little impact on the average crystallite size, with only a 1–2 nm increase when the reaction time was extended from 0.5 h to 4 h (Table 3.3). Moreover, it was observed that the origin of the sulfurizing agent had a slight effect on the crystallite size of covellite, as the values for this parameter were lower by 2–5 nm for each experimental point in the reference sample (Table 3.3). Therefore, the temperature of the hydrothermal treatment played a crucial role in stimulating crystal growth.

Morphology of synthesis products

Based on the *Scanning Electron Microscopy* (SEM) images, the waste samples displayed a morphology characterised by round-shaped plates. However, as the temperature increased, the particles agglomerated and formed clusters resembling flower shapes (Fig. 3.7). The tabular structure of the synthesis products was also confirmed by TEM images (Fig. 3.8).

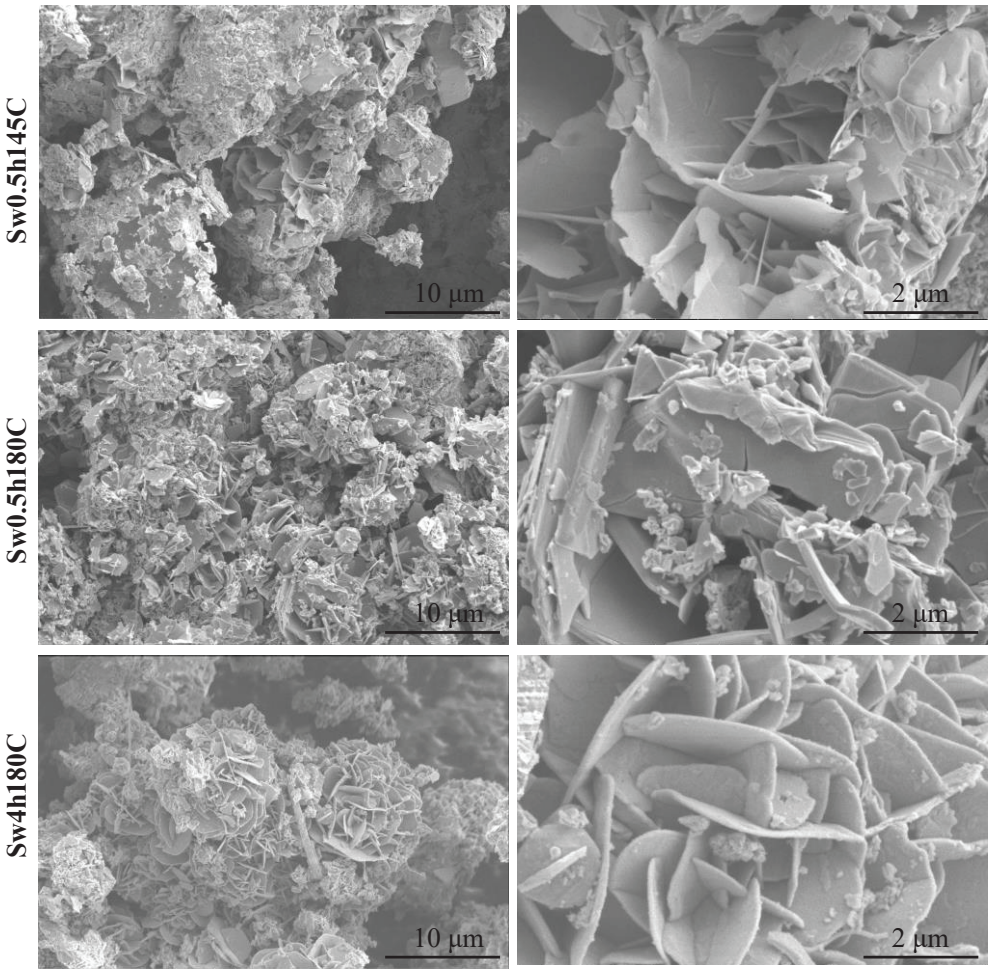

Fig. 3.7. SEM images of sulfur waste-based synthesized CuS samples

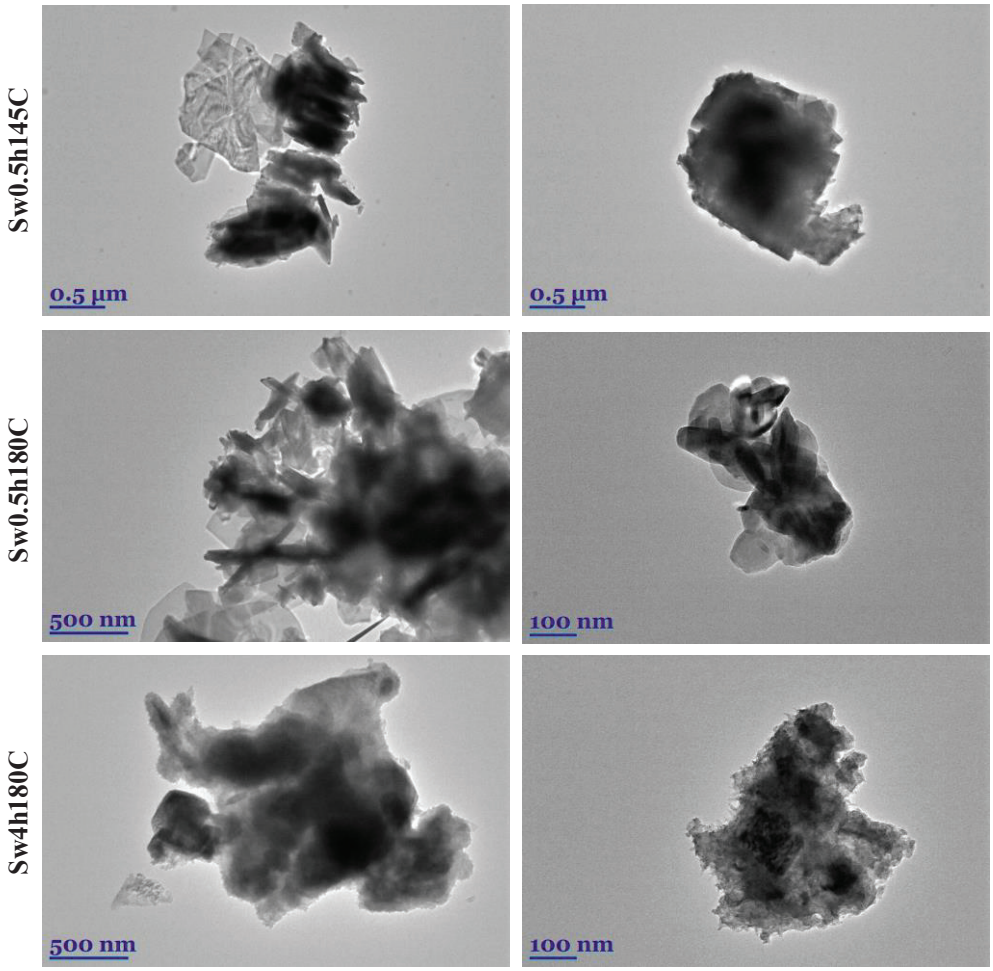

Fig. 3.8. TEM images of synthesized samples

The waste samples were also analysed by using energy dispersive X-ray spectroscopy. The analysis revealed that, in the samples of Sw0.5h145C and Sw0.5h180C, the observed S-to-Cu ratio is 1:1, thus confirming that the synthesized compound Cu_xS_y was actually covellite (Table 3.4).

Table 3.4. Average quantification of EDX spectra of different sulfur waste samples

Synthesized sample	Atomic ratio Cu:S
Sw0.5h145C	1.01:1
Sw0.5h180C	1.06:1
Sw4h180C	0.87:1

Although the Cu:S ratio in sample Sw4 h180C was approximately 0.9:1, which indicates the formation of a sulfur-rich copper sulfide compound, the XRD results did not indicate the presence of this compound (Fig. 3.5, Table 3.4). Therefore, it is possible that the obtained results were influenced by an error in the instrumentation.

Mass balance of sulfur and copper

Furthermore, the elemental composition of the liquid medium after hydrothermal synthesis was investigated by XRF analysis. The obtained results revealed that all of the samples contained sulfuric compounds, which goes into agreement with thermodynamic estimations stating the possible presence of colloidal sulfur, dissolved SO_2 and H_2S gases, and HSO_3^- anion in the reacting medium (Equation 3.6). It was determined that, by increasing the reaction temperature from 145 to 180 °C, the amount of sulfur-containing components in the liquid medium increased on average by 0.127 and 0.203% in sulfur waste and the sulfur reference samples, respectively (Table 3.5). Meanwhile, the increase of the duration of the reaction did not affect the sulfur content in the liquid significantly (Table 3.5).

Moreover, thermodynamic estimations based on Equations 3.5 and 3.7 indicating the presence of Cu^{2+} cations in the reacting medium were also confirmed by XRF analysis, since the copper element was detected in the liquid. Nevertheless, the highest content of Cu was detected in the samples synthesized in 0.5 h at 145 °C, whereas, by raising the reaction temperature to 180 °C, the amount of Cu slightly decreased (Table 3.5). Meanwhile, in samples Sw4h180C and Sr4h180C, Cu element was measured in the range of 19–35 PPM, which proves the time-dependent consumption of released Cu^{2+} for the formation of CuS (Table 3.5).

Table 3.5. Content of sulfur and copper in liquid medium after hydrothermal treatment

Sample	S content, %	Cu content, %
	Average value ± st. dev.	Average value ± st. dev.
Sw0.5h145C	0.589±0.058	0.586±0.122
Sw0.5h180C	0.716±0.023	0.034±0.025
Sw4h180C	0.701±0.044	0.000±0.000
Sr0.5h145C	0.530±0.005	0.053±0.030
Sr0.5h180C	0.733±0.003	0.059±0.028
Sr4h180C	0.720±0.042	0.000±0.000

To evaluate the effectiveness of the copper sulfide synthesis, the component mass distribution of sulfur and copper throughout different phases of the experimental system was investigated. For this reason, the mass balance of S and Cu was constituted. It is worth noting that the mass balance was not constituted for samples Sw0.5h145C and Sr0.5h145C due to the presence of unreacted components, such as S and CuO in the samples, which would distort the results.

The mass distribution of sulfur after hydrothermal treatment was evaluated while considering that S element as distributed throughout the solid phase in a form of CuS, the liquid medium, losses due to the processing, and, possibly, gaseous compounds. Furthermore, it is worth noting that the losses due to the processing were calculated according to the losses of Cu in the system; thus, the possible contribution of sulfur to the generated amount of gaseous compounds was estimated. In addition, it was determined that, despite the hydrothermal synthesis conditions, the majority of

the supplied sulfur reacted with CuS since 59–68% of the supplied sulfur was found in the solid phase which consisted of CuS (Table 3.6). Therefore, considering the amount of sulfuric compounds in the liquid and the losses of processing, up to 16% of the supplied sulfur was used to form gaseous sulfur compounds (Table 3.6).

Table 3.6. Mass distribution of sulfur after hydrothermal synthesis

Material phase	Sample			
	Sr0.5h180C	**Sw0.5h180C**	**Sr4h180C**	**Sw4h180C**
	Mass distribution ± standard dev., %			
solid	67.68±2.05	66.52±1.34	59.19±1.39	62.32±1.34
liquid	19.49±0.15	20.17±0.92	19.13±1.11	19.74±1.23
gaseous	12.83±2.19	16.30±2.26	14.59±0.28	15.95±1.11
losses	0.00±0.01	0.1±0.00	7.10±0.00	0.61±0.01

Meanwhile, up to 99% of the supplied copper reacted to CuS (Table 3.7).

Table 3.7. Mass distribution of copper after hydrothermal synthesis

Material phase	Sample			
	Sr0.5h180C	**Sw0.5h180C**	**Sr4h180C**	**Sw4h180C**
	Mass distribution ± standard dev., %			
solid	98.81±0.94	99.27±0.49	89.3±0.00	100.00±0.2
liquid	1.19±0.95	0.72±0.49	0.00±0.00	0.00±0.00
losses	0.00±0.01	0.01±0.00	10.70±0.00	0.00±0.02

In addition, the percentage mass distribution of S and Cu elements goes in good agreement with thermodynamic estimations, thus proving the formation of gaseous sulfur compounds during the synthesis.

Most importantly, on the grounds of XRD, SEM-EDX and TEM analysis, in 0.5 h hydrothermal treatment of a mixture of sulfur waste and copper sulfide in an aqueous solution in 145–180 °C temperature, copper sulfide – covellite – was synthesized in the tabular shape with 27–40 nm-sized crystallites on average.

Acknowledgements:

Reprinted/Adapted with permission from MDPI: *Materials* / Aqueous-Based Synthesis of Photocatalytic Copper Sulfide Using Sulfur Waste as Sulfurizing Agent/ G. Sarapajevaite, D. Morselli, K. Baltakys, 15(15):5253. 2022. https://doi.org/10.3390/ma15155253

3.4. Thermal Stability Investigation of Synthesized Covellite

According to the literature review, the application of synthesized copper sulfide may also involve conditions in a higher than ambient temperature, such as the temperature of operating field photovoltaic or electronic devices [122]. Furthermore, during the heat treatment of the samples, constituent recrystallisation takes place, and this phenomenon notably affects the nanoparticle size [123]. As the particle size significantly influences the electrochemical and optical properties of nanostructured

sulfides, exploring the thermal stability and recrystallisation becomes vital. However, the data on the thermal stability and recrystallisation are not only limited; these data also exhibit inconsistencies across different sources, thereby implying that thermal decomposition and stability depend on the synthesis approach and conditions. For these reasons, the thermal stability and the decomposition process of the synthesized samples was investigated further.

DSC analysis of the synthesized samples was performed across a temperature range of 25–600 °C. The obtained data revealed that the samples, which were synthesized at 145 °C in 0.5 h synthesis by using both sulfur waste and elemental sulfur, still contained elemental sulfur since the endothermic effect was noticed in both samples at 118–119 °C showing the melting of sulfur (Fig. 3.9).

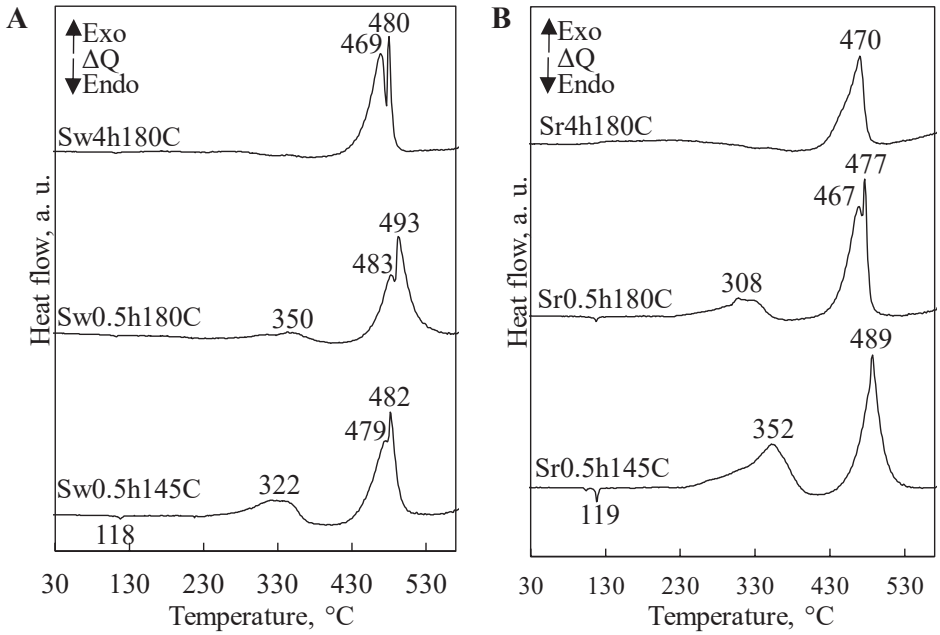

Fig. 3.9. DSC analysis curves of synthesized samples from sulfur waste (A) and reference sulfur (B)

Moreover, two exothermic reactions proceeded during the thermal treatment of Sw0.5h145C and Sr0.5h145C. The first exothermic effect was observed from 235±5 (onset) to 379±22 °C (offset) (Fig. 3.9). Meanwhile, the second exothermic reaction proceeded from 418±2 to 523±3 °C (Fig. 3.9). It is important to note that the endothermic effect, characteristic to sulfur melting, was not noticed in the samples originating from sulfur waste synthesized at 180 °C in 0.5 h and 4 h, which confirms the absence of sulfur in the samples (Fig. 3.9).

Moreover, two exothermic reactions also were observed in the samples synthesized at 180 °C in 0.5 h of treatment. The first exothermic effect was in the temperature range of 245±15–385±15 °C, with the peak temperatures at 350 and 308 °C for the waste and reference samples, respectively (Fig. 3.9). It is worth noting that the samples fabricated at 180 °C released a lower amount of heat by 149 and 120 J/g

for the waste and reference samples, respectively, compared to the ones synthesized at 145 °C (Fig. 3.9, Table 3.8). The second exothermic reaction proceeded from 414±4 to 518 ±22 °C for samples Sw0.5h180C and Sr0.5h180C, respectively (Fig. 3.9).

Meanwhile, the samples obtained during 4 h synthesis showed only one exothermic effect in a temperature range from 405±5 to 497±8 °C (Fig. 3.9). It was observed that this single-peak exothermic effect was characteristic of sample Sr4h180C, while sample Sw4h180C exhibited a duplex peak during the exothermic reaction at peak temperatures of 469 and 480 °C (Fig. 3.9).

Table 3.8. Heat flow of synthesized samples

Sample	Sw0.5h180C		Sw4h180C		Sr0.5h180C		Sr4h180C	
Thermal effect	Peak, °C	Heat, J/g	Peak, °C	Heat, J/g	Peak, °C	Heat, J/g	Peak, °C	Heat, J/g
	350	92			308	232		
	483; 493*	595*	469; 480*	541*	469; 477*	643*	470	455

*– peak temperatures and the value of heat flow during the thermic effect possessing a duplex peak

The discrepancy in the exothermic reaction pattern was attributed to the mineralogical composition of samples Sw4h180C and Sr4h180C. XRD analysis of the synthesized samples revealed that the intensity of the diffraction peaks in sample Sr4h180C was 32–51% lower compared to Sr0.5h180C, which indicates poorer crystallization in Sr4h180C (Table 3.2). On the other hand, the crystallinity of samples Sw0.5h180C and Sw4h180C was approximately at the same level, as the intensity of diffraction peaks varied by approximately 3–8% between the two (Table 3.2). Additionally, when comparing the samples of the waste origin, it was observed that the released heat in sample Sw4h180C was lower by 54 J/g compared to the amount of the released heat in Sw0.5h180C (Table 3.8). Accordingly, in the samples originating from the sulfur reference, the amount of the released heat was lower by 188 J/g in sample Sr4h180C compared to Sr0.5h180C (Table 3.8). Hence, the duration of the synthesis significantly influenced the pathway of decomposition together with the amount of the released heat.

As it was confirmed by DSC analysis, the samples synthesized at 145 °C temperature still contained elemental sulfur, which reveals that the formation of covellite was not finished. For this reason, the thermal stability of the latter samples was not investigated. To investigate the decomposition mechanism of covellite, thermal treatment experiments were conducted to observe the mineralogical changes occurring during the heating of the material.

According to the data of XRD analysis, there were no noticeable mineralogical alterations in samples Sr0.5h180C and Sw0.5h180C compared to their initial composition in the synthesis products when the temperature was increased to 300 °C (Fig. 3.10). The initial changes in the mineralogical composition were noticed in the

samples heated at 400 °C, since traces of anilite (Cu_7S_4) (PDF 04-007-1772, *d*-spacing = 0.336 nm) and digenite (Cu_9S_5) (PDF 00-047-1748, *d*-spacing = 0.321, 0.196, and 0.168 nm) were observed in both samples (Fig. 3.10). These findings suggest that the decomposition of covellite into digenite and anilite began at temperatures higher than 300 °C, thus explaining the exothermic effect observed by DSC in the temperature range of 235–379 °C (Equations 3.8–3.9, Fig. 3.9).

$$9CuS \rightarrow Cu_9S_5 + 4S \quad (3.8)$$

$$7CuS \rightarrow Cu_7S_4 + 3S \quad (3.9)$$

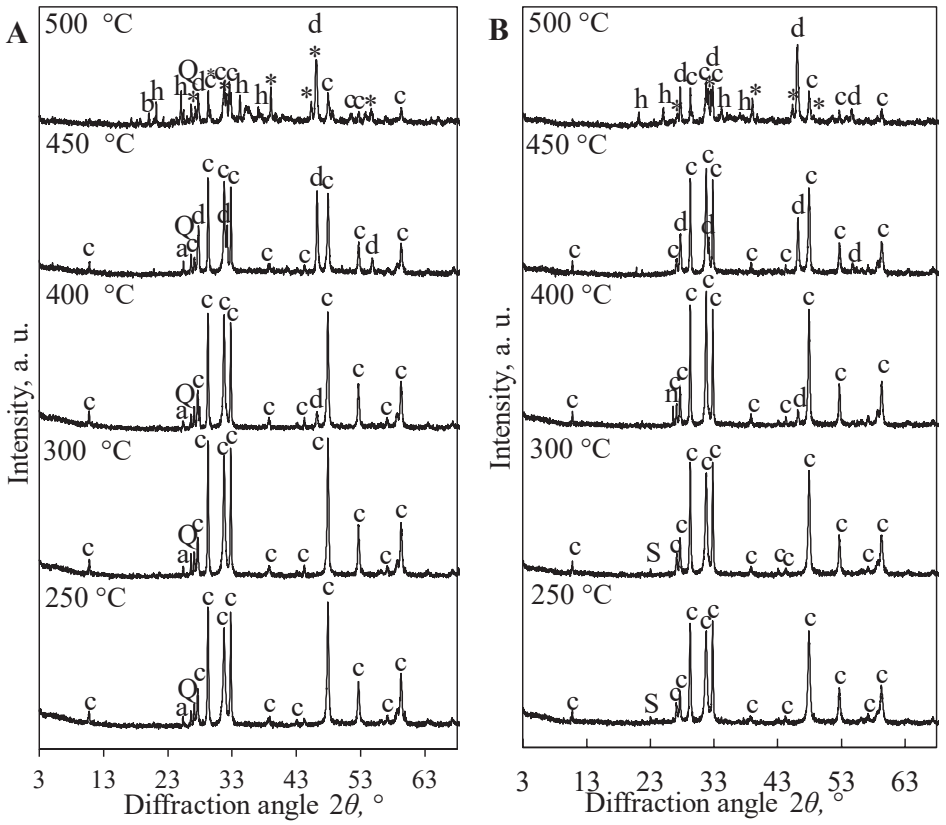

Fig. 3.10. XRD patterns of samples Sw0.5h180C (A) and Sr0.5h180C (B) thermally treated at different temperatures. Indices: S – sulfur; Q – quartz; a – anhydrite; c – covellite; n – anilite; d – digenite; * – $Cu_{1.81}S$; h – chalcocyanite; b – bonattite

Moreover, the intensity of the diffraction maximums of digenite increased in samples heated at 450 °C, although no new intermediate compounds were identified. The most prominent changes in the phase composition of samples Sr0.5h180C and Sw0.5h180C were noticed in the samples heated at 500 °C, since the dominant compounds were digenite and copper sulfide with a stoichiometric ratio of Cu and S being equal to 1.81 to 1 ($Cu_{1.81}S$) (PDF 04-003-4437, *d*-spacing = 0.231, 0.197 nm) (Equation 3.10) (Fig. 3.10). Moreover, the oxidation of covellite occurred in a

temperature range of 450–500 °C, since the diffraction peaks of covellite decreased by more than a half, and chalcocyanite ($CuSO_4$) (PDF 04-008-0844, *d*-spacing = 0.419, 0.355, 0.262 nm) was also one of the main constituents of the samples (Equation 3.11) (Fig. 3.10). The latter findings also corresponded to the data of DSC analysis showing the exothermic effect at 418–523 °C (Fig. 3.9).

$$1.81CuS \rightarrow Cu_{1.81}S + 0.81S \quad (3.10)$$

$$CuS + 2O_2 \rightarrow CuSO_4 \quad (3.11)$$

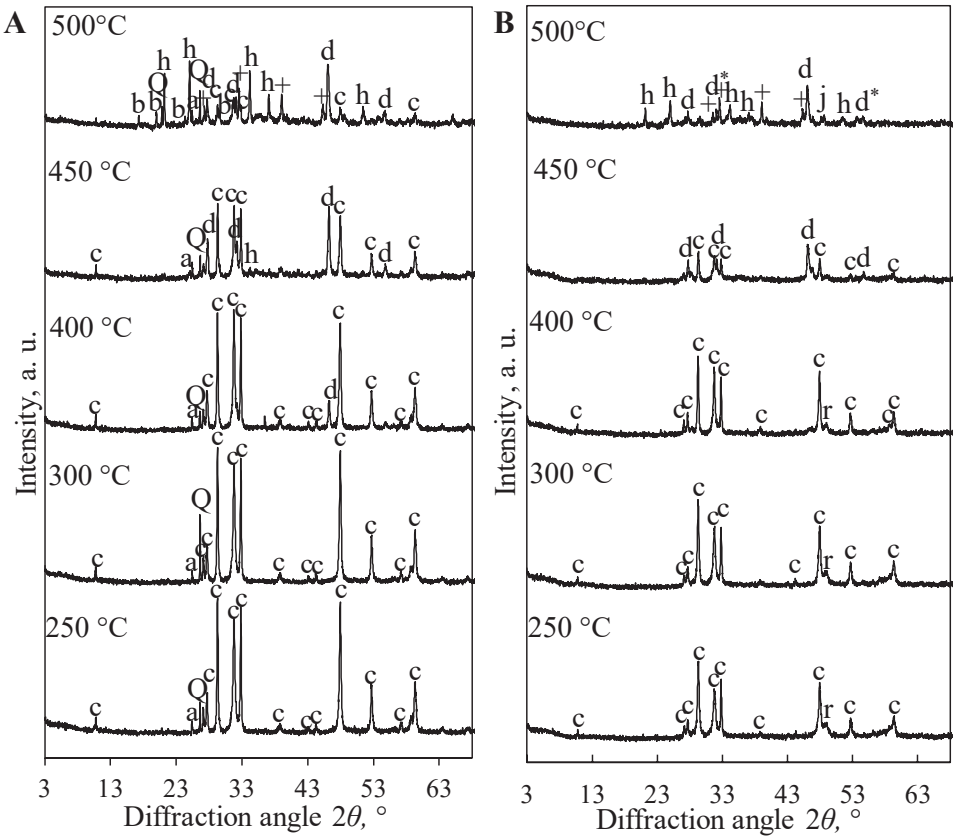

Fig. 3.11. XRD patterns of samples Sw4h180C (A) and Sr4h180C (B) thermally treated at different temperatures. Indices: S – sulfur; a – anhydrite; Q – quartz; c – covellite; d – digenite; d*– digenite high; r – roxbyite; + – Cu_2S; h – chalcocyanite; b – bonattite

By comparing samples synthesized by hydrothermal treatment of 0.5 and 4 h, only minor mineralogical changes of the phase composition were noticed in the sample heated at the same temperature. For instance, the compounds originating from waste such as quartz and anhydrite remained unreacted in both samples Sw0.5h180C and Sw4h180C, thus proving the inertness throughout the whole temperature range of thermal treatment (Figs. 3.10A, 3.11A).

Furthermore, the intermediate compound roxbyite ($Cu_{1.8125}S$) (PDF 04-019-1452, *d*-spacing = 0.186 nm) was only noticed in sample Sr4h180C at low thermal treatment temperatures between 250–300 °C (Fig. 3.11B). Moreover, Cu_2S (PDF 04-024-2237, *d*-spacing = 0.275, 0.230, 0.171 nm) was identified instead of $Cu_{1.8}S$ in the samples heated at 500 °C (Figs. 3.11B, 3.12). The latter samples also consisted of digenite high ($Cu_{7.2}S_4$) (PDF 04-024-0061, *d*-spacing = 0.279, 0.197 nm) and bonattite ($CuSO_4 \cdot (H_2O)_3$) (PDF 04-010-6576, *d*-spacing = 0.511, 0.442, 0.326 nm) (Fig. 3.11).

$$2Cu_{1.8}S + 0.2O_2 \rightarrow 1.8CuS + 0.2SO_2 \quad (3.12)$$

It is of importance to highlight that the most significant distinctions between the reference and the waste samples were observed in the intensity values of the main diffraction peaks associated with covellite. It was determined that the intensities of the diffraction maximums of sample Sw4h180C heated at 250 °C were higher by 47–62% compared to sample Sr4h180C, which was thermally treated at the same temperature (Fig. 3.11, Table 3.9).

Table 3.9. Intensity of the diffraction maximums characteristic to covellite in thermally treated samples

Sample	Thermal treatment, °C	*d*-spacing, nm				
		0.305	**0.282**	**0.273**	**0.190**	**0.174**
Sw0.5h180C	250	2372	1916	2264	2496	872
	300	2744	2411	2591	2663	990
	400	2324	2272	2135	2338	857
Sw4 h180C	250	2687	2280	2501	2616	944
	300	2702	2292	2461	2641	900
	400	2330	2368	2214	2071	737
Sr0.5 h180C	250	1999	1824	2047	1870	707
	300	2277	2008	2258	2116	792
	400	2459	2714	2329	2288	851
Sr4 h180C	250	1422	888	1104	1041	358
	300	1657	1104	1109	1114	446
	400	1547	1302	1130	1182	394

The tendency remained the same across all the samples thermally treated at different temperatures. It is also worth noting that sulfur was formed during thermal decomposition according to Equations 3.8–3.10. However, the endothermic effect corresponding to elemental sulfur at 119 °C was not observed in all the curves of samples DSC analysis due to the sulfur oxidation reaction in the air environment (Equation 3.13).

$$S + O_2 \rightarrow SO_2 \quad (3.13)$$

To the contrary of the claims of the literature, CuO or Cu_2O was not indicated in any product heated at 250–500 °C [124,125].

The crystallite size of covellite in the initial samples ranged from 27 to 40 nm on average, and there was no notable variation in the crystallite size observed among different initial samples. Additionally, an increase of the heating temperature to 400 °C did not lead to a significant alteration in the crystallite size of covellite, which demonstrates the stability of the synthesized covellite (Table 3.10).

Table 3.10. Change of the covellite crystallite size

Sample	Synthesized sample			
	Sr0.5h180C	Sr4 h180C	Sw0.5 h180C	Sw4 h180C
	Range of crystallite size (min–max), nm			
250	23–45	23–51	23–47	26–53
300	28–52	26–51	26–46	28–51
400	34–57	28–49	29–51	32–56

Moreover, it is noteworthy that the changes in the mass observed during the experiments of thermal treatment also supported the XRD findings. It was also observed that, as the heating temperature was increased from 250 to 450 °C, the mass of sulfur waste-based and the reference-based samples, synthesized in 0.5 h, decreased by up to 11% (Table 3.11). This reduction in mass was attributed to the withdrawal of sulfur from covellite, as indicated by XRD analysis.

However, the mass reduction was lower in the samples synthesized in 4 h by approximately 8% (Table 3.11). Furthermore, in the temperature range of 450–500 °C, where oxidation occurred, both samples of 4 h processing showed a 5–7% increase in the mass, which was attributed to the formation of a compound of a higher molar mass, specifically, copper sulfate (Table 3.11).

Table 3.11. Mass change of samples during thermal treatment

Heating temperature, °C	Synthesized sample			
	Sr0.5h180C	Sr4h180C	Sw0.5h180C	Sw4h180C
	-Δm, %			
250	0.62	0.48	0.64	0.68
300	3.40	1.50	2.66	0.86
400	8.87	3.00	4.94	5.18
450	10.91	7.40	10.29	8.41
500	14.11	2.18	7.06	1.46

Samples Sr0.5h180C and Sr4h180C heated at 500 °C were investigated by SEM–EDX analysis, and the obtained results corresponded to the XRD data (Fig. 3.12). It was noticed that both samples mainly consisted of small size bulk material distributed on the surface of large crystals (Fig. 3.12A,D). According to spectra 1 of EDX analysis of both samples Sr0.5h180C and Sr4h180C, the large particles corresponded to Cu_2S compound since the ratio of the atomic mass is 2:1 (Fig. 3.12B,E). Meanwhile, $CuSO_4$ was formed in small-size bulk material, since the EDX

spectra indicated a large amount of oxygen together with copper and sulfur (Fig. 3.12C,F).

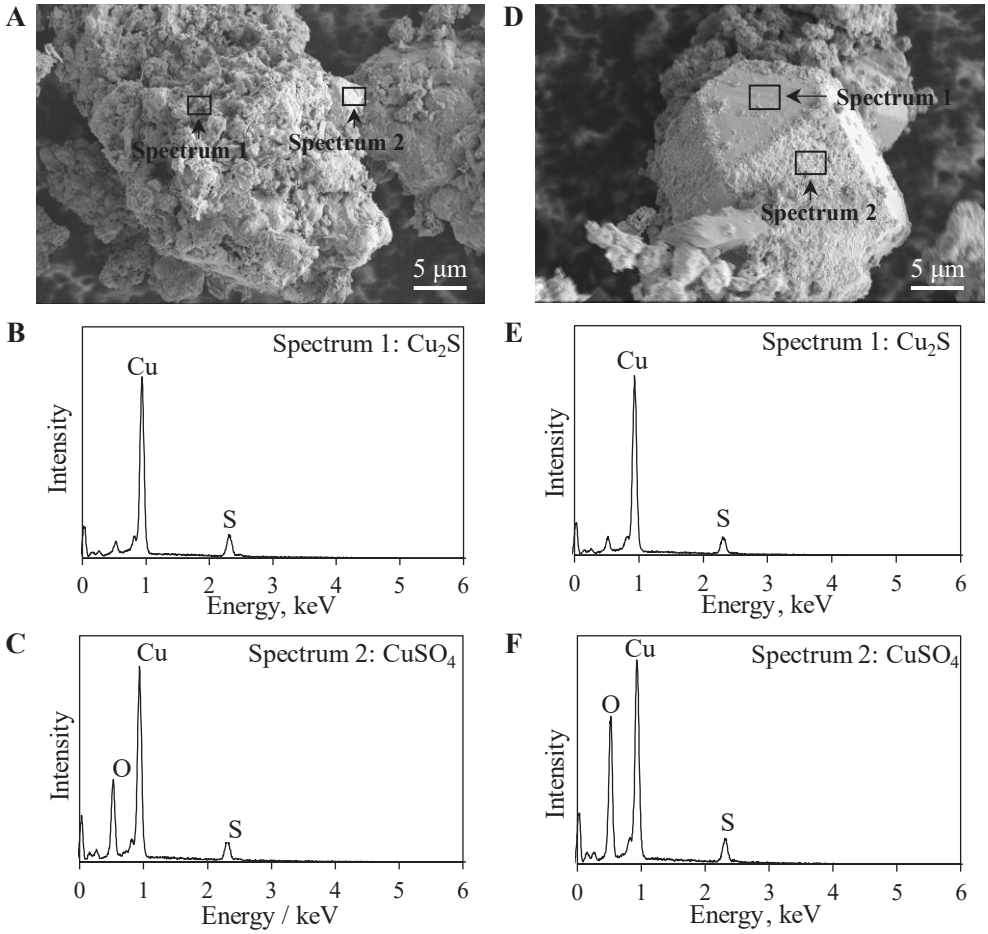

Fig. 3.12. SEM image of sample Sr0.5h180C thermally treated at 500 °C (A), EDX spectra of sample Sr0.5h180C heated at 500 °C (B, C). SEM image of sample Sr4h180C thermally treated at 500 °C (D), EDX spectra of sample Sr4h180C heated at 500 °C (E, F)

After the mineralogical investigation of the heated samples was performed, it was clear that the exothermic reaction across an approximate temperature range from 240±14 to 382±22 °C appeared due covellite decomposition to digenite. Meanwhile, the exothermic reaction in the temperature from 412±7 to 513±19 °C occurred due to the covellite oxidation reaction to copper sulfate.

For the further exploration of the thermal properties of the synthesized samples, DSC analysis was performed on heated samples to confirm the absence of presumably formed new compounds during the thermal treatment of covellite samples. The results demonstrated that the thermograms of thermally treated samples originating from sulfur waste followed the same heat releasing pattern as the heated samples originating

from sulfur reference (Fig. 3.13). It is also worth noting that the first exothermic effect was absent or was insignificant in all of the heated samples (Fig. 3.13).

By increasing the temperature of the thermal treatment, the amount of the released heat during the exothermic effect at temperatures approximately from 412±7 to 513±19 °C decreased in all of the samples compared to the data of the synthesis products (Table 3.12). These data go in good agreement with the XRD data, which suggests that, by raising the heating temperature, covellite decomposed to intermediate copper sulfides; therefore, a lower amount of reactive covellite was sufficient for the oxidation reaction in the sample heated at 400 °C than that for the sample heated at 250 °C.

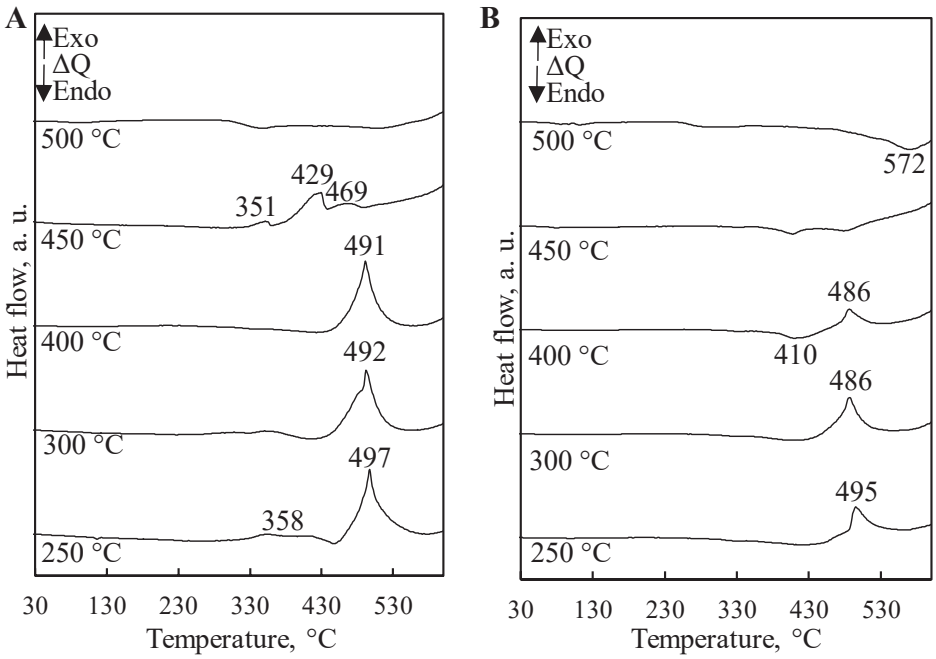

Fig. 3.13. DSC analysis curves of samples Sr0.5h180C (A) and Sr4h180C (B) thermally treated at different temperatures

However, the amount of the released heat differed depending on the duration of hydrothermal synthesis. For instance, in samples Sr0.5h180C and Sw0.5h180C, which were the samples heated at 400 °C, the amount of the released heat was lower by 7 and 64 J/g, respectively, compared to the heat amount released by the primary samples (Table 3.12). Meanwhile, samples Sr4h180C and Sw4h180C heated at 400 °C released the amount of heat which was lower by 296 and 168 J/g compared to the synthesis products (Table 3.12).

Moreover, by increasing the heating temperature up to 450 °C, the amount of the released heat in samples Sr0.5h180C and Sw0.5h180C was reduced significantly by 331 and 351 J/g compared to the synthesis products (Table 3.12). However, sample Sw4h180C released only 61 J/g of heat; meanwhile, this effect was absent in sample Sr4h180C (Table 3.12). Since the effect indicating the covellite oxidation reaction

was absent or insignificant, it was discovered that the oxidation reaction in the samples obtained with 4 h synthesis started at a lower temperature than oxidation which occurred in samples synthesized in 0.5 h. In addition, the duration of synthesis influenced the oxidation rate of covellite.

Table 3.12. Values of released or consumed heat during thermal analysis of heated synthesized samples

Sample	Sw0.5h180C		Sr0.5h180C		Sw4h180C		Sr4h180C	
Thermal treat. temp., °C	Peak, °C	Heat, J/g	Peak, °C	Heat, J/g	Peak, °C	Heat, J/g	Peak, °C	Heat, J/g
250	504	↑496	358 497	↑216 ↑717	489; 497*	↑480*	495	↑304
300	467; 480*	↑466*	357 492	↑ 164 ↑686	479; 491*	↑424*	486	↑374
400	475; 485*	↑531*	491	↑636	492	↑373	410 486	↓82 ↑159
450	493	↑244	351 429; 469*	↑25 ↑312*	335 461	↓64 ↑61	408 480	↓55 ↓26
500	452 520	↓58 ↓74	–	–	466 540	↓110 ↓79	289 –	↓64 –

* – peak temperatures and the value of the heat flow during the thermic effect possessing a duplex peak;
↓ – consumed heat;
↑ – released heat.

Moreover, it was determined that the amount of the heat released by thermally treated samples during exothermic reactions was lower in the samples synthesized by 4 h of hydrothermal treatment than those involving 0.5 h of thermal treatment. For instance, by comparing Sr4h180C samples heated at 250, 300, 400 °C temperatures, the released heat for the second exothermic effect was higher by 57.6, 45.5, 75.0%, respectively, for 0.5 h treatment samples compared to the 4 h-treated samples (Fig. 3.12, Table 3.12). These results also corresponded to the data of synthesized CuS. This suggests that the samples obtained by 4 h synthesis were more stable and less reactive in the oxidation process than 0.5 h-treated samples. However, it is worth noting that the influence of the synthesis duration for the amount of the released heat was less significant in sample Sw4h180C since the difference was 3.2, 9.0, and 29.8% (Table 3.12). Furthermore, all the samples heated at 500 °C temperature did not release heat in temperatures characteristic to the covellite oxidation reaction; therefore, it was determined that the transition temperature from CuS to $CuSO_4$ was a higher temperature than 450 °C (Fig. 3.13).

It is also worth noting that the application of different sulfurizing agents for hydrothermal synthesis did not affect the phase changes of the thermal treatment

products within a temperature range of 250–400 °C. Nevertheless, the sulfurizing agent and the synthesis duration were the key reasons in the variation of the amount of the released heat during thermal treatment.

In addition, the decomposition of covellite (CuS) started through the minor reactions of decomposing covellite to anilite (Cu_7S_4) and digenite (Cu_9S_5) at a temperature higher than 300 °C. However, the major reaction of the decomposition of covellite to digenite occurred at a higher temperature than 400 °C. These results prove the thermal stability of the synthesized copper sulfide samples proceeds at least up to 300 °C, which is a higher temperature of stability than that reported in the literature [125,126]. By increasing the temperature, anilite further decomposed to $Cu_{1.81}S$, and the latter compound was also produced from covellite at a temperature higher than 450 °C. Meanwhile, part of digenite was oxidised to Cu_2S simultaneously. It was determined that, at a temperature higher than 450 °C, the oxidation of covellite to copper sulfate (chalcocyanite, bonattite) occurred. It is worth noting that the latter reaction also occurred at a higher temperature than the value reported in the literature [124].

Acknowledgements:

Reprinted/Adapted with permission from *Springer Nature*: *Journal of Thermal Analysis and Calorimetry* / Thermal stability and decomposition mechanism of synthetic covellite samples / G. Sarapajevaite, K. Baltakys. 147:10951-10963. 2022. https://doi.org/10.1007/s10973-022-11313-8; license No. 5756430078164

3.5. Photocatalytic Properties of Synthesized Samples

Investigation of photocatalytic properties

As it was revealed by XRD and DSC analysis, samples Sw0.5h145C and Sr0.5h145C still contained unreacted sulfur and copper oxide, which lowered the possible maximum content of CuS and also incorporated impurities to the composition. This possibly could have distorted the results of the further investigation. Therefore, only the samples synthesized at 180 °C during 0.5 or 4 h hydrothermal treatment were examined for the further investigation of photocatalytic properties. Furthermore, the samples synthesized under the above outlined conditions – despite using sulfur reference as a sulfurizing agent – were also investigated for comparison purposes and sulfur origin validation reasons. The latter samples shall be referred further as the reference samples.

Photocatalytic characteristics are among the most important properties of semiconductors. For this reason, samples obtained during 0.5 and 4 h synthesis at a temperature of 180 °C were further examined by DRS. The reflectance spectra of the samples were measured across a wavelength range of 200–900 nm, which revealed a broad absorption peak in the visible light wavelength (Fig. 3.14A). Consequently, the band gap energy of the synthesized samples was calculated based on Tauc plot obtained from the Kubelka–Munk function [110]. For this function, the value of n characteristic to covellite, which is the main component of the synthesized samples, is 1/2 [64].

In addition, the determined band gap of the CuS sample obtained from waste during 0.5 h synthesis at 180 °C is 1.78 eV (Fig. 3.14B). Furthermore, the duration of the synthesis did not have an impact on the band gap in the waste samples, since sample Sw4h180C also possessed the band gap value of 1.78 eV (Fig. 3.14B). However, the duration of the hydrothermal treatment did affect the band gap in the reference sample. By increasing the duration of the synthesis from 0.5 to 4 h, the values of the band gap decreased from 1.81 eV to 1.72 eV (Fig. 3.14B). Comparatively, the literature suggests that the band gap energy characteristic of covellite samples typically varies around 2.0 eV [127]. Therefore, the proposed hydrothermal method allowed synthesizing particles of covellite with a slightly lower experimental bandgap energy than the value which was theoretically expected.

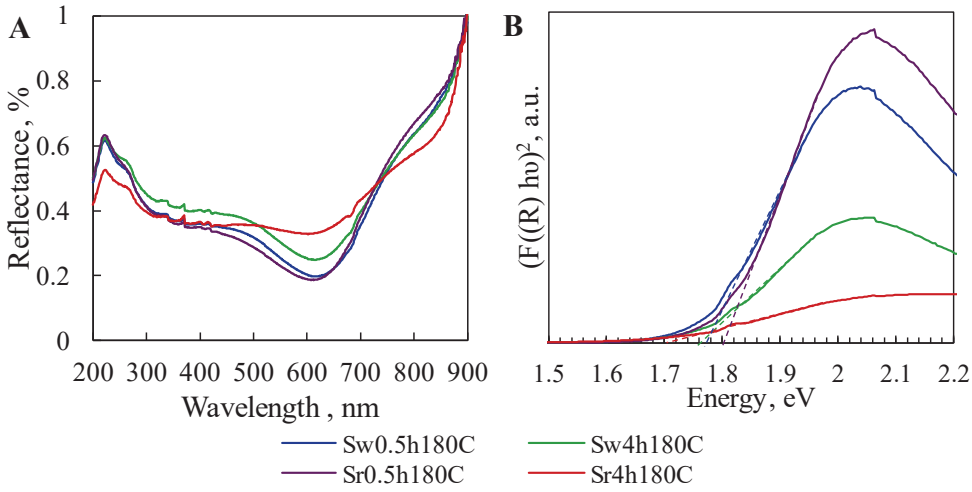

Fig. 3.14. DRS spectra of the synthesized samples (A). Curves of Kubelka–Munk function of the synthesized samples (B)

According to the obtained band gap, the wavelength of the electromagnetic wave which initiates the formation of free charge carriers was calculated (Equation 3.14, Table 3.13) [128].

$$\lambda = \frac{hc}{E_g} = \frac{1239.83}{E_g} \tag{3.14}$$

Where: λ – the wavelength of exciting irradiation, m;
H – Planck's constant;
C – speed of light, m/s.

In addition, the estimated wavelength to excite free charge carriers varied from 685 to 721 nm (Table 3.13). This indicated that the synthesized samples were able to generate free electrons-holes when stimulated by visible light irradiation. Therefore, the photocatalytic degradation performance of the CuS samples was assessed under visible light irradiation.

Table 3.13. Values of the band gap of the samples and the wavelength of charge carrier excitement

Sample	E_g value, eV	Wavelength of charge carrier excitement, nm
Sw0.5h180C	1.78	698
Sw4h180C	1.78	698
Sr0.5h180C	1.81	685
Sr4h180C	1.72	721

Despite the origin of the sulfurizing agent, the target photocatalytic compound – covellite – was already a dominant compound in the samples synthesized during 0.5 h of hydrothermal synthesis. By prolonging the synthesis from 0.5 to 4 h, no significant effect was made on the band gap value of the samples, since the aimed value of the latter parameter (which covers the absorption of the visible light wavelength) was already reached in the samples synthesized in 0.5 h. For the above mentioned reasons, while also considering the economic point of view, the photocatalytic properties of samples Sw4h180C and Sr4h180C were not tested. Therefore, the experiments were focused on two specific samples, Sw0.5h180C and Sr0.5h180C. In particular, the latter sample was investigated to validate the application of covellite of the waste origin.

Photodegradation of methylene blue by powder synthesized samples

The photocatalytic properties of Sw0.5h180C and Sr05h180C samples were further investigated by performing the degradation of organic molecules under visible light irradiation. For this reason, methylene blue was used as a model organic molecule to be degraded.

Figure 3.15 illustrates the dependence of the degradation efficiency and the irradiation time. Initially, there was a significant decrease in the characteristic absorbance peak of methylene blue at 664 nm within the first few minutes of the experiment (Fig. 3.15A).

The calculations of MB degradation efficiency revealed that, during the initial stage of irradiation, the DE value achieved by the waste origin sample was 7% higher compared to the one achieved by the reference sample (Fig. 3.15B). As the irradiation time increased up to 30 min, the waste sample degraded 73% of the dye, whereas the reference sample achieved 61% degradation of MB particles (Fig. 3.15B). By the end of the 180 min experiment, both samples exhibited a degradation efficiency of 96% (Fig. 3.15B).

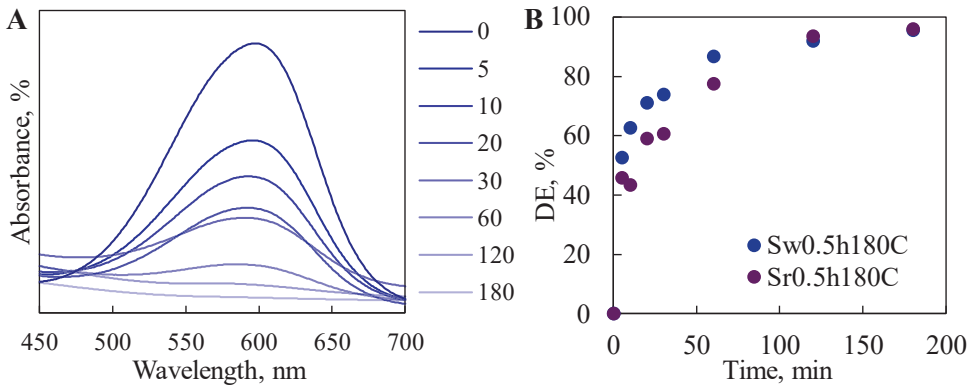

Fig. 3.15. Representative peak of methylene blue spectra during photodegradation for sample Sr0.5h180C (A). Dependence of photocatalytic degradation efficiency on time for samples Sw0.5h180C and Sr0.5h180C (B)

It is already known that methylene blue particles are able to decompose by themselves due to photolysis [129]. Furthermore, hydrogen peroxide by itself is able to produce the hydroxyl radical; therefore, it directly participates in the degradation of organic molecules. In order to eliminate the influence of extrinsic sources on the degradation efficiency and, consequently, in order to evaluate only the contribution of synthesized photocatalysts, comparison experiments were performed.

According to the obtained data, methylene blue did not degrade in the presence of H_2O_2 during the reaction in the dark, while, under visible light irradiation, DE was 45% after 180 min (Fig. 3.16).

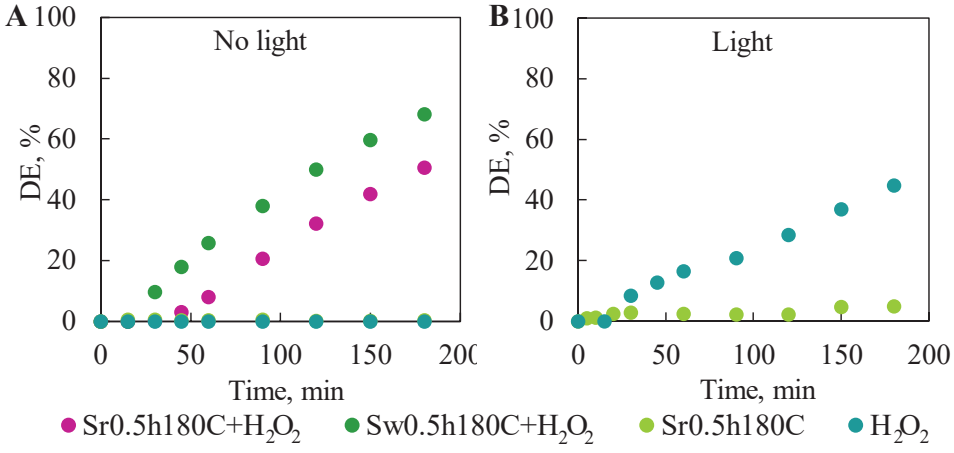

Fig. 3.16. Photocatalytic degradation efficiency of comparison tests without (A); and with visible light irradiation (B)

It is also worth noting that the degradation efficiency values are also obtained by samples Sw0.5h180C and Sr0.5h180C in the presence of hydrogen peroxide, while performing the experiment in the dark (Fig. 3.16A). Nevertheless, these values are

imitative since copper sulfide does not possess the catalytic properties to degrade organic molecules by itself, which suggests that the adsorption of the dye molecule on the photocatalyst's surface is responsible for the decrease of the UV-vis absorption peak intensity.

It is important to emphasise that the presence of H_2O_2 had a significant influence on the degradation efficiency values during the initial reaction. For instance, during the first 20 min of the reaction the DE values achieved by Sw0.5h180C and Sr0.5h180C were 71 and 59%, respectively (Fig. 3.16B). Meanwhile, the degradation of MB did not start by using the photocatalyst without hydrogen peroxide (Fig. 3.16B).

According to the literature, copper sulfide is a narrow band gap semiconductor in which the excited electrons in the conductive band immediately return to the valence [35,38]. This phenomenon is known as recombination, and it has been known to be characteristic for copper sulfides [38]. Nevertheless, one of the ways to reduce recombination is to employ H_2O_2 for photocatalytic reactions, since it has been known to be a better electron acceptor than pure CuS, consequently limiting the recombination of electrons and holes [38,130].

Furthermore, the initial reaction kinetics of MB photocatalytic degradation were also investigated. It was determined that photodegradation followed the pseudo-first-order model for both photocatalysts. During the first 20 min of the reaction, a first-order rate constant achieved by sample Sw0.5h180C was 0.0725 min^{-1}, while sample Sr0.5h180C had a rate constant of 0.052 min^{-1} (Fig. 3.17).

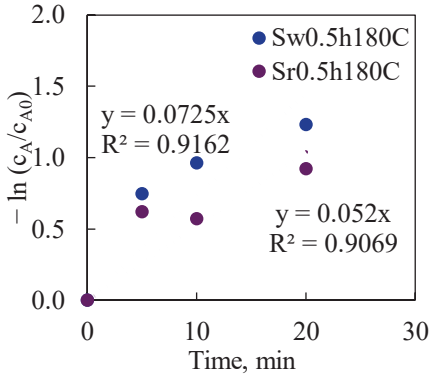

Fig. 3.17. Plot of first order kinetics during photocatalytic degradation

The lower reaction rate for the reference sample is a corresponding result with lower degradation efficiency values during the first half of the experiment, since the DE values were higher by 7–20% in the waste sample than in the reference sample (Fig. 3.15B). The latter results can be attributed to the variation of the crystallite size of the photocatalyst. According to the literature, a bigger crystallite size of the photocatalyst can result in a higher degradation rate [131,132]. In addition, sample Sw0.5h180C had a larger average crystallite size compared to Sr0.5h180C (39 nm and 35 nm, respectively), which led to a higher degradation efficiency value during the initial reaction and a higher reaction rate constant (Table 3.3).

It is noteworthy that the obtained reaction rate constants and degradation efficiency rates aligned and even exceeded the data reported in the literature. For example, the degradation of MB in the presence of H_2O_2 under visible light irradiation by CuS in flake or sheet nanostructures, or microflowers, possessed a lower reaction rate constant (e.g., 0.0226 min^{-1}, 0.0492 min^{-1}) [50,133,134].

In addition, it is worth emphasising that the valorisation of sulfur waste by using it as a sulfurizing agent resulted in the synthesis of particles with photocatalytic properties comparable to the ones of CuS obtained through the conventional sulfurizing agent. Specifically, the rate of dye degradation and the degradation efficiency after 180 min exhibited highly similar values in both tested samples.

Acknowledgements:

Reprinted/Adapted with permission from MDPI: *Materials* / Aqueous-Based Synthesis of Photocatalytic Copper Sulfide Using Sulfur Waste as Sulfurizing Agent/ G. Sarapajevaite, D. Morselli, K. Baltakys. 15(15):5253. 2022. https://doi.org/10.3390/ma15155253

3.6. Application of Synthesis Products for Degradation of Organic Molecules

The CuS samples obtained from industrial sulfur waste synthesized by 0.5 h hydrothermal synthesis at 180 °C temperature demonstrated promising photocatalytic properties. However, to employ photocatalyst in the bulk powder form for industrial degradation of organic molecules, several economic drawbacks need to be noted. For example, a further technological step to effectively separate the powder material from the flow of organic molecules is required, thus consequently increasing the costs of processing [89]. Therefore, a more industry-applicable approach is to incorporate the synthesized powder photocatalyst to an easily removable solid matrix. For this reason, the synthesized CuS samples were embedded into the polymeric matrix which served as the supporting material for the photocatalyst. The composites were formed in the film and porous architecture, and both samples Sw0.5h180C and Sr0.5h180C were investigated in terms of the degradation of organic material (Fig. 3.18).

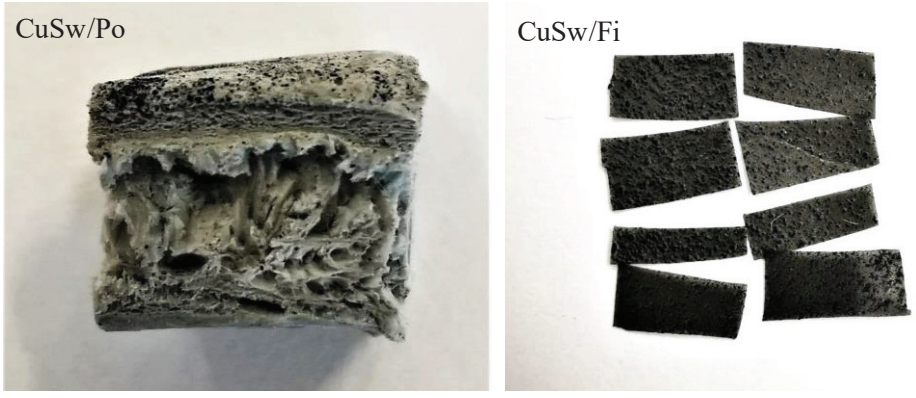

Fig. 3.18. Optical images of prepared composite samples

Investigation of the structure of composites

Firstly, XRD analysis was conducted on both neat and composite samples. It was noticed that the composite samples predominantly consisted of semi-amorphous PHBV and hexagonal covellite (CuS), which matched the reference pattern of powder (PDF 04-006-9635) (Fig. 3.19).

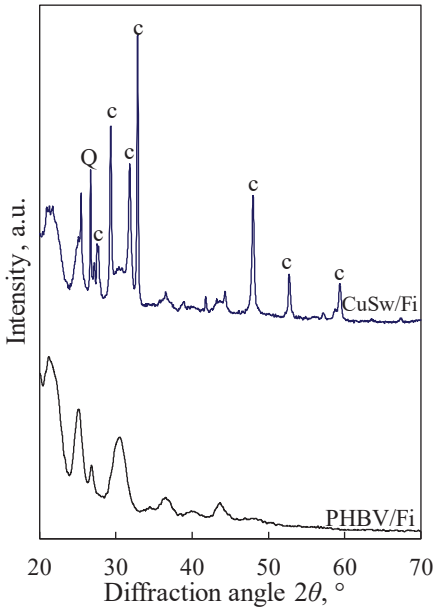

Fig. 3.19. XRD patterns of neat PHBV and CuSw/Fi composite sample. Indices: c– covellite; Q – quartz

These findings align perfectly with the composition of sample Sw0.5h180C in the powder form, which proves that samples Sw0.5h180C and Sr0.5h180C did not change their phase composition in the polymeric matrix, and that no new compounds were formed between PHBV and the photocatalyst.

Additionally, further analysis was performed by using a field emission scanning electron microscope (FE-SEM) to examine the dispersion and distribution of the incorporated photocatalyst as well as the formation of the desired porous structure. To enhance the visibility of inorganic particles within the surrounding polymeric matrix, the top-view FE-SEM images of both film and porous composites were captured with backscattered electrons (Fig. 3.20, Fig. 3.21). In both samples, the micrographs revealed a uniform distribution and effective dispersion for samples Sw0.5h180C and Sr0.5h180C (Fig. 3.20, Fig. 3.21).

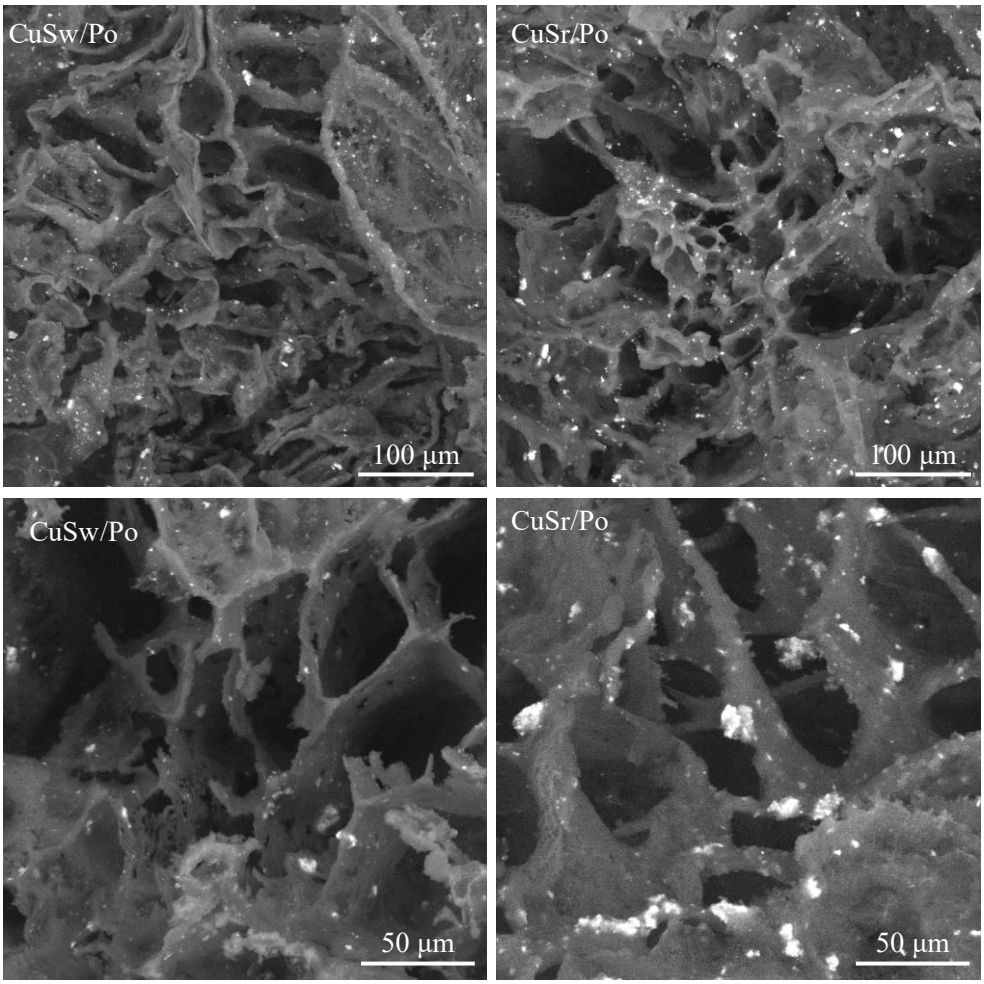

Fig. 3.20. FE-SEM top view images of porous composites with Sw0.5h180C and Sr0.5h180C fillers as photocatalyst

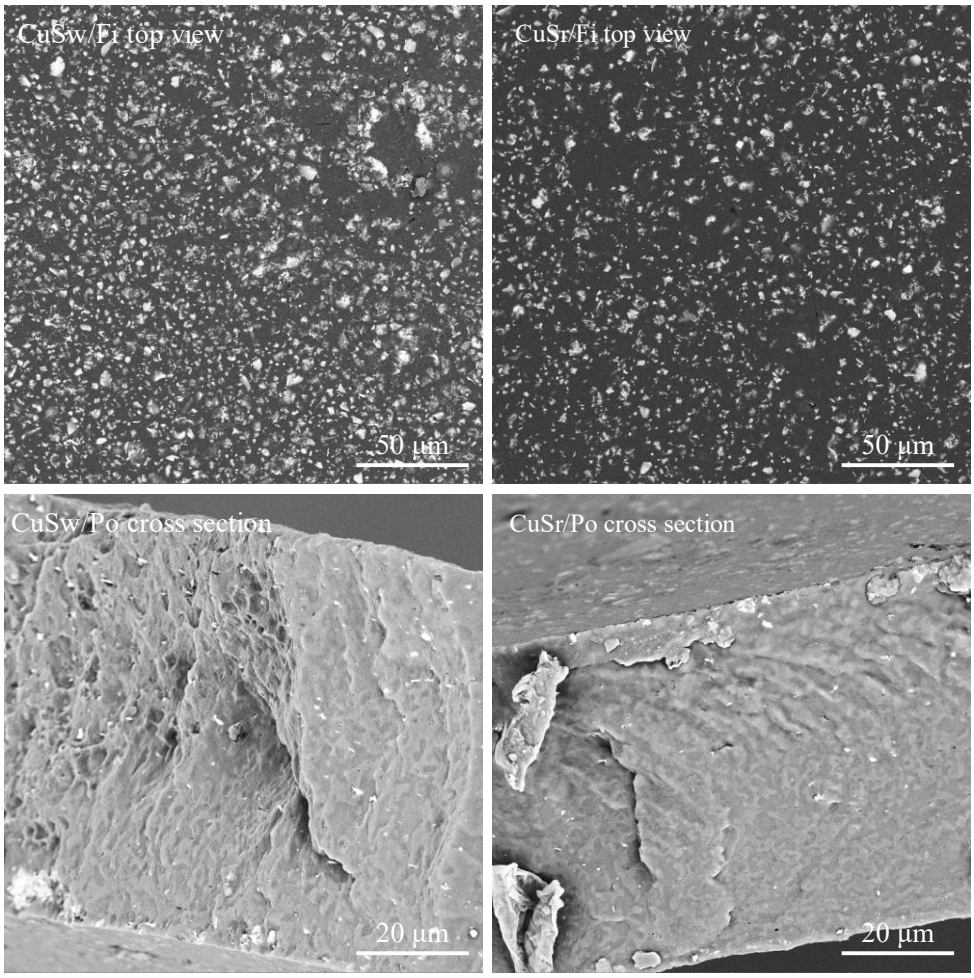

Fig. 3.21. FE-SEM top view images of film composites with Sw0.5h180C and Sr0.5h180C fillers as photocatalyst

Furthermore, it is known that PHBV is a hydrophobic polymer, possibly possessing a *Water Contact Angle* (WCA) of approximately 128° [135]. The high hydrophobicity of the samples could possibly limit the contact between the aqueous solution of organic molecules to the composite's surface, which leads to a slower degradation of organic pollutants. In order to enhance the contact between the organic molecule flow and the photocatalyst's surface, the WCA of the polymer needs to be reduced. For this reason, MFC, which contains hydroxyl groups in its structure and which has been previously found to decrease the hydrophobicity of other polymers, was introduced to the composition of composites [136].

The WCA measurements of neat samples proved that PHBV is a highly hydrophobic polymer possessing the WCA of 117° and 93° for porous and film matrices, respectively (Table 3.14, Fig. 3.22).

However, the incorporation of MFC to the composition of composites significantly improved the wettability of porous composites by reducing the water

contact angle by 11° (Table 3.14). Meanwhile, the wettability of the film samples was only marginally affected by MFC since WCA was reduced by only 4° compared to the neat sample (Table 3.14). It is worth noting that the standard deviation values of the WCA measurements were low, which indicates a homogeneous distribution of MFC and the effectiveness of the MFC dispersion method, as each WCA measurement is given as an average of five repetitions taken from different areas of the sample's surface.

Table 3.14. Water contact angle of neat PHBV and composites with and without MFC

Sample	WCA ± std. dev.		
	Neat polymer	**Without MFC**	**With MFC**
Porous	117.1±0.29	126.1±0.36	115.1±0.58
Film	93.3±0.44	94.8±0.8	91.1±0.56

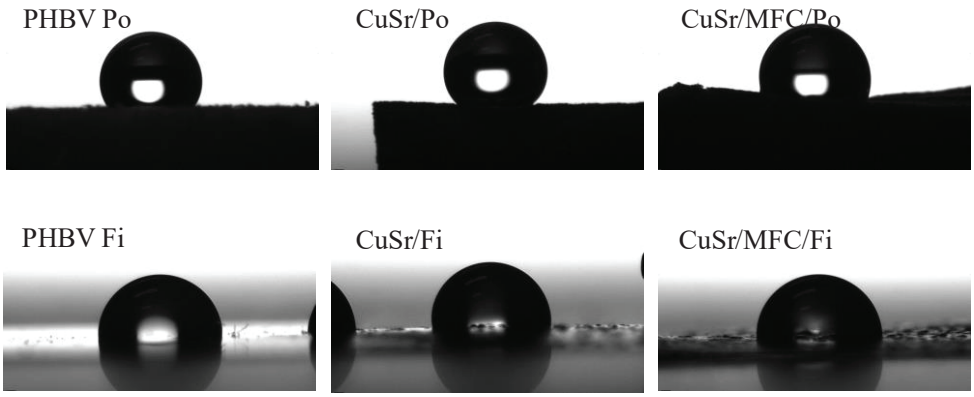

Fig. 3.22. Representative images of a water drop used for shape analysis under static conditions to determine the contact angle on different tested samples

The samples with MFC filler were also investigated by FE-SEM. It is worth noting that the presence of CuS particles is less evident in CuSw/MFC/Fi compared to CuSw/Fi (Fig. 3.21, Fig. 3.23). This was attributed to the overshadowing effect of MFC, which is primarily composed of carbon atoms, as well as the polymeric matrix. However, due to the significantly larger surface area of the porous structure compared to the films, this phenomenon was not observed in the porous samples (Fig. 3.24). Importantly, the FE-SEM images clearly demonstrated the successful achievement of highly interconnected porosity in porous composites with a homogeneous distribution of CuS (Fig. 3.24). It is also worth noting that the examination of film cross-sections by using FE-SEM revealed that CuS particles exhibited partial aggregation throughout the thickness of the film (Fig. 3.24).

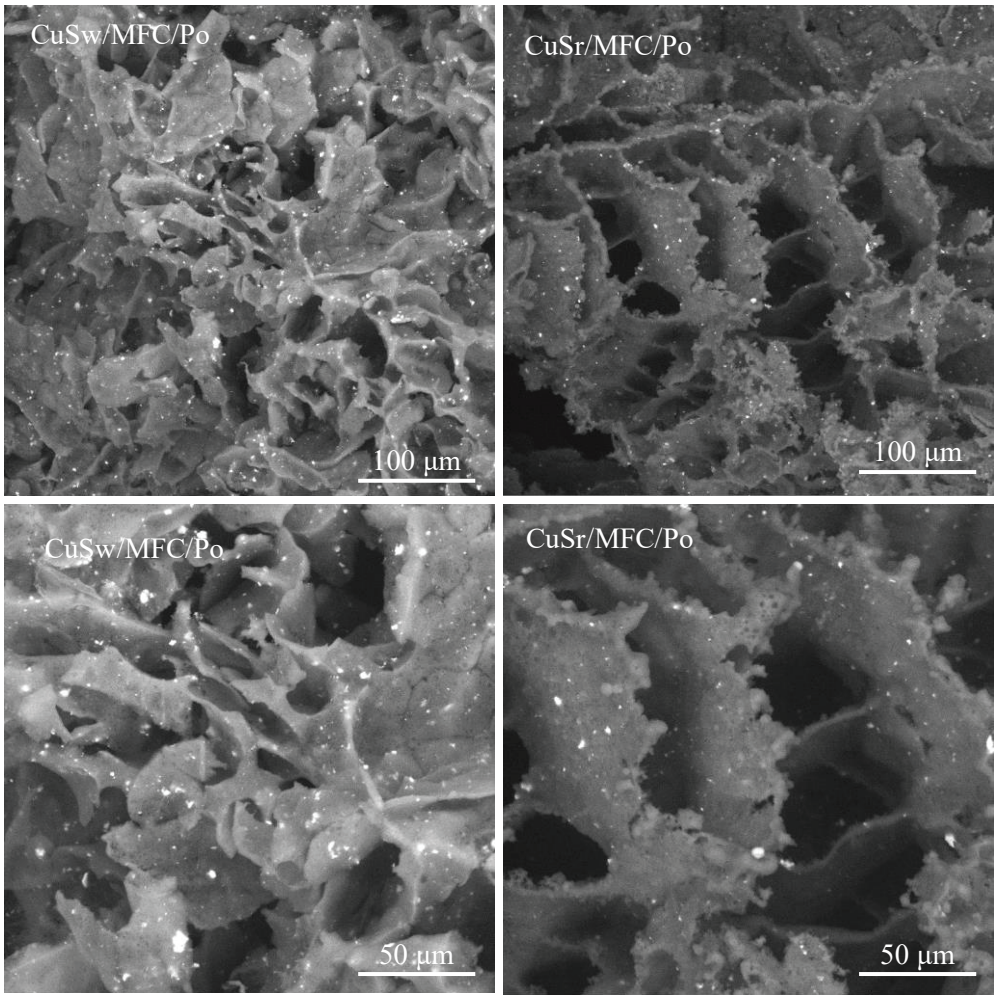

Fig. 3.23. FE-SEM top view images of film composites modified with MFC and Sw0.5h180C and Sr0.5h180C fillers

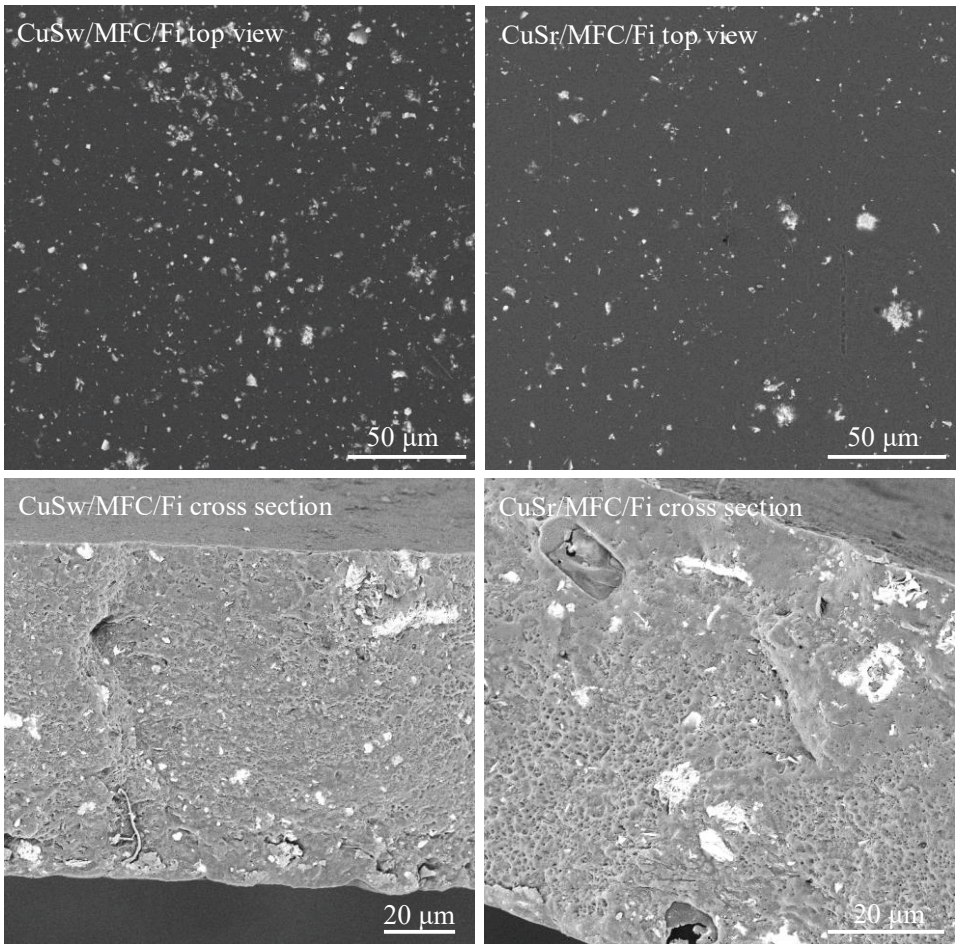

Fig. 3.24. FE-SEM top view images of porous composites modified with MFC and Sw0.5h180C and Sr0.5h180C fillers

Photodegradation of organic molecules by composites

To assess the photocatalytic properties of Sw0.5h180C and Sr0.5h180C samples within the composite assembly, tetracycline (TC) was chosen as a model organic molecule to be degraded under visible light.

Before irradiating the samples with visible light, the experiment was performed in dark in order to obtain the absorption-desorption equilibrium of organic molecules on the surface of the photocatalyst. During this period, there was a negligible decrease in the intensity of the UV-vis absorption peak (Fig. 3.25). According to the literature, typically, within the initial 10 min in the dark, pollutant absorption takes place [64,137].

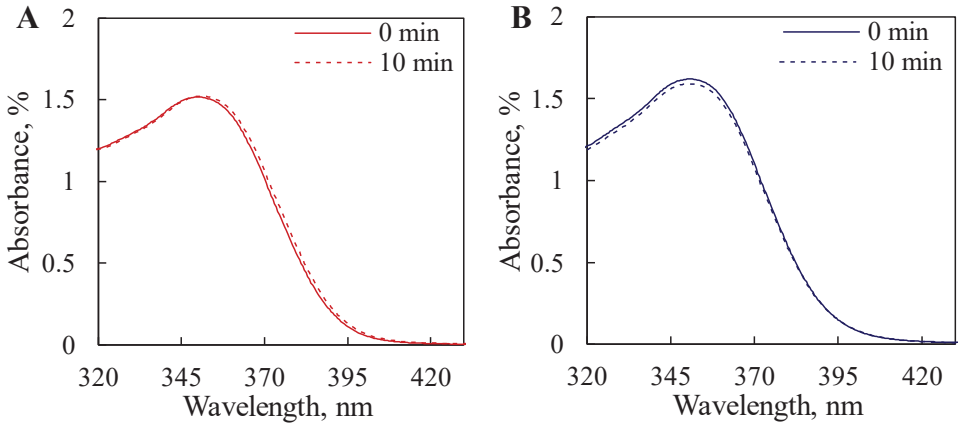

Fig. 3.25. Representative UV absorption peak at 351 nm characteristic of TC during the experiment in the dark by CuSw/MFC/Po (A) and CuSw/Fi samples (B)

In addition, after conducting the experiment in the dark, the irradiation was the following. Specifically, the degradation efficiency was determined by monitoring the decrease of the TC characteristic UV-vis absorbance peak at 351 nm (Fig. 3.26).

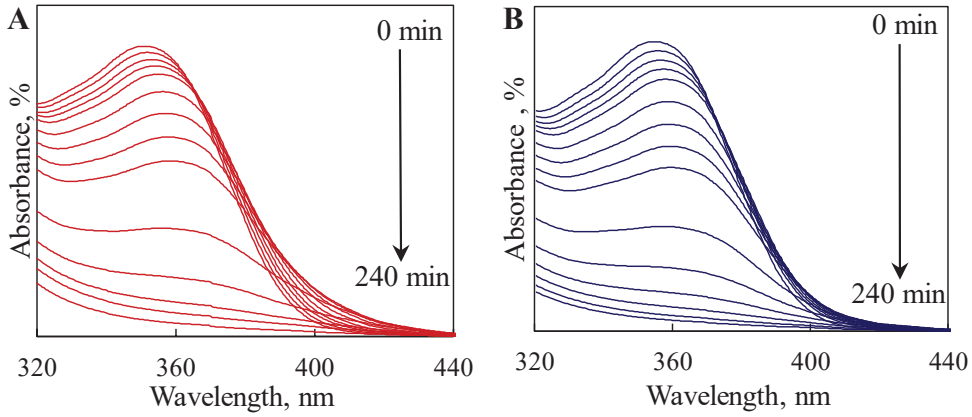

Fig. 3.26. Representative decrease of the UV absorption peak at 351 nm characteristic of TC during photodegradation experiments by CuSw/MFC/Po (A) and CuSw/Fi (B) samples

The kinetic curves of TC degradation under visible light using either porous or film composites as photocatalysts were investigated. According to the degradation efficiency data, it is evident that the majority of the tested samples achieved 100% degradation efficiency within 180 min of photooxidation regardless of the composite architecture (Fig. 3.27). Furthermore, no significant differences in the degradation efficiency were observed between the samples with the photocatalyst of Sw0.5h180C or Sr0.5h180C (Fig. 3.27). For example, after 120 min, CuSr/Po and CuSw/Po samples exhibited degradation rates of 56% and 60% for the pollutants, respectively (Fig. 3.27A).

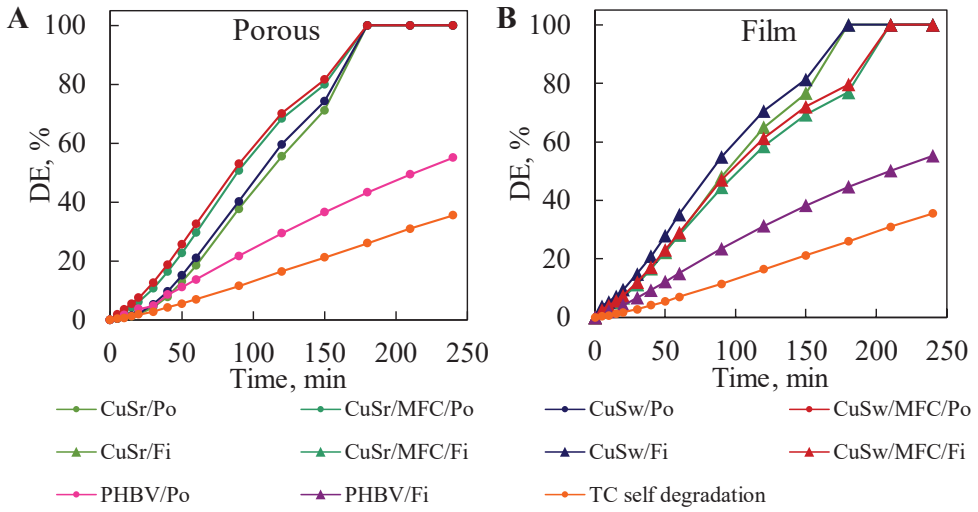

Fig. 3.27. Degradation efficiency as a function of time evaluated by degrading TC with (A) porous and (B) film composites

The initial reaction rate of photodegradation showed similarities between the waste and the reference origin samples with a porous architecture, since the reaction's rate constant was 0.0863 min^{-1} (Fig. 3.28A, Appendix 6). The latter value was slightly higher than the value achieved by the neat porous sample (0.0786 min^{-1}), which highlights the contribution achieved by the photocatalyst. However, in the film samples, the degradation rate was 1.4 times higher for CuS particles derived from waste (CuSw/Fi sample –0.5203 min^{-1}; CuSr/Fi – 0.3834 min^{-1}) (Fig. 3. 28B, Appendix 6). A slightly lower value of the reaction rate constant achieved by the reference sample compared to the waste one corresponds to the photocatalytic properties of bulk Sw0.5h180C and Sw0.5h180C samples, which is attributed to the influence of the crystallite size of the powder material, as mentioned before.

The inclusion of MFC in the porous composites demonstrated a positive effect on TC degradation, resulting in an enhancement of the degradation efficiency by up to 13% over the entire irradiation period (Fig. 3.27A). Notably, the initial reaction rate constants for CuSr/MFC/Po and CuSw/MFC/Po samples were found to be 3.3 and 4.2 times higher, respectively, compared to the samples without MFC (Fig. 3.28A). This confirms that the presence of MFC in the porous samples promotes a faster photocatalytic reaction. Due to the decreased WCA of the surface of the porous samples, the latter phenomenon is related to the enhanced wettability and permeability of the porous structure to the TC aqueous solution, which leads to a larger active surface area exposed to the solution.

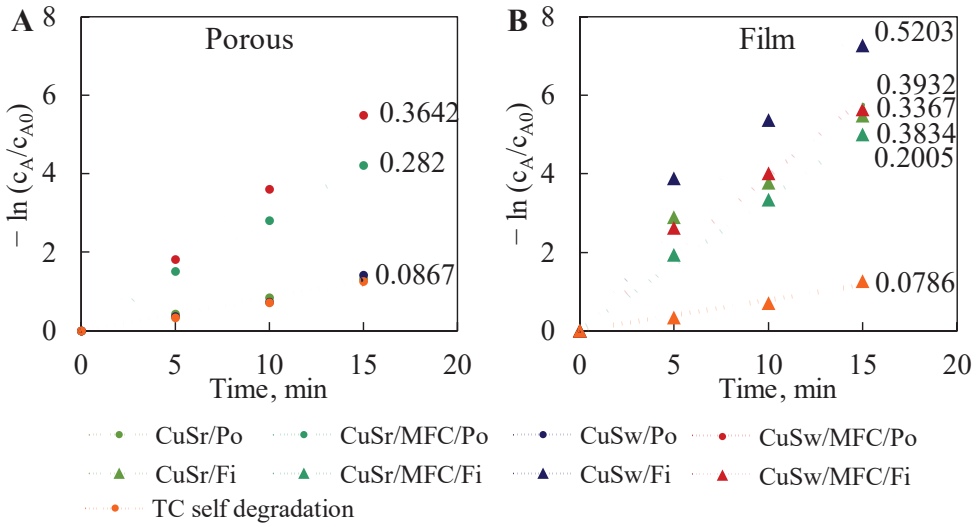

Fig. 3.28. Pseudo-first order kinetic curves of TC photocatalytic degradation by (A) porous and (B) film composite

On the contrary, the incorporation of MFC had a negative impact on the degradation efficiency of the film composites when both types of photocatalysts were used (Fig. 3.27B). Specifically, complete degradation of TC was achieved after 150 min of irradiation without MFC (CuSw/Fi and CuSr/Fi), while the addition of MFC to the film composites delayed complete degradation by 30 min (Fig. 3.27B). The reaction rate constants were also slightly lower (specifically, by 12% and 24%) for CuSr/MFC/Fi and CuSw/MFC/Fi, respectively (Fig. 3.28B). In the film samples, both types of fillers were distributed throughout a flat substrate, which offered a smaller free surface area compared to the porous composites. Consequently, the photocatalyst particles in the film samples were more likely to be partially shielded by MFC, which resulted in a lower concentration of the exposed particles on the surface, as revealed by FE-SEM investigations (Fig. 3.23). Additionally, MFC did not significantly reduce WCA in the film samples. The decrease in the number of electrons/holes involved in photodegradation together with the unaltered permeability of the film samples to the TC aqueous solution led to an overall reduction in the degradation efficiency.

The composite architecture also influenced the photodegradation rate. The degradation was significantly faster in the film samples compared to the porous samples, with an initial reaction rate constant of 0.083 min^{-1} for CuSw/Po and 0.5203 min^{-1} for CuSw/Fi, which is approximately six times higher (Fig. 3.28). However, the addition of MFC increased the degradation rate of porous composites, thereby bringing it to the values comparable to the values of film samples with the same composition. Specifically, the initial reaction rate constants achieved with CuSw/MFC/Fi and CuSw/MFC/Po were 0.3932 and 0.3642 min^{-1}, respectively (Fig. 3.28).

In addition, tests of TC photodegradation by composites with copper sulfide obtained from sulfur (sample Sw0.5h180C) revealed comparable results as the

composite with CuS synthesized from the reference sulfur (sample Sr0.5h180C). In addition, considering the importance of sustainability, only composites containing sample Sw0.5h180C were chosen for further investigation. Moreover, due to the highest values of the initial reaction rate and the degradation efficiency over the entire irradiation period, only samples CuSw/MFC/Po and CuSw/Fi were selected for further analysis.

Reusability of composites

The reusability of composites for the photodegradation of fresh pollutant batches is a crucial aspect to consider. The research findings demonstrated that both CuSw/MFC/Po and CuSw/Fi samples can be reused for at least five cycles, while achieving 100% degradation of TC after each cycle (Fig. 3.29).

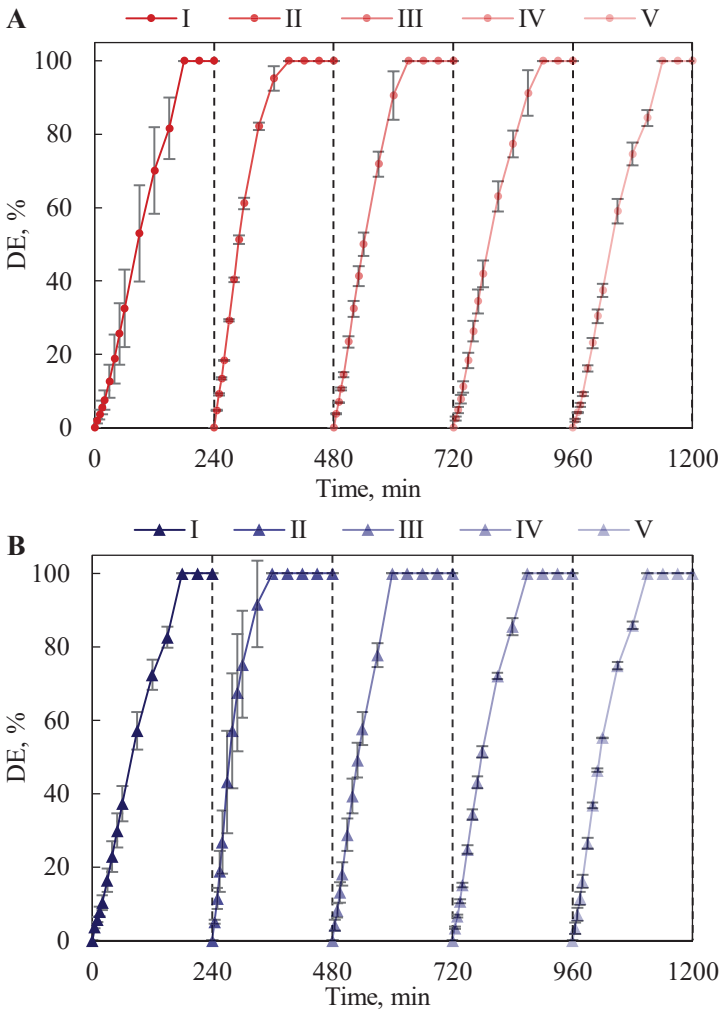

Fig. 3.29. Degradation efficiency obtained by degrading TC with CuSw/MFC/Po (A) and CuSw/Fi (B) composites by reusing each sample for five cycles

Furthermore, it has been noticed that the DE values obtained during the second cycle were higher compared to the ones achieved in the first cycle. Specifically, after 60 min of irradiation during the initial cycle, CuSw/MFC/Po and CuSw/Fi samples exhibit degradation efficiencies of 33% and 37%, respectively (Fig. 3.30). Meanwhile, during the second cycle, the degradation efficiency was doubled for both samples, by reaching values of 61% and 75% by CuS/MFC/Po and CuSw/Fi, respectively, after 60 min of irradiation (Fig. 3.30). Nonetheless, in the second cycle, both samples achieved 100% degradation of TC 30 min faster compared to the data of the first cycle (Fig. 3.30).

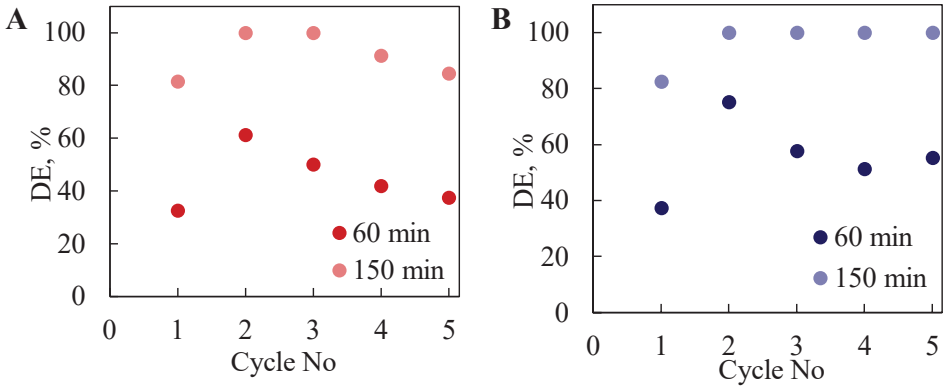

Fig. 3.30. Degradation efficiency as a function of the number of cycles for CuSw/MFC/Po (A) and CuSw/Fi (B) samples after 60 and 150 min of irradiation

Most importantly, a clear performance enhancement in the organic molecule photodegradation performance for both sample types has been demonstrated. Moreover, the faster initial reaction kinetics were also noticed during the second cycle since the initial reaction rate constant for CuSw/MFC/Po increased by 2.5 times, specifically, from 0.3642 min^{-1} to 0.9036 min^{-1} (Fig. 3.31). Similarly, the reaction rate constant for CuSw/Fi increased by 2.3 times, thus reaching a value of 1.2051 min^{-1} compared to the initial cycle value of 0.5203 min^{-1} (Fig. 3.31). Consequently, both tested samples exhibited improved degradation efficiency values as well.

This unexpected phenomenon indicated that, in the second cycle, photodegradation was initiated by harvesting the charge carriers which were already generated during the first cycle and subsequently became trapped in the subsurface of the semiconductor material [138].

Regardless the composite sample in use, the reaction rate constant gradually decreased after the second cycle and continued to increase further with an increase of the cycle number. This effect was attributed to the mild photocorrosion of the photocatalyst, since the latter process typically occurs in metal sulfides as observed in a number of previous studies [96,139,140]. In the course of photocorrosion, the generated charge carriers oxidise sulfur ions in CuS. In this process, the SO_4^{2-} anion is formed in the oxygen environment, or else elemental sulfur is formed under deficiency of O_2. In any case, it results in the depletion of the active sites on the photocatalyst's surface as well as in the reduction of photocatalytic activity [139].

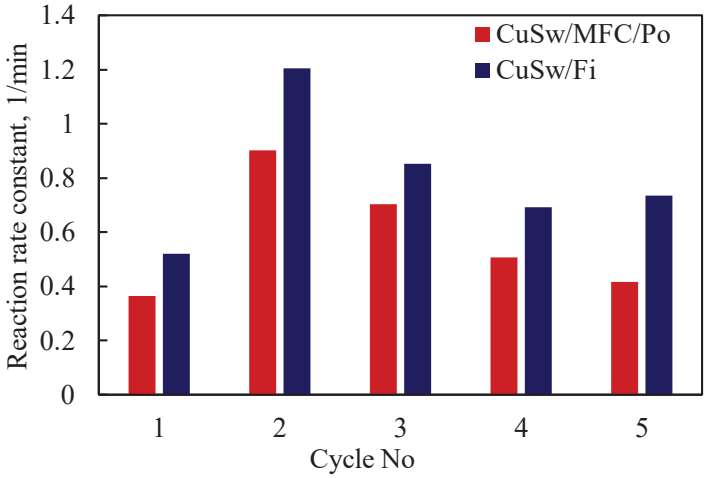

Fig. 3.31. Reaction rate constant as a function of the number of cycles for CuSw/MFC/Po and CuSw/Fi

However, it is noteworthy that the photodegradation process exhibited a slightly higher reaction rate during the last four cycles compared to the first cycle (Fig. 3.31). Additionally, the degradation efficiency of both composites decreased by 20% after 60 min of irradiation in the reusability experiments (Fig. 3.30). Nevertheless, these values remained higher than those observed in the first cycle, with an 18% and 5% increase for CuSw/Fi and CuSw/MFC/Po, respectively (Fig. 3.30). This observation suggests that the holes and electrons became trapped on the surface of the photocatalyst. As the trapped charge carriers can persist for extended periods, even months, the immediate generation of radicals is assumed to occur during the subsequent cycles of photodegradation [138]. Consequently, this phenomenon contributes to a higher degradation efficiency and a faster degradation rate when reusing composites compared to their initial application. Importantly, CuSw/Fi composite achieved 100% degradation of TC after 150 min of visible light irradiation, while maintaining this level of performance even after the fifth cycle of the composite usage (Fig. 3.30). It is worth mentioning that many studies employing free particles typically exhibit a rapid degradation rate, but experience a decline in efficiency as early as after the initial cycle [108,141–144].

Furthermore, the chemical stability of the photocatalyst which was used in this study was also confirmed through XRD analysis performed on the composite before and after five cycles. According to XRD, powder sample Sw0.5h180C incorporated in CuSw/Fi composite, which was chosen as a representative, maintained the identical chemical compound composition even after undergoing five cycles of TC photodegradation (Fig. 3.32). This indicates that the polymer exhibits a safeguarding influence on the CuS particles.

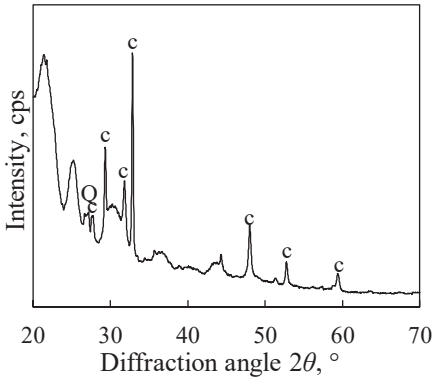

Fig. 3.32. XRD pattern of CuSw/Fi composite sample after 5 cycles. Indices: c– covellite; Q – quartz

Simultaneous degradation of multiple organic molecules by composites

Further investigation was conducted to assess the potential of the prepared composites to simultaneously degrade different organic molecules in the same solution. For this reason, CuS/MFC/Po and CuSw/Fi samples were tested for the photodegradation of MB (10 mg/L) and TC (100 mg/L) mixture under visible light. The results demonstrated that both CuSw/MFC/Po and CuSw/Fi composites were capable of simultaneously degrading both organic molecules by reaching 100% of degradation during 4 h of the reaction. Throughout the entire irradiation process, the porous samples exhibited a higher degradation efficiency for TC and MB compared to the films (Fig. 3.33A). Specifically, after 150 min of irradiation, CuSw/Fi composite degraded 78.5% of TC and 89.9% of MB, while the degradation efficiency achieved by CuSw/MFC/Po was higher by 5.7 and 6.3 percentage points, respectively (Fig. 3.33).

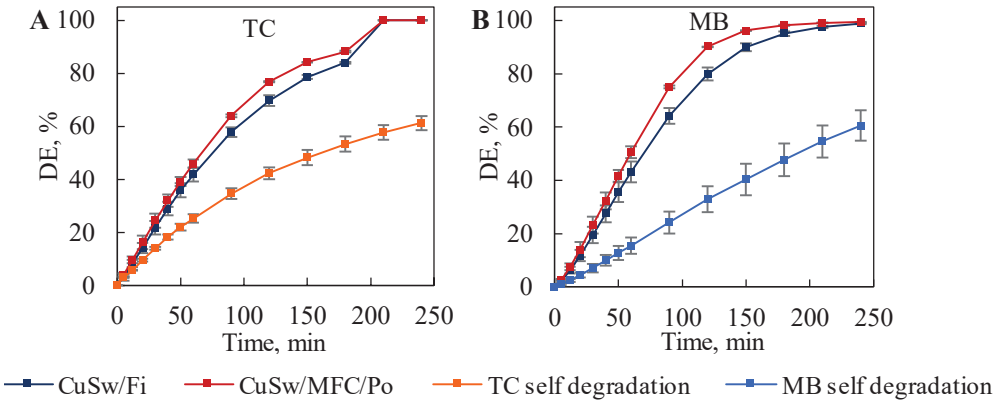

Fig. 3.33. Degradation efficiency obtained with CuSw/MFC/Po and CuSw/Fi composites by simultaneous degradation of tetracycline (A) and methylene blue (B)

Furthermore, the reaction rate constants achieved by CuSw/Fi sample were 0.6979 min^{-1} and 0.5635 min^{-1} for TC and MB, respectively (Fig. 3.34). It was also

observed that photodegradation was initiated more rapidly in the porous composite compared to the film sample, since the reaction rate constants for TC and MB were 0.8044 min^{-1} and 0.6744 min^{-1}, respectively, in the CuSw/MFC/Po sample (Fig. 3.34). Nonetheless, both types of samples achieved 100% photodegradation for both organic molecules within 210 min, which indicates the absence of any significant differences in this experiment (Fig. 3.34).

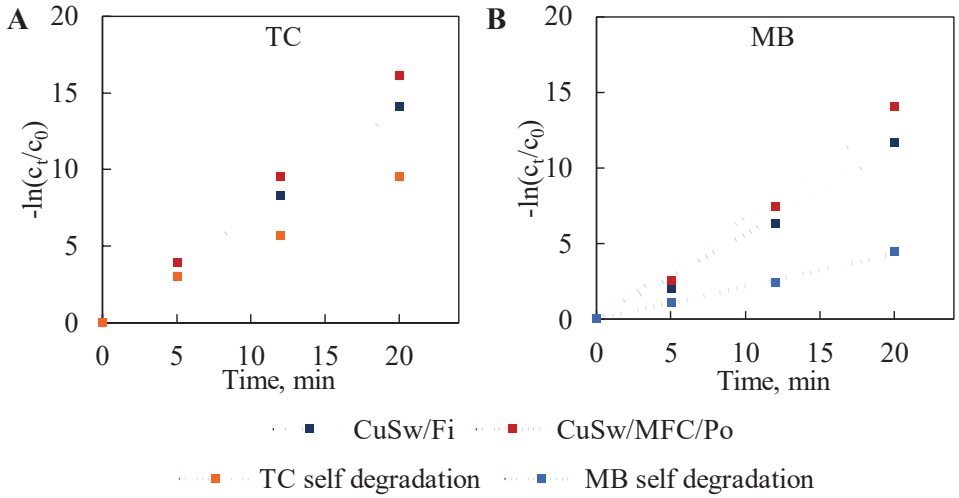

Fig. 3.34. Pseudo-first order kinetic curves of photocatalytic simultaneous degradation of tetracycline (A) and methylene blue (B) by CuSw/MFC/Po and CuSw/Fi

It is noteworthy that, for this particular experiment, the concentration of TC was doubled from 50 mg/L to 100 mg/L. Despite the increase of the TC concentration, both samples achieved complete degradation of the pollutant within 210 min. By increasing the TC concentration, the reaction rate constant for CuSw/Fi composite was also higher by 1.4 times, while the value for the CuSw/MFC/Po composite was doubled (Appendix 8). This confirms that composites are capable of effectively degrading even higher concentrations of TC.

In addition, waste-based copper sulfide samples were successfully incorporated into the biopolymer-based matrix for the purposes of large-scale organic molecule degradation under visible light. The results have revealed that waste-based CuS–PHBV composite samples are able to effectively degrade tetracycline up to 100% in 3 h; they can also be reused at least for 5 cycles. Furthermore, the results also provide proof for broad application of composites to degrade multiple pollutants of different origins simultaneously.

Acknowledgements:

Reprinted/Adapted with permission from *Wiley-VCH GmbH*: *Advanced Sustainable Systems* / Sustainable PHBV/CuS Composite Obtained from Waste Valorization for Wastewater Purification by Visible Light-Activated Photocatalytic

Activity/ G. Sarapajevaite, K. Baltakys, M. Degli Esposti, D. Morselli, P. Fabbri. 7(8): 2300112. 2023. https://doi.org/10.1002/adsu.202300112

3.7. Technological Recommendations

Simulation of processing conditions by Aspen HYSIS

According to the thermodynamic estimations for the formation of copper sulfides from sulfur and copper oxide in the water medium, the initial reaction is the generation of sulfurous gaseous compounds.

According to the proposed theoretical reaction mechanism based on thermodynamic calculations, to form the target product of synthesis – copper sulfide – the generation of sulfuric reactants SO_2 and H_2S took place in the initial reaction (Equation 3.1). Therefore, the production of the latter compounds is the key reaction which has the effect on the formation of the desired products.

In addition, the possibility to produce the SO_2 and H_2S compounds from elemental sulfur in the water environment was investigated by the *Aspen HYSIS* modelling program (Fig. 3.35).

It is worth noting that, during the hydrothermal treatment performed at a high temperature in a limited-volume system, typically, the equilibrium between water molecules in the gaseous and liquid phase is established. However, based on the proposed copper sulfide formation mechanism, part of gaseous water participated in the reaction with elemental sulfur to form H_2S and SO_2, which led to the reduction of the amount of water molecules in the system and altered the liquid-vapour equilibrium. To avoid the influence of the latter phenomenon on the reaction performance, the modelling was performed by assuming the state of water in the gaseous phase.

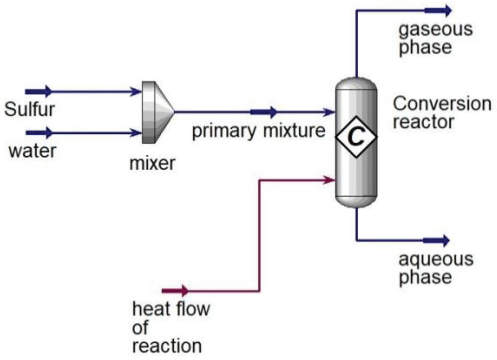

Fig. 3.35. Process scheme of the formation of sulfuric compounds

By simulating the processing conditions in the course of hydrothermal synthesis, the stream after treatment consisted only of the vapour phase (Table 3.15). According to performed simulation based on the used amounts of sulfur and water, H_2S and SO_2 were generated in the vapour phase by the amounts of 0.00133 and 0.00125 kg respectively, which contained 0.014 and 0.007 of the total molar fraction in the gaseous phase (Table 3.15).

It is important to note that elemental sulfur was no longer identified in any of the product streams, which shows the complete consumption of the component (Table 3.15). Since water was also employed not only as a reactant but also as the reaction medium, 0.979 of the gaseous stream molar fraction consisted of water (Table 3.15).

Table 3.15. Composition by molar fraction of the products stream

Component	Gaseous phase	Aqueous phase
H_2O	0.979	0
S	0	0
H_2S	0.014	0
SO_2	0.007	0

Furthermore, the amount of heat required to produce sulfuric gaseous compounds has been estimated. For this reason, a hypothetical model simulating the temperature in the products stream leaving the reactor (T_{out}) was created. The simulation was performed under the assumption that no additional external amount of heat was supplied to carry out the reaction. Typically, under no generation of heat during the reaction and isothermal conditions, the temperature of the outlet stream is supposed to be the same as in the inlet (Fig. 3.36). However, during the simulation, it was estimated that, following Reaction 3.1, the temperature in the outlet is lower by 35–38 °C, compared to the temperature of the supplied stream of water and sulfur (Fig. 3.36). These estimations indicate that the generation of sulfur dioxide and hydrogen sulfide from elemental sulfur and water proceeds as an endothermic reaction (Fig. 3.36).

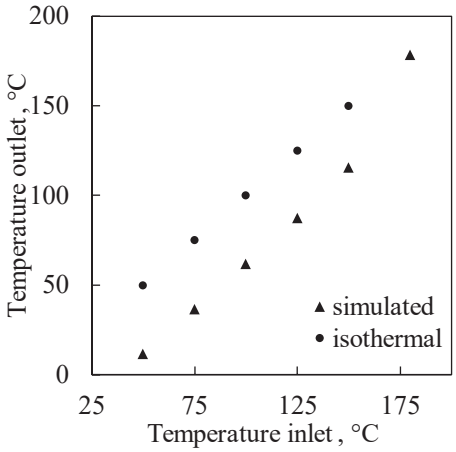

Fig. 3.36. Hypothetical estimations of temperature in the process outlet stream depending on the inlet temperature

To validate the theoretical *Aspen Hysis* simulation of the reaction mechanism, the temperature and the generated pressure were measured together with the heat flow supplied by an outer autoclave heater during hydrothermal treatment (Fig. 3.37B). According to the measured supplied amount of heat by the heater, 84.32 kJ of total heat was required to achieve a temperature of 180 °C in the autoclave, and for

isothermal maintenance, while treating sample Sw0.5h180C (Fig. 3.37). Meanwhile, for the empty experiment while processing only water, the required amount of heat was 77.00 kJ. In addition, to produce H_2S and SO_2 according to the reverse Claus reaction, the needed amount of heat was 7.31 kJ. The proposed endothermic reaction also goes in good agreement with the literature, since the direct Claus reaction has been known to be exothermic [121].

The pressure generated during temperature rise in the 'empty' experiment was 7.57 bar, while, within the reaction mixture, the achieved pressure was 7.23 bar. By the end of isothermal conditions at 180 °C, the pressure in the reactor with the empty experiment was 9.53 bar, while, with the reaction mixture, the pressure was 9.43 bar (Fig. 3.37A).

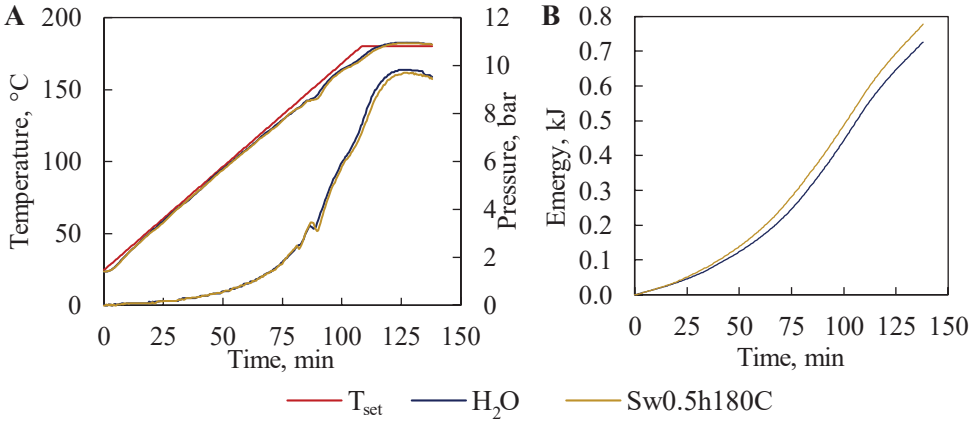

Fig. 3.37. Change of temperature and pressure in the reactor during hydrothermal treatment of primary mixture (A) and the total heat of the reaction (B)

In addition, simulation together with the experimental results validated the reaction of elemental sulfur and water to generate hydrogen sulfide and sulfur dioxide, consequently proving the mechanism of copper sulfide formation in water medium at a temperature of 180 °C.

4. CONCLUSIONS

1. It has been determined that the origin of the sulfurizing agent (conventional/secondary raw material) did not significantly affect the formation of CuS under hydrothermal conditions. CuS-based samples have been synthesized in aqueous solution from secondary raw material of sulfur and copper oxide at temperatures between 145–180 °C in 0.5–4 h of hydrothermal treatment. It has been determined that the secondary raw material origin CuS-based sample without the primary reactant compounds was produced at 180 °C during 0.5 h of synthesis.
2. Depending on the experimental conditions, the average crystallite size of synthetic CuS ranged from 27 to 40 nm, while the band gap varied from 1.72 to 1.81 eV. By increasing the temperature of the synthesis, the crystallite size of CuS increased by 6–8 nm on average in all of the samples, regardless the used type of sulfurizing agent. Meanwhile, the duration of isothermal treatment did not affect the size of CuS crystallites.
3. Synthetic CuS is thermally stable up to 300 °C. Samples of diverse phase composition ($Cu_{1.81}S$, Cu_2S, $CuSO_4$) were formed at temperatures higher than 450 °C. The increase of isothermal treatment duration from 0.5 to 4 h led to the extinction of the thermal effect at 245–385 °C, and a lower amount of heat was released.
4. Composites of biopolymer poly(3-hydroxybutyrate-co-3-hydroxyvalerate) and synthesized CuS samples were produced in porous (pore size <50 μm) and film (thickness 100 μm) structures by employing the thermally induced phase separation technique and film casting. The produced biocomposites were eligible to degrade organic molecules, for instance, tetracycline by up to 100% in 3 h of photocatalytic reaction. The highest values of the degradation efficiency and the fastest initial photodegradation kinetics were observed in the samples containing CuS obtained from secondary raw material of sulfur in the film architecture, as well as with a porous structure modified by microfibrillated cellulose. Moreover, the prepared composites were reused for at least five cycles, while consistently degrading tetracycline up to 100%.
5. It has been noted that the produced composites were eligible to effectively and concurrently degrade methylene blue and tetracycline and that they reached 100% of degradation efficiency for both molecules within 4 h of the photocatalytic reaction.

5. SANTRAUKA

5.1. Įvadas

Per pastarąjį dešimtmetį sukaupti stebėjimų duomenys, analizuojantys atliekų neutralizavimo tendencijas, rodo nerimą keliančią padėtį atliekų tvarkymo srityje. Tyrimai atskleidžia, kad įvairūs sieros turintys nevertingi junginiai ar medžiagos yra paplitę aplinkoje tiek kietu, tiek dujiniu pavidalu. Minėtų junginių buvimas aerobinėmis sąlygomis sukelia pavojingų medžiagų, neigiamai veikiančių aplinką ir žmogaus sveikatą, formavimąsi.

Be to, nuolat didėjantis žmonijos įprastinių ir inovatyvių patogumų poreikis didina naudojamų iškastinių žaliavų kiekį, kuris daro didesnį neigiamą antropogeninį poveikį aplinkai. Kadangi gamtos ištekliai yra riboti, o žmogaus veikla gali turėti neigiamų negrįžtamų padarinių aplinkai, būtina ieškoti sprendimų, kaip tvariai valdyti žaliavas. Žiedinės ekonomikos diegimas, ypač naudojant atliekas kaip antrinę žaliavą, yra vienas iš būdų mažinti gaminamų nevertingų produktų bei iškastinio kuro kiekius.

Didėjantis poreikis atrasti naujų efektyvių technologinių sprendimų daugelyje aplinkosaugos sričių lemia mokslininkų siekį tobulinti funkcinių junginių savybes. Taigi tyrimai, kuriuose nagrinėjami pramoninių atliekų neutralizavimo būdai išgaunant vertingus junginius, yra labai reikalingi.

Pereinamųjų metalų chalkogenidai, ypač vario sulfidai (Cu_xS_y), yra pigūs, stabilūs ir netoksiški junginiai, pasižymintys savybėmis, priklausančiomis nuo sintezės metu pasiekto dydžio ir formos. Cu_xS_y pasižymi tokiomis siekiamomis p-tipo puslaidininkių savybėmis, tokiomis kaip aukšta teorinė specifinė krūvio talpa, didelė laisvų krūvininkų koncentracija ir puikūs gebėjimai sugerti šviesą. Šios savybės lemia jų taikymą fotokatalizei, tvariai kaupiant energiją ar gaminant žaliąjį vandenilį. Cu_xS_y savybė pagaminti laisvuosius krūvininkus, sugeriant regimojo šviesos spektro spinduliuotę, yra išnaudojama taikant junginį pažangios oksidacijos procesui, kuriuo skaidomi organiniai dažai bei antibiotikai. Minėtos organinės molekulės yra visuotinai žinomos kaip nuotekų teršalai, kurių patekimas į vandens ciklą lemia pagreitėjusį žmonių antimikrobinį atsparumą ir toksišką poveikį augalams ir gyvūnams.

Nors mokslininkai pasiūlė daugybę Cu_xS_y sintezės būdų, dar nėra išvystytas pramoninės paskirties metodas, kuriuo gaminami išskirtinių funkcinių savybių junginiai. Be to, daugelio vertingų produktų sintezė naudoja iškastinio kuro prigimties reagentus, mokslininkams stokojant tvarumo bei vengiant Jungtinių Tautų tvaraus vystymosi tikslų įgyvendinimo. Taigi, aplinkosaugos požiūriu, antrinių žaliavų naudojimas utilizuojant atliekas yra pageidautinas technologinis būdas sintetinant aukštos vertės junginius, tokius kaip vario sulfidai. Pažymėtina, jog būtina patvirtinti antrinės žaliavos kilmės produktų funkcinių savybių patikimumą.

Potencialios Cu_xS_y taikymo sritys galimai apimtų aukštesnės nei kambario temperatūros sąlygas, pavyzdžiui, naudojimas fotovoltiniems ar elektroniniams įrenginiams pagaminti. Apdorojant bandinius termiškai, gali atsirasti kristalo gardelės komponentų pokyčių, smarkiai veikiančių nanodalelių dydį. Atsižvelgiant į pastarojo parametro svarbą, būtina tirti tiek terminį stabilumą, tiek rekristalizacijos fenomeną, nustatant vario sulfido elektrochemines ir optines savybes.

Darbo tikslas – sukurti tvarų vario sulfido (CuS) gamybos būdą panaudojant sieros rūgšties gamybos atlieką ir pagaminti CuS–PHBV biokompozitą, tinkantį organinėms molekulėms skaidyti.

Darbo uždaviniai:

1. Nustatyti sieros rūgšties gamybos atliekos sudėties ir hidroterminės sintezės parametrų įtaką CuS susidarymo procesams.
2. Ištirti geriausiomis savybėmis pasižyminčių sintetinių bandinių morfologines ir fotokatalitines savybes bei sintetinio CuS terminio skilimo ore mechanizmą.
3. Pagaminti skirtingos struktūros biokompozitus iš sintetinio CuS ir poli(3-hidroksibutirato-co-3-hidroksivalerato) bei nustatyti jų gebą skaidyti organines molekules.

Disertacijos ginamieji teiginiai

1. Įrodyta, kad sieros rūgšties gamybos atlieka yra tinkama CuS, pasižyminčio fotokatalitinėmis ir kitomis funkcinėmis savybėmis, tvariai sintezei.
2. Sintetinio CuS bandinių biokompozitai skaido tetracikliną iki 100 % per 3 val. regimosios šviesos spinduliuotės.

Mokslinio darbo naujumas

1. Termiškai stabilus (250–300 °C) CuS gaunamas hidroterminėmis sintezės sąlygomis S–CuO–H_2O sistemoje per 0,5–4 val. 145–180 °C temperatūroje bei pasižymi 27–40 nm kristalitų dydžiu ir 1,72–1,81 eV energetinės draustinės juostos pločiu.
2. Pirmą kartą nustatyta, kad pagamintas CuS–PHBV biokompozitas pakartotinai (ne mažiau nei 5 kartus) skaido tetracikliną ir metileno mėlį.

Praktinė vertė

Pasiūlytas tvarus CuS gamybos būdas iš sieros rūgšties gamybos atliekos ir vario oksido mišinio. Nustatyta, kad sintezės produktai pasižymi pastovia chemine sudėtimi ir terminiu stabilumu iki 300 °C. Sintetinis CuS panaudotas skirtingos struktūros CuS–PHBV biokompozito gamyboje. Ištirta, jog minėtas gaminys gali būti taikomas organiniams teršalams ir jų mišiniams nuotekose skaidyti: ciklišKai skaido tiek pavienius, tiek organinių junginių (tetraciklino – metileno mėlio) mišinius.

Darbo aprobavimas ir publikavimas

Doktorantūros studijų metu disertacijos tematika buvo paskelbtos 4 mokslinės publikacijos *Clarative Analytics Web of Science* duomenų bazėje: *Waste and Biomass Valorization, Journal of Thermal Analysis and Calorimetry, Materials and Advanced Sustainable Systems.* Taip pat rezultatai pristatyti 6 tarptautinėse konferencijose.

Autorės ir bendraautorių mokslinis indėlis

Gabrielė Šarapajevaitė atliko vario sulfido sintezę iš sieros rūgšties gamybos atliekos, nustatė susintetintų mėginių morfologines ir fotokatalizines savybes bei ištyrė CuS terminį stabilumą. Minėti tyrimo žingsniai atlikti KTU vadovaujant prof.

dr. Kęstučiui Baltakiui, kuris konsultavo eksperimentinės eigos klausimais ir recenzavo mokslinių publikacijų rankraščius.

Taip pat autorė gamino kompozitus, atliko fotoskaidymo tyrimus bei eksperimentinių duomenų apdorojimą. Kompozitų gamyba ir jų fotokatalitinių savybių tyrimas buvo atliktas Bolonijos universitete, vadovaujant prof. Paulai Fabbri. Dr. Micaela Degli Esposti konsultavo kompozitų gamybos ypatumų klausimais bei redagavo mokslinių publikacijų rankraščius. Dr. Davide'as Morselli konsultavo kompozitų ruošimo, mėginių apibūdinimo ir fotokatalitinių savybių nustatymo temomis bei recenzavo mokslinių publikacijų rankraščius.

Darbo apimtis

Disertaciją sudaro įvadas, literatūros apžvalga, doktorantūros studijų metu naudotos medžiagos ir taikyti instrumentinės analizės metodai, pasiekti rezultatai ir išvados. Taip pat pateikiamas 144 bibliografinių šaltinių literatūros sąrašas. Rezultatai aptariami 134 puslapiuose, įskaitant 20 lentelių, 38 paveikslus ir 8 priedus.

5.2. Medžiagos ir metodai

5.2.1. Medžiagos

Sieros atlieka

Pramoninė sieros atlieka, kuri buvo naudojama kaip sieros antrinė žaliava, yra šaltinis produktas, susidarantis sieros rūgšties gamybos metu cheminių junginių gamykloje „Lifosa“ (Kėdainiai, Lietuva). Atlieka susiformuoja elementinės sieros (grynumas 99,98 %) lydymo metu. Žaliavoje esančios priemaišos yra atskiriamos iš lydalo filtruojant, toliau yra surenkamos ir išdžiovinamos.

Kitos naudotos medžiagos

- Etaloninė elementinė siera, (99,99 %, AB „Lifosa“, Lietuva);
- Vario oksidas (CuO, 99 %, „Reachem“, Slovakija);
- Poli(3-hydroksibutirat-*co*-3-hidroksivaleratas) (PHBV), (M_n 209,300 g/mol, M_w 586,000 g/mol, 20 mol % 3HV vienetų) buvo pirktas iš „Merck“ grupės. Prieš atliekant eksperimentus, PHBV buvo išgrynintas tirpinant biopolimerą chloroforme, filtruojant pro ceolitinį filtrą ir nusodinant kietą medžiagą šaltame metanolyje.
- Sausa mikrofibrilinė celiuliozė (MFC) pagaminta pagal [108].

Chloroformas ($CHCl_3$, an. gr.), 1,4-dioksanas (DIOX, ≥99,0 %), etilo alkoholis (EtOH, ≥99,8%), vandenilio peroksidas (H_2O_2, 30 %), metileno mėlis (MB, $C_{16}H_{18}ClN_3S \cdot 3H_2O$) ir tetraciklino hidrochloridas (TC, $C_{22}H_{24}N_2O_8 \cdot HCl$, an. gr.) buvo pirkti iš „Merck“ grupės, JAV.

5.2.2. Metodai

Pradinio mišinio paruošimas

Pramoninė sieros atlieka (sieros antrinė žaliava), gauta iš gamyklos lydinio gabalų pavidalu, 70 min. buvo smulkinta rutuliniame malūne, kurio talpa 6,6 l,

pripildytame 21 % rutulinės formos žaliavos, kurios vidutinis skersmuo 42 mm. Po to 30 g miltelių buvo malami 150 ml planetariniame malūne (Pulverisette 9, „Fritsch“, Italija) 600 aps./min greičiu 2 min.

Pradinis sintezės mišinys buvo paruoštas sumaišius antrinę sieros žaliavą su vario oksidu, kai S ir CuO molinis santykis buvo lygus 1,5:1. Pirmiausia abi medžiagos 1 h homogenizuotos homogenizatoriuje (Turbula Type T2F, „Willy A Bachofen“ AG, Šveicarija) 34 aps./min greičiu. Po to 10 g mišinio buvo malama 50 ml planetiniame malūne „Pulverisette 9" 1 min 600 aps./min greičiu.

Siekiant pripažinti antrinės žaliavos kilmės bandinių savybių tinkamumą, kita pirminio mišinio partija buvo paruošta tomis pačiomis eksperimentinėmis sąlygomis, tačiau kaip sieros žaliavą naudojant etaloninę elementinę sierą.

Hidroterminė sintezė

Hidroterminė sintezė buvo atlikta 150 ml nerūdijančio plieno autoklave (Series 4560, „Parr instruments“, JAV). Sintezė buvo vykdyta maišant 5 g pirminio mišinio su 50 ml vandens suspensijos (50 aps./min). Eksperimentai buvo atlikti 145–180 °C temperatūroje išlaikant izotermines sąlygas 0,5–4 h (5.1 lentelė). Temperatūra buvo pasiekta 100 °C per valandą greičiu. Po izoterminio išlaikymo reakcijos indas buvo natūraliai atvėsintas iki kambario temperatūros. Tuomet gauta mėginio suspensija buvo nufiltruota, o juodos nuosėdos buvo išdžiovintos oro atmosferoje 104 °C temperatūroje 12 valandų. Tada išdžiovinta kieta medžiaga buvo sutrinta, persijota per 100 μm sietą ir išanalizuota atliekant instrumentinę analizę.

5.1 lentelė. Sintezės eksperimentinės sąlygos

Sieros žaliava	Trukmė, h	Temperatūra, °C	Trumpinys
Sieros atlieka	0,5	145	Sw0.5h145C
		180	Sw0.5h180C
	4		Sw4h180C
Sieros etalonas	0,5	145	Sr0.5h145C
		180	Sr0.5h180C
	4		Sr4h180C

Terminio stabilumo tyrimas

Sintetinių bandinių terminio stabilumo tyrimas atliktas naudojant vamzdinę krosnį (RT 50/250/11, „Nabertherm“, Vokietija). Kiekvienas sintetinis bandinys, sveriantis 0,5 g, buvo termiškai apdorotas 250, 300, 400, 450 ir 500 °C temperatūroje oro aplinkoje. Temperatūra buvo didinama 10 °C/min greičiu. Pasiekus reikiamą temperatūrą, mėginys buvo nedelsiant išimtas iš krosnies ir atvėsintas eksikatoriuje. Po to degti produktai buvo analizuoti taikant DSK (diferencinės skenavimo kalorimetrijos) ir RSDA (rentgeno spindulių difrakcinės analizės) metodus. Tiksliau, kiekviename degtame bandinyje buvo nustatytas tikslinio sintezės produkto – CuS (kovelito) (PDF 04-006-9635) – kristalitų dydžio pokytis.

Sintetinių bandinių fotokatalitinės savybės

Sintetinių miltelių pavidalo bandinių fotokatalitinės savybės buvo nustatytos skaidant metileno mėlį (MB) apšviečiant regimosios šviesos spektru. Šio eksperimento metu buvo tirti tik Sw0.5h180C ir Sr0.5h180C bandiniai. 15 mg susintetinto fotokatalizatoriaus buvo sumaišyta su 100 ml vandeninio MB tirpalo (20 mg/l) ir 4 ml H_2O_2. Prieš apšviečiant mišinys buvo magnetiškai maišomas tamsoje 10 min kambario temperatūroje, kad būtų pasiekta adsorbcijos ir desorbcijos pusiausvyra. Po to suspensija buvo apšviesta regimosios šviesos spektru (23 W LED lempa). Reakcijos metu nustatytais intervalais buvo paimtas 5 ml eksperimentinės suspensijos kiekis ir 5 min centrifuguota, kad būtų atskirtos fotokatalizatoriaus dalelės nuo eksperimentinio mišinio. Toliau matuotas gauto MB tirpalo UV-Vis (ultravioletinės ir regimosios spinduliuotės) spektras naudojant UV-vis spektrofotometrą (PerkinElmer Lambda 25, JAV). Siekiant nustatyti MB koncentraciją, buvo išmatuotas MB būdingos absorbcijos smailės, kurios centras yra 664 nm, intensyvumas. Skaidymo efektyvumas (DE) buvo apskaičiuotas taip:

$$DE = \left(1 - \frac{A_t}{A_0}\right) \cdot 100\%, \tag{5.1}$$

čia A_t – MB absorbcijos smailės intensyvumo vertė tam tikru laiko momentu;
A_0 – MB absorbcijos smailės intensyvumo vertė prieš pradedant eksperimentą.

Bandinio apšvietimas regimuoju šviesos spektru truko 180 min. Palyginimui buvo atlikti papildomi bandymai be šviesos, tiek su, tiek be fotokatalizatorių, taip pat su ir be vandenilio peroksido. Skaidymo greitis buvo apskaičiuotas pagal pseudopirmojolaipsnio kinetikos modelį (5.2). Reakcijos greičio konstanta nustatyta analizuojant pirminį fotoskaidymo etapą, taikant reakcijos kinetinių kreivių tiesinę dalį per pirmąsias 15 eksperimento minučių.

$$ln\left(\frac{c_t}{c_0}\right) = -kt, \tag{5.2}$$

čia c_t – MB koncentracija tam tikru laiko momentu, mg/l;
c_0 – pradinė MB koncentracija prieš pradedant apšvietimą, mg/l;
k – reakcijos greičio konstanta, min^{-1};
t – laikas, min.

Kompozitų paruošimas

Kompozitai buvo formuojami porėta ir plėvelės struktūra. Kompozitams formuoti buvo naudojami tik Sw0.5h180C ir Sr0.5h180C bandiniai. Dėl teksto aiškumo, kompozitų formavimo tyrimo etape Sw0.5h180C ir Sr0.5h180C bandiniai toliau vadinami atitinkamai CuSw ir CuSr.

Porėta struktūra buvo pagaminta disperguojant 15 % masės Sw0.5h180C/Sw0.5h180C bandinio PHBV polimeriniame tirpale (1,08 g polimero ištirpinto 30 ml dioksane). Siekiant užtikrinti kruopštų sumaišymą, dispersija buvo maišoma ir 3 h 95 °C temperatūroje naudojant panardinamąjį ultragarsinį maišymą. Dispergavus fotokatalizatorių polimeriniame mišinyje, porėta kompozito struktūra

buvo pasiekta naudojant termiškai indukuoto fazių atskyrimo (angl. *thermally induced phase separation*, TIPS) metodą.

Siekiant padidinti mėginių hidrofiliškumą taip pagerinant kompozito drėkinamumą, prieš ultragarsinį maišymą į dispersiją buvo pridėta 5 % masės MFC.

Kompozitinės plėvelės buvo paruoštos liejimo būdu, naudojant tą pačią mišinio sudėtį, kaip ir paruošiant porėtus bandinius, tačiau kaip tirpiklį naudojant chloroformą. Tiksliau, vario sulfido bandiniai ir MFC buvo disperguojami kartu 3 h naudojant panardinamąjį ultragarsinį maišymą 50 °C temperatūroje. Tada gautas mišinys buvo išlietas į 11 cm skersmens Petri lėkštelėje ir paliktas per naktį džiūti kambario temperatūroje. Paruoštų bandinių sudėtys yra pateiktos 5.2 lentelėje.

5.2 lentelė. CuS–PHBV kompozitų sudėtys

Bandinio struktūra	Sieros kilmė gaminant fotokatalizatorių	Hidrofiliškumo stipriklis	Trumpinys
Porėta	etalonas	–	CuSr/Po
	atlieka	–	CuSw/Po
	etalonas	MFC	CuSr/MFC/Po
	atlieka	MFC	CuSw/MFC/Po
	–	–	PHBV/Po
Plėvelė	etalonas	–	CuSr/Fi
	atlieka	–	CuSw/Fi
	etalonas	MFC	CuSr/MFC/Fi
	atlieka	MFC	CuSw/MFC/Fi
	–	–	PHBV/Fi

Organinių molekulių fotoskaidymo CuS–PHBV kompozitais tyrimas

Siekiant nustatyti paruoštų bandinių fotoskaidymo savybes, buvo tirti porėtos ir plėvelės struktūros kompozitai. Atliekant šiuos eksperimentus tetraciklinas (TC) buvo pasirinktas kaip skaidoma organinė molekulė. Eksperimentai buvo atlikti 4 ml kvarco kiuvetėje maišant tirpalą, apšviečiant regimuoju šviesos spektru ($\lambda > 420$ nm, Philips PL-S, 900 lm). 3 ml TC tirpalo (50 mg/l) buvo sumaišyti su 60 μm H_2O_2. Porėtas kompozitinis mėginys, paruoštas 1x1x1 cm kubo forma, buvo panardintas į eksperimentinį tirpalą. O plėvelės struktūros kompozito bandinys (1 cm^2 ploto) supjaustytas į 8 vienodas dalis ir panardintas į TC tirpalą. Siekiant nustatyti adsorbcijos ir desorbcijos pusiausvyrą, prieš pradedant reakciją bandiniai 10 min buvo laikomi tamsoje. Po to eksperimentinis tirpalas buvo apšviestas regimosios šviesos spektru. Organinių junginių koncentracija buvo nustatyta tam tikrais laiko intervalais matuojant UV-Vis absorbcijos smailę ties 351 nm bangos ilgiu, kuri būdinga TC. Šiems matavimams naudotas UV-Vis spektrofotometras (V-650, „Jasco“, Japonija). Skaidymo efektyvumas buvo nustatytas ir reakcijos greičio konstanta apskaičiuota pagal pseudopirmojo laipsnio kinetikos modelį, analizuojant tiesinę kinetinės kreivės dalį per eksperimento pirmąsias 15 min (5.1–5.2).

Siekiant ištirti kompozitų pakartotinį naudojimą, buvo taikyti tik CuSw/MFC/Po ir CuSw/Fi bandiniai. Po pradinio fotoskaidymo eksperimento kompozitai buvo išdžiovinti oru kambario temperatūroje ir pakartotinai naudojami dar keturis kartus kartojant eksperimentą.

Be to, buvo įvertinti paruoštų kompozitų gebėjimai skaidyti kelias organines molekules vienu metu. Dėl to buvo paruoštas 100 mg/l TC ir 10 mg/l MB mišinys. Fotoskaidymo eksperimentai buvo atlikti tomis pačiomis sąlygomis, kaip aprašyta anksčiau.

Rentgeno spinduliuotės difrakcinė analizė

Mėginių fazinei sudėčiai nustatyti buvo naudojama rentgeno spindulių difrakcijos analizė (RSDA). Po hidroterminės sintezės gauti miltelių bandiniai buvo ištirti D8 Advance difraktometru („Bruker AXS“, Karlsrūhė, Vokietija) su CuKα rentgeno vamzdeliu, veikiančiu 40 kV ir 45 mA. Junginių kristalitų dydis ir difrakcijos smailių intensyvumas apskaičiuotas naudota RSDA programine įranga „Diffract. Eva“.

Terminė analizė

Diferencijuojama skenuojamoji kalorimetrija (DSK) buvo naudota matuojant susintetintų bandinių išskirtą šilumos kiekį kovelito terminio stabilumo tyrimų metu. Analizės metu naudotas terminis analizatorius (DSC 214 Polyma, „Netzsch“, Vokietija), kurio parametrai: temperatūros kėlimo greitis 10 °C/min, tiriamas temperatūros diapazonas 25–600 °C, etalonas – tuščias aliuminio tiglis. Atmosfera krosnyje – azotas, kurio srauto debitas 20 ml/min. Eksperimentai buvo atlikti uždaruose tigliuose su E tipo termopora.

UV-regimosios šviesos difuzinio atspindžio spektroskopija

Sintetinės kietos medžiagos optinės savybės buvo įvertintos atliekant UV-regimosios šviesos difuzinio atspindžio spektroskopiją (DRS), naudojant Jasco V-650 UV-vis-NIR spektrofotometrą. Matavimai buvo atlikti kintant bangos ilgiui nuo 200 iki 900 nm. Prieš atliekant matavimus, spektrofotometras buvo sukalibruotas naudojant $BaSO_4$ etaloną. Sintezės produktų energetinės draustinės juostos plotis buvo įvertintas taikant Kubelkos ir Munko teorijos lygtį (5.3–5.4)

$$R = \frac{R_{bandinys}}{R_{etalonas}}, \tag{5.3}$$

$$F(R) = \frac{(1-R)^2}{2R}, \tag{5.4}$$

$$F(R) = \frac{A\left(1-E_g\right)^n}{h\upsilon}, \tag{5.5}$$

čia R – atspindys nuo bandinio;

E_g – draustinės juostos plotos, eV;

$h\upsilon$ – šviesos energija, eV;

A – proporcingumo konstanta;

n – a vertė, priklausanti nuo elektrono šuolio tipo, pavyzdžiui, esant tiesioginiam šuoliui n = 1/2, esant draustiniam tiesioginiam šuoliui n = 3/2, esant netiesioginiam šuoliui n = 2, esant netiesioginiam draustiniam šuoliui n = 3.

Skenuojamoji elektroninė mikroskopija

Kompozitinių bandinių struktūros susidarymas ir užpildo pasiskirstymas polimerinėje matricoje tirtas panaudojant skenuojamąjį elektronų mikroskopą su lauko emisijos šaltiniu (FE-SEM) (Mira3, „Tescan“, Čekija).

Drėkinimo kampo nustatymas

Statiniai kompozitų drėkinimo kampo (DK) matavimai atlikti drėkinimo kampo goniometru (DSA30, „Kruss Scientific“, Vokietija), kuriame buvo įrengta skaitmeninė kamera. Matuojant drėkinimo kampą, ant bandinių paviršiaus buvo dedama 4 μl Milli-Q vandens lašelių.

5.3. Rezultatai ir aptarimas

5.3.1 Sintezės produktų apibūdinimas

Atlikus hidroterminį vario oksido ir sieros žaliavos apdorojimą, buvo ištirta susintetintų miltelių mėginių fazinė sudėtis. Pastebėta, kad bandiniuose, kuriuose sieros žaliava buvo atlieka arba etalonas, po 0,5 h hidroterminio apdorojimo 145 °C temperatūroje buvo susintetintas heksagoninės singonijos CuS – kovelitas (PDF 04-006-9635) (5.1 pav.). Pažymėtina, jog bandiniai, pagaminti 180 °C temperatūroje per 0,5 arba 4 h, taip pat susidarė iš kovelito (5.1 pav.).

Be to, priemaišos, esančios bandiniuose dėl antrinės žaliavos kilmės, tokios kaip kvarcas ir anhidritas, liko nesureagavusios visuose sieros atliekos kilmės bandiniuose, apdorotuose skirtingomis hidroterminės sintezės sąlygomis (5.1 pav., A). Paminėtina, kad elementinė siera buvo nustatyta Sw0.5h145C bandinyje, o tai rodo, kad sintezės 145 °C temperatūra apdorojant mišinį 0,5 h yra nepakankama visiškai sureaguoti reagentams (5.1 pav., A). O visuose skirtingomis sąlygomis susintetintuose bandiniuose, kuriuose siera yra etaloninės kilmės, buvo nesureagavusios sieros (5.1 pav., B). Pažymėtina, kad Sr0.5h145C bandinyje taip pat buvo nesureagavusio tenorito (5.1 pav., B). Kadangi CuO ir S difrakcijos smailės buvo intensyvesnės bandiniuose, kuriuose siera antrinės žaliavos kilmės, palyginti su etalono kilmės bandiniais, teigiama, kad CuS etaloniniame bandinyje kristalizavosi lėčiau. Pastarasis reiškinys grindžiamas skirtingu sieros reagentų reaktyvumu, kurį lėmė skirtingas mechaninis sieros žaliavos paruošimas.

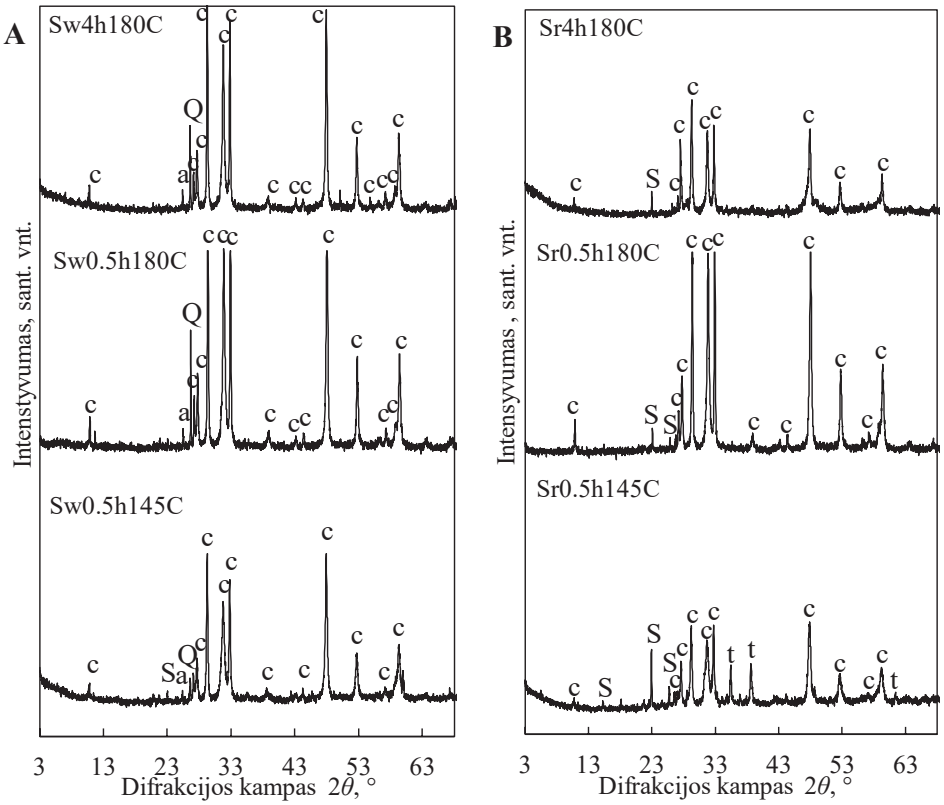

5.1 pav. Sintezės produktų, pagamintų naudojant sieros atlieką (A) ir sieros etaloną (B), RSDA difraktogramos. Žymenys: c – kovelitas, S – siera, Q – kvarcas, t – tenoritas, a – anhidritas

Proceso sąlygos, tokios kaip apdorojimo terpė ir džiovinimo parametrai, paprastai turi įtakos miltelinių medžiagų dalelių dydžiui. Priešingai, kristalitų dydis, kuris yra parametras, lemiantis puslaidininkinių medžiagų funkcines savybes, yra skirtingai veikiamas. Pastebėta, kad bandiniai, susintetinti 0,5 h hidroterminio apdorojimo metu 145 °C temperatūroje, pasižymėjo mažiausiu kristalitų dydžiu (5.3 lentelė). Vidutiniškai kovelito kristalitų dydis sieros antrinės žaliavos ir etalono kilmės bandiniuose atitinkamai buvo 33 nm ir 27 nm (5.3 lentelė). Hidroterminio apdorojimo temperatūrą padidinus iki 180 °C, sieros atliekos bandinyje kristalitų dydis padidėjo 6 nm, o etaloniniame bandinyje – 8 nm (5.3 lentelė). Tai parodė, kad kristalų dydžio augimas paspartėjo esant aukštesnei reakcijos temperatūrai. Vis dėlto sintezės trukmė neturėjo didelės įtakos vidutiniam kristalitų dydžiui, kadangi kai reakcijos laikas buvo pratęstas nuo 0,5 iki 4 h, identifikuotas padidėjimas tik 1–2 nm (5.3 lentelė). Be to, buvo pastebėta, kad sieros žaliavos kilmė turėjo nedidelį poveikį kovelito kristalitų dydžiui, nes šio parametro vertės buvo 2–5 nm mažesnės kiekviename etaloninio bandinio eksperimentiniame taške (5.3 lentelė). Taigi, hidroterminio apdorojimo temperatūra turėjo lemiamą poveikį skatinant kristalitų dydžio didėjimą.

5.3 lentelė. Sintetinio CuS kristalitų dydis

Sintezės sąlygos	Sieros atliekos bandinys	Sieros etalono bandinys
	Kristalitų dydžio diapazonas (min–max, nm	
0,5 h 145 °C	19,9–42,7	18,3–42,3
0,5 h 180 °C	27,3–49,0	25,8–50,3
4 h 180 °C	28,7–50,6	27,8–53,0

Remiantis RSDA analize, Sw0.5h145C ir Sr0.5h145C bandiniai buvo sudaryti iš nesureagavusios sieros ir vario oksido, taip sumažinant galimą maksimalų CuS kiekį ir galimai iškreipiant tolesnius tyrimo rezultatus. Taigi, toliau nustatant fotokatalitines savybes, buvo tirti tik bandiniai, pagaminti 180 °C temperatūroje 0, 5 arba 4 h hidroterminio apdorojimo metu. Be to, bandiniai, susintetinti atitinkamomis sąlygomis, naudojant sieros etaloną kaip sieros žaliavą, taip pat buvo tirti siekiant palyginti rezultatus bei pripažinti sieros antrinės žaliavos kilmės tinkamumą gaminant vario sulfidą.

Fotokatalitinės charakteristikos yra viena iš svarbiausių puslaidininkių savybių. Dėl šios priežasties bandiniai, gauti 0,5 ir 4 h sintezės metu 180 °C temperatūroje, buvo toliau tiriami DRS. Remiantis susintetintų Tauko diagrama, gauta iš Kubelka-Munk funkcijos, buvo apskaičiuotas energijos draustinės juostos plotis [110]. Nustatyta, jog CuS bandinio, gauto iš sieros antrinės žaliavos 0,5 h sintezės metu 180 °C temperatūroje, draustinės juostos plotis yra 1,78 eV (5.2 pav.). Be to, sintezės trukmė neturėjo įtakos sieros atliekos kilmės bandinių juostos pločio vertei, nes Sw4h180C taip pat pasižymėjo 1,78 eV juostos pločiu (5.2 pav.). Vis dėlto hidroterminio apdorojimo trukmė lėmė bandinių, pagamintų naudojant sieros etaloną, draustinės juostos pokyčius, kadangi, padidinus trukmę nuo 0,5 iki 4 h, juostos pločio vertės sumažėjo nuo 1,81 eV iki 1,72 eV (5.2 pav.). Remiantis literatūra, kovelitui būdingas energijos draustinės juostos plotis įprastai svyruoja apie 2,0 eV [127]. Taigi, siūlomu hidroterminės sintezės metodu susintetinamas CuS su šiek tiek mažesne eksperimentine energinės juostos energija, nei tikėtasi.

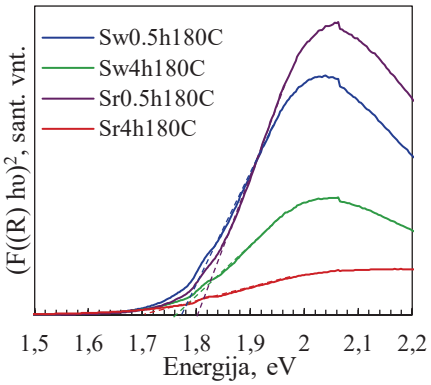

5.2 pav. Sintetinių bandinių Kubelkos ir Munko funkcijos kreivės

Metileno mėlio skaidymas susintetintais miltelių būsenos bandiniais

Sw0.5h180C ir Sr0.5h180C bandinių fotokatalitinės savybės toliau buvo tirtos atliekant organinių molekulių skaidymą, apšviečiant regimosios šviesos spektru. Šio tyrimo metu buvo naudotas metileno mėlis (MB) kaip skaidoma organinė molekulė.

Atlikus MB skaidymo tyrimus, buvo nustatyta, kad pradinėje fotokatalitinės reakcijos stadijoje sieros atliekos kilmės bandiniu pasiekta skaidymo efektyvumo vertė buvo 7 % didesnė nei bandiniu, pagamintu iš etaloninės sieros (5.3 pav.). Apšvietus bandinius 30 min, Sw0.5h180C bandiniu suskaidyta 73 % metileno mėlio, o etaloniniu bandiniu MB dalelės buvo suirusios 61 % (5.3 pav.). Pasibaigus eksperimentui po 3 h, skaidymo efektyvumas, pasiektas abiem bandiniais, buvo 96 % (5.3 pav.).

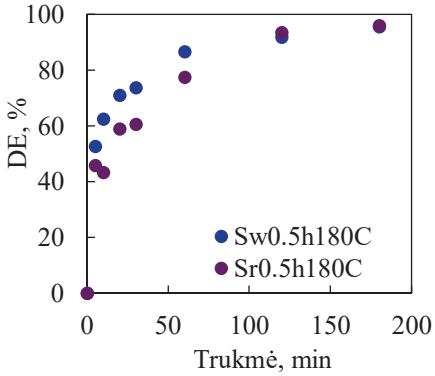

5.3 pav. Fotokatalitinio skaidymo efektyvumas Sw0.5h180C and Sr0.5h180C bandiniais (A) ir pseudopirmojo laipsnio kinetinės kreivės per pirminį skaidymo laiką (B)

Taigi naudojant antrinę sieros žaliavą buvo susintetintos CuS dalelės su analogiškomis fotokatalitinėmis savybėmis, kaip ir bandiniai, gauti naudojant įprastą etaloninę sierą.

5.3.2. Sintetinio kovelito terminio stabilumo tyrimai

Susintetintų bandinių DSK analizė buvo atlikta 25–600 °C temperatūroje. Rezultatai parodė, kad antrinės žaliavos kilmės bandinių termogramos atitiko tą patį šilumos išsiskyrimo modelį, kaip ir bandinių, pagamintų iš etaloninės sieros žaliavos. Remiantis gautais rezultatais, termiškai apdorojant Sw0.5h180C ir Sr0.5h180C įvyko dvi egzoterminės reakcijos. Pirmasis egzoterminis efektas buvo pastebėtas esant 245±15–385±15 °C temperatūrai, kai antrinės žaliavos ir etalono kilmės bandiniuose didžiausia efekto temperatūra atitinkamai buvo 350 ir 308 °C (5.4 pav.). Antroji egzoterminė reakcija vyko nuo 414±4 iki 518±22 °C atitinkamai Sw0.5h180C ir Sr0.5h180C (5.4 pav.). Pažymėtina, jog 4 h sintezės metu gauti bandiniai pasižymėjo tik vienu egzoterminiu efektu temperatūroje nuo 405±5 iki 497±8 °C (5.4 pav.). Be to, pastebėta, jog 467–493 °C temperatūroje vykusio egzoterminės reakcijos metu bandiniai, susintetinti per 0,5 h, išskyrė mažiau šilumos, palyginti su bandiniais, gautais per 4 h. Pavyzdžiui, Sw4h180C bandinys išskyrė 54 J/g mažiau šilumos,

palyginti su išsiskiriančios šilumos kiekiu Sw0.5h180C, o sieros etalono kilmės bandiniuose išskiriamos šilumos kiekis Sr4h180C mėginyje buvo 188 J/g mažesnis, palyginti su Sr0.5h180C. Taigi, sintezės trukmė reikšmingai paveikė terminio apdorojimo metu vykusias reakcijas kartu su išsiskiriančios šilumos kiekiu.

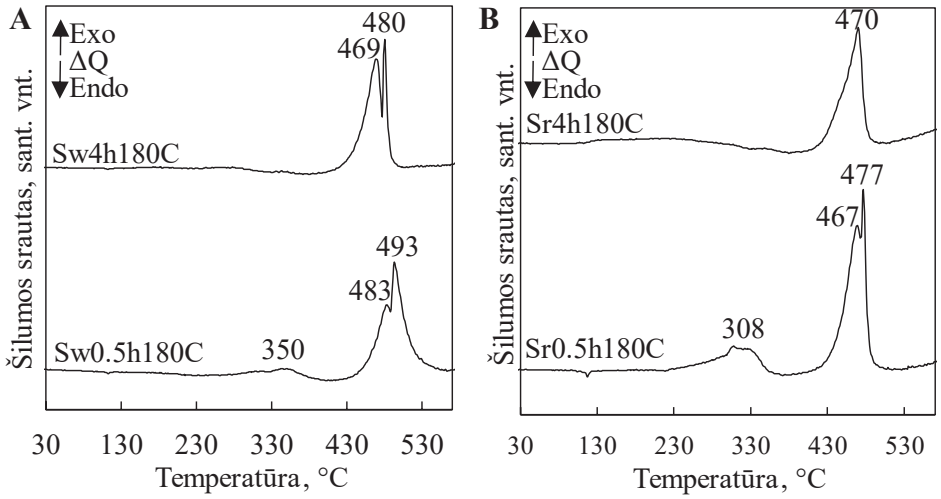

5.4 pav. Sintezės produktų, pagamintų naudojant sieros atlieką (A) ir sieros etaloną (B), DSK analizės kreivės

Toliau siekiant ištirti bandinį sudarančių komponentų skilimo mechanizmą, buvo atlikti degimo eksperimentai, stebint fazinės sudėties pokyčius terminio apdorojimo metu.

Pastebėta, kad, padidinus temperatūrą iki 300 °C, antrinės žaliavos ir etalono kilmės bandinių, susintetintų per 0,5 h hidroterminį apdorojimą, fazinė sudėtis nepakito, palyginti su pradine atitinkamų bandinių sudėtimi (5.5 pav.). Pirmieji fazinės sudėties pokyčiai buvo pastebėti 400 °C temperatūroje degtų bandinių sudėtyje identifikuojant naujų junginių, tokių kaip anilitas (Cu_7S_4) (PDF 04-007-1772, *d*-tarpplokštuminis atstumas – 0,336 nm) ir digenitas (Cu_9S_5) (P PDF 00-047-1748, *d*-spacing–0,321; 0,196; 0,168 nm), pėdsakų (5.5 pav., A).

Be to, digenito difrakcinių maksimumų intensyvumas padidėjo bandinius išdegus 450 °C temperatūroje, nors naujų tarpinių junginių nebuvo nustatyta. Didžiausi faziniai sudėties pokyčiai pastebėti išdegus Sr0.5h180C ir Sw0.5h180C bandinius 500 °C temperatūroje, kadangi identifikuotos intensyvios dominuojančios digenito ir vario sulfido (Cu ir S stechiometrinis santykis 1,81:1 ($Cu_{1,81}S$)) (PDF-04-003-4437, *d*- tarpplokštuminis atstumas–0,231; 0,197 nm) difrakcinės smailės (5.5 pav., A). Be to, kovelito oksidacija įvyko 450–500 °C temperatūroje, kadangi kovelito difrakcijos smailės sumažėjo daugiau nei perpus, o chalkocianitas ($CuSO_4$) (PDF 04-008-0844, *d*-tarpplokštuminis atstumas – 0,419; 0,355; 0,262 nm) taip pat buvo vienas iš pagrindinių junginių bandinyje (5.5A pav.).

Palyginus 0,5 ir 4 h hidroterminio apdorojimo metu susintetintus bandinius, pastebėti nedideli faziniai sudėties pokyčiai, termiškai apdorojus analogiškomis temperatūromis. Pavyzdžiui, antrinės žaliavos prigimties junginiai, tokie kaip kvarcas

ir anhidritas, liko nesureagavę tiek Sw0.5h180C, tiek Sw4h180C bandiniuose, parodant inertiškumą visame terminio apdorojimo temperatūrų intervale (5.5 pav.). Be to, tarpinis junginys roksbitas ($Cu_{1,8125}S$) (PDF 04-019-1452, *d*-tarpplokštuminis atstumas – 0,186 nm) buvo pastebėtas tik Sr4h180C mėginyje esant žemai degimo temperatūrai 250–300 °C (5.5B pav.). Padidinus terminio apdorojimo temperatūrą iki 500 °C, bandinius sudarė Cu_2S (PDF 04-024-2237, d-tarpplokštuminis atstumas – 0,275; 0,230; 0,171 nm), aukšto kristališkumo digenitas ($Cu_{7,2}S_4$) (PDF 04-024-0061, *d*-tarpplokštuminis atstumas – 0,279; 0,197 nm) ir bonatitas ($CuSO_4 \cdot (H_2O)_3$) (PDF 04-010-6576, *d*-tarpplokštuminis atstumas – 0,511; 0,442; 0,326 nm), įrodantis įvykusią oksidaciją didesnėje temperatūroje nei 450 °C (5.5 pav., B).

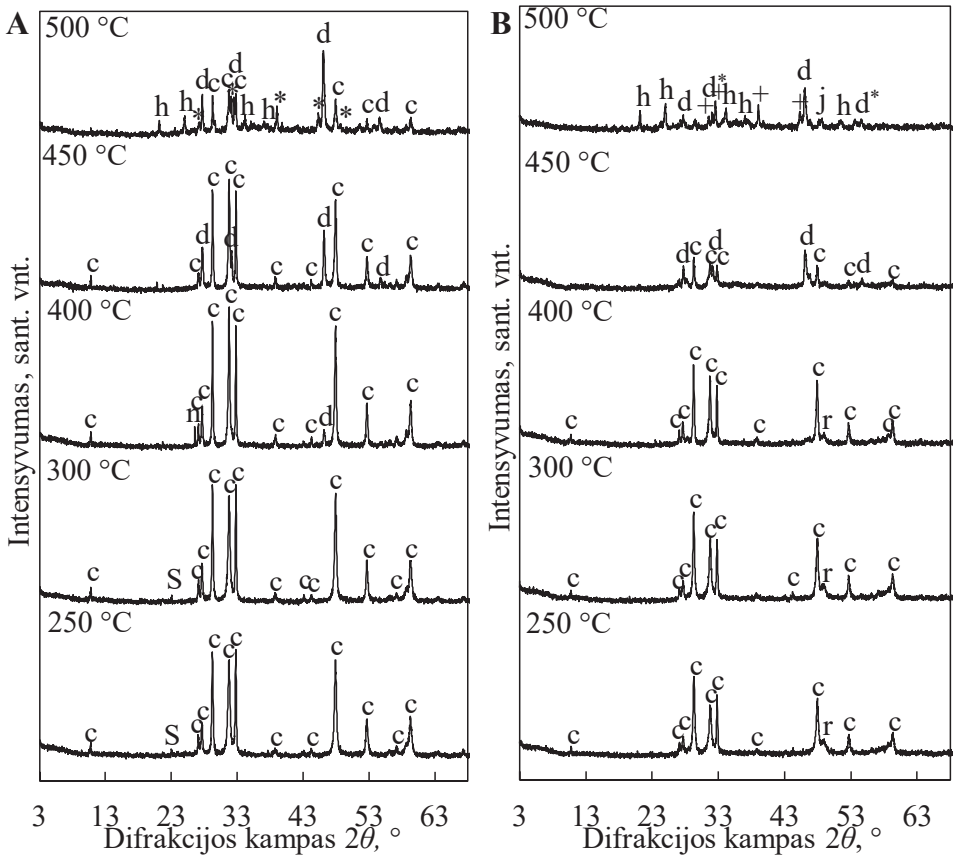

5.5 pav. Bandinių Sr0.5h180C (A) ir Sr4h180C (B) RSDA analizės kreivės atlikus terminį apdorojimą. Žymenys: c – kovelitas, n – anilitas, d – digenitas, * – $Cu_{1.81}S$, h – chalkocianitas, d*– aukšto kristališkumo digenitas, r – roksibitas, + – Cu_2S

Palyginus termiškai apdoroto kovelito kristalitų dydžius su pradinius bandinius sudarančio kovelito duomenimis, reikšmingų šio parametro pakitimų nebuvo pastebėta (5.4 lentelė). Taigi, šie duomenys rodo susintetinto kovelito stabilumą didinant temperatūrą iki 400 °C.

5.4 lentelė. Kovelito kristalitų dydžio pokytis

Degimo temperatūra,	Sintetinis bandinys			
	Sr0.5h180C	Sr4h180C	Sw0.5h180C	Sw4h180C
	Kristalitų dydžio diapazonas (min–max), nm			
250	23–45	23–51	23–47	26–53
300	28–52	26–51	26–46	28–51
400	34–57	28–49	29–51	32–56

Taigi, ištyrus termiškai apdorotų junginių fazinės sudėties pokyčius, paaiškėjo, kad egzoterminės reakcijos, vykusios 240±14–382±22 °C temperatūroje, metu kovelitas skilo iki digenito. Didinant terminio apdorojimo temperatūrą 412±7–513±19 °C, įvyko antroji egzoterminė reakcija, kurios metu kovelitas oksidavosi iki vario sulfato.

Tolimesniam sintetintų bandinių terminių savybių tyrimui buvo atlikta degtų bandinių DSK analizė. Verta paminėti, kad egzoterminis efektas, pastebėtas 240±14–382±22 °C temperatūroje, nebuvo identifikuotas visų degtų bandinių termogramose (5.6 pav.).

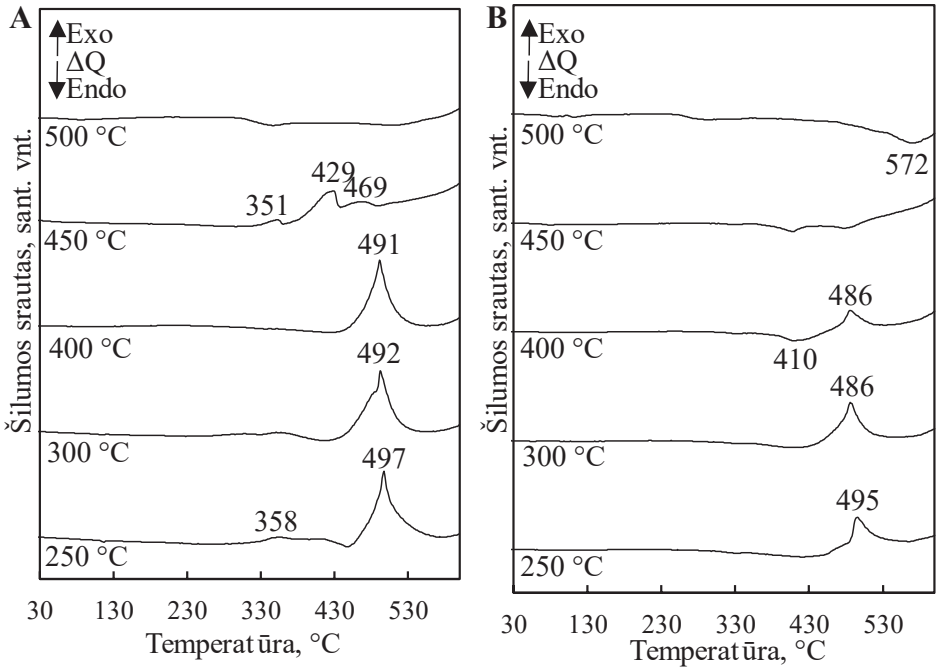

5.6 pav. Sr0.5h180C (A) ir Sr4h180C (B) bandinių, termiškai apdorotų skirtingose temperatūrose, termogramos

Didinant terminio apdorojimo temperatūrą, visų bandinių išskiriamas šilumos kiekis vykusios 412±7–513±19 °C temperatūroje egzoterminės reakcijos metu sumažėjo, palyginti su sintezės produktų duomenimis. Pažymėtina, jog išsiskiriančios

šilumos kiekis skyrėsi priklausomai nuo hidroterminės sintezės trukmės. Pavyzdžiui, Sr0.5h180C ir Sw0.5h180C bandiniai, termiškai apdoroti 400 °C temperatūroje, išsiskyrė 7 ir 64 J/g mažiau šilumos, palyginti su sintezės produktų išskiriamu šilumos kiekiu. Nustatyta, jog Sr4h180C ir Sw4h180C bandiniai, degti 400 °C temperatūroje, taip pat išskiria atitinkamai 296 ir 168 J/g mažesnį šilumos kiekį, palyginti su sintezės produktais. Be to, nė vienas bandinys, termiškai apdorotas 500 °C temperatūroje, neišskyrė šilumos tokioje temperatūroje, kuri būdinga kovelito oksidacijos reakcijai; todėl nustatyta, kad perėjimo iš CuS į $CuSO_4$ temperatūra buvo aukštesnė nei 450 °C (5.6 pav.).

Pažymėtina, kad skirtingos sieros žaliavos panaudojimas hidroterminei CuS sintezei neturėjo įtakos fazių pokyčiams 250–400 °C temperatūroje. Nepaisant to, sieros žaliavos kilmė ir sintezės trukmė buvo pagrindinės priežastys, lėmusios terminio apdorojimo metu išsiskiriančios šilumos kiekio pokyčius.

Nustatyta, jog kovelito (CuS) neryškus skilimas prasidėjo aukštesnėje nei 300 °C temperatūroje dėl kovelito neryškaus skilimo į anilitą (Cu_7S_4) ir digenitą (Cu_9S_5). Vis dėlto reikšmingas kovelito skilimas iki digenito įvyko aukštesnėje nei 400 °C temperatūroje. Taigi pastarieji rezultatai įrodo susintetintų vario sulfido mėginių stabilumą bent iki 300 °C, o tai yra aukštesnė stabilumo temperatūra, nei skelbiama kitų autorių literatūroje [125,126]. Didinant terminio apdorojimo temperatūrą, anilitas toliau suskilo iki $Cu_{1.81}S$, pastarasis junginys taip pat buvo pagamintas iš kovelito aukštesnėje nei 450 °C temperatūroje. Paminėtina, jog vienalaikiškai dalis digenito sureagavo į Cu_2S. Nustatyta, kad aukštesnėje nei 450 °C temperatūroje įvyko kovelito oksidacija iki vario sulfato (chalkocianito, bonatito). Pažymėtina, kad pastaroji reakcija taip pat įvyko aukštesnėje temperatūroje, nei nurodyta literatūroje [124].

5.3.3. Sintezės produktų taikymas organinėms molekulėms skaidyti

Kompozitų struktūros tyrimas

Toliau susintetinti CuS mėginiai buvo įtvirtinti į polimerinę matricą, siekiant suteikti atramą fotokatalizatoriui ir išvengti pastarojo komponento atskyrimo stadijos iš tirpalo. Kompozitai buvo suformuoti porėtos ir plėvelės struktūros. Pažymėtina, kad tik Sw0.5h180C, tiek Sr0.5h180C bandiniai buvo panaudoti gaminant kompozitus, kurie taikyti organinių junginių skaidymo tyrimui.

FE-SEM analizė buvo atlikta siekiant ištirti fotokatalizatoriaus dispersiją ir pasiskirstymą polimerinėje matricoje bei analizuojant norimos porėtos struktūros susidarymą. Pažymėtina, jog gauti mikroskopijos vaizdiniai atskleidė efektyvią sklaidą ir tolydų Sw0.5h180C ir Sr0.5h180C mėginių pasiskirstymą bei sklandžiai suformuotą porų struktūrą (5.7 pav.)

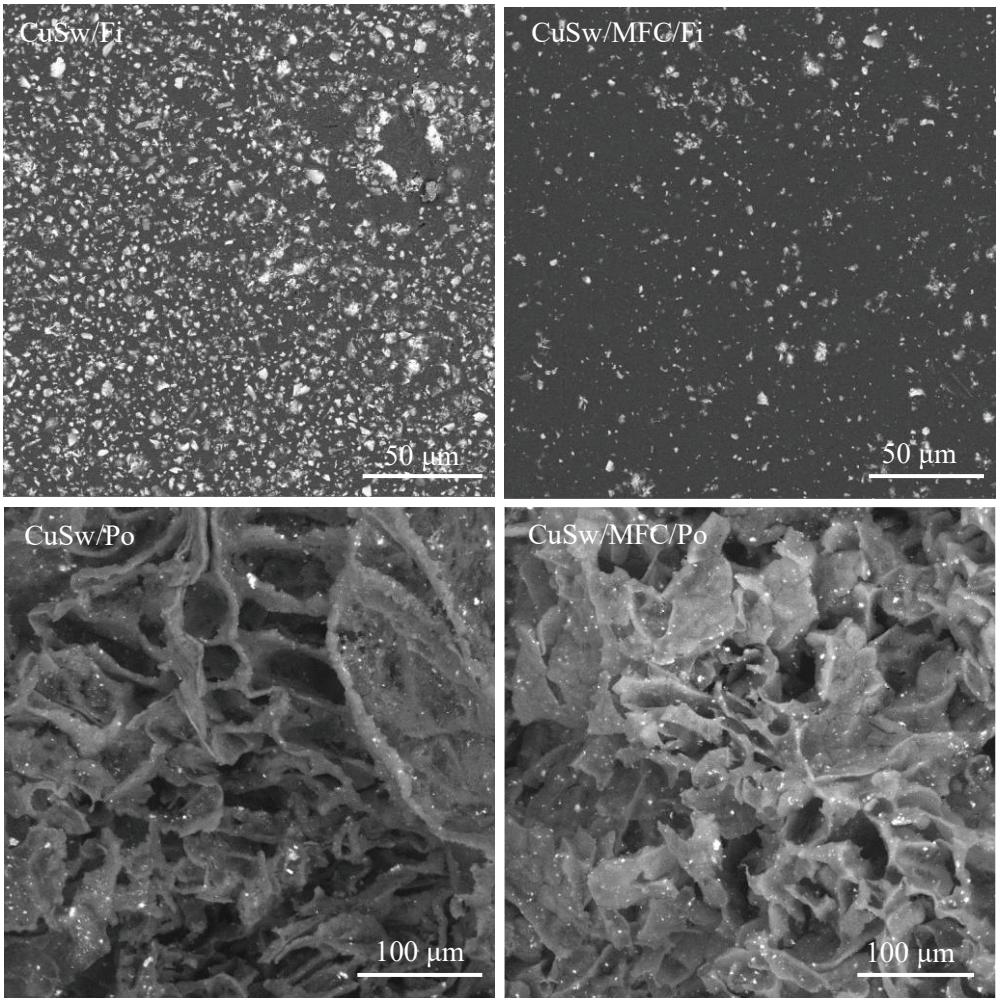

5.7. pav. CuS–PHBV kompozitų SEM vaizdiniai

Siekiant pagerinti kontaktą tarp organinės molekulių srauto ir fotokatalizatoriaus paviršiaus, buvo mažinamas hidrofobinio PHBV polimero drėkinimo kampas. Dėl šios priežasties į kompozitų sudėtį buvo įmaišyta mikrofibrilinės celiuliozės (MFC), kurios struktūroje yra hidroksilo grupių, mažinančių ir kitų polimerų hidrofobiškumą [136].

Nustatyta, jog MFC kompozito struktūroje smarkiai pagerino porėtų bandinių drėkinamumą, sumažindamas drėkinimo kampą 11° (5.4 lentelė). O plėvelės bandinių drėkinamumą MFC paveikė tik nedaug, kadangi DK sumažėjo tik 4°, palyginti su grynu bandiniu (5.4 lentelė). Verta paminėti, kad WCA matavimų standartinių nuokrypių vertės buvo mažos, o tai rodo homogenišką MFC pasiskirstymą ir MFC dispersijos metodo efektyvumą.

5.5 lentelė .Gryno polimero ir kompozitų su ir be MFC drėkinimo kampas

Bandinys	DK ± standartinis nuokrypis, °		
	Grynas polimeras	Kompozitas be MFC	Kompozitas su MFC
Porėtas	117,1±0,29	126,1±0,36	115,1±0,58
Plėvelė	93,3±0,44	94,8±0,8	91,1±0,56

Organinių molekulių fotoskaidymas kompozitais

Vertinant Sw0.5h180C ir Sr0.5h180C bandinių fotokatalitines savybes kompozito struktūroje, tetraciklinas (TC) buvo pasirinktas kaip regimosios šviesos spektre skaidoma organinė molekulė.

Remiantis TC skaidymo kinetinėmis kreivėmis, akivaizdu, kad dauguma tirtų bandinių pasiekė 100 % skilimo efektyvumą per 180 min reakcijos, nepriklausomai nuo kompozito struktūros (5.8 pav.). Be to, lyginant Sw0.5h180C arba Sr0.5h180C bandiniais pasiektą skaidymo efektyvumą, reikšmingų duomenų neatitikimų nepastebėta (5.8 pav.). Pavyzdžiui, po 120 min CuSr/Po ir CuSw/Po bandiniais buvo suskaidyta atitinkamai 56 % ir 60 % organinių molekulių (5.8 pav.).

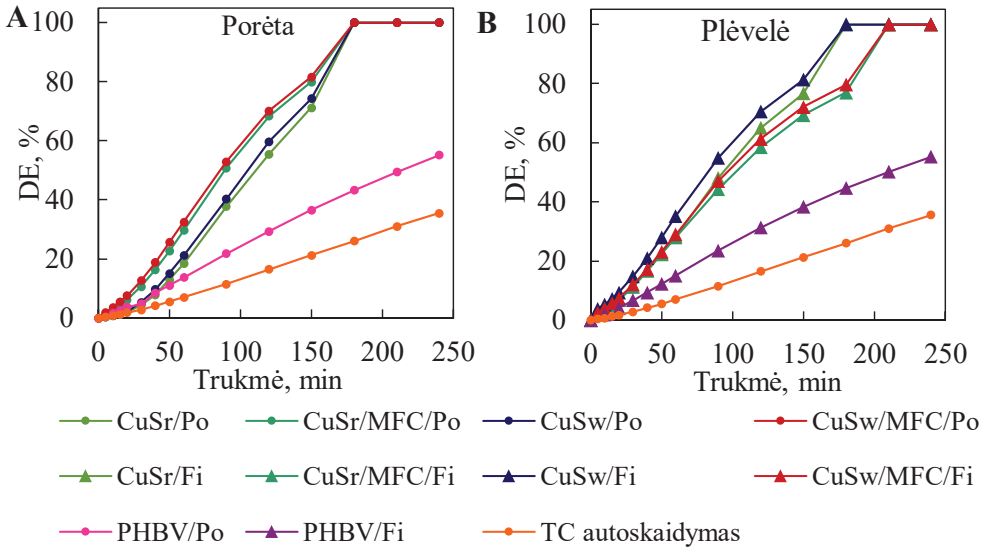

5.8 pav. TC skaidymo efektyvumo porėtais (A) ir plėvelės formos (B) kompozitais priklausomybė nuo reakcijos trukmės

Pradinis fotoskaidymo reakcijos greitis porėtais sieros atliekos ir etalono kilmės bandiniais buvo analogiškas, kadangi pasiekta reakcijos greičio konstanta atitinkamai buvo 0,0863 min^{-1} ir 0,0786 min^{-1} (5.9 pav.). Vis dėlto plėvelės struktūros bandiniai, kuriuose vario sulfidas pagamintas iš antrinės žaliavos, pasižymėjo 1,4 karto didesniu skaidymo greičiu nei etaloninės sieros kilmės CuS (CuSw/Fi – 0,5203 min^{-1}; CuSr/Fi – 0,3834 min^{-1}) (5.9 pav.). Paminėtina, jog šiek tiek mažesnė reakcijos greičio konstantos vertė, pasiekta etaloniniu bandiniu, palyginti su atliekos kilmės bandiniu,

atitinka fotokatalitinių savybių rezultatus, pasiektus miltelių formos Sw0.5h180C ir Sw0.5h180C bandiniais, kuriuos lėmė miltelinės medžiagos kristalitų dydžio įtaka, kaip minėta anksčiau.

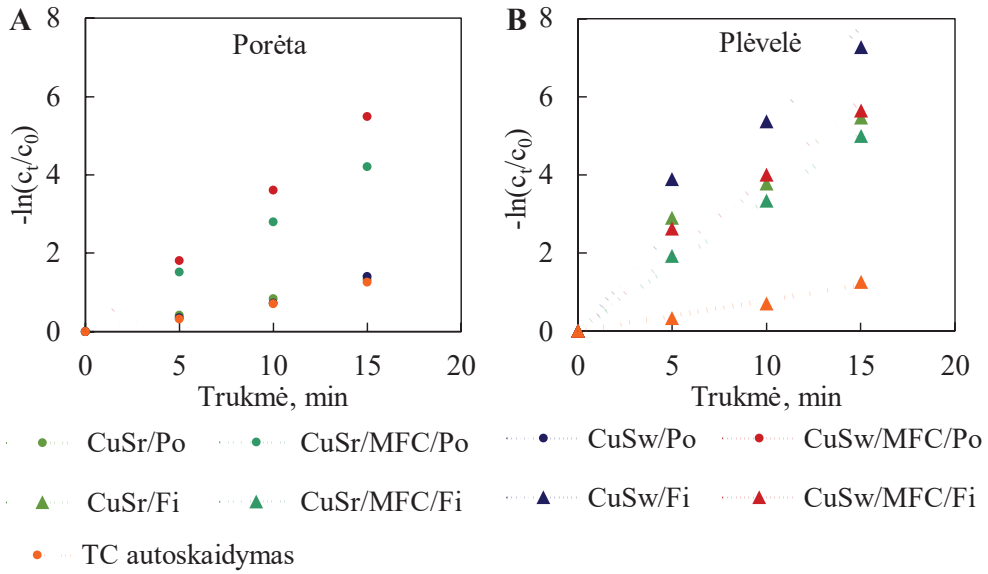

5.9 pav. Pseudopirmojo laipsnio kinetinės kreivės fotokatalitiškai skaidant TC porėtos (A) ir plėvelės (B) struktūros kompozitu

Pažymėtina, jog MFC įtraukimas į kompozitų sudėtį teigiamai paveikė TC skaidymą porėtais bandiniais, kadangi skaidymo efektyvumas padidėjo iki 13 % per visą apšvietimo laikotarpį (5.8 pav.). Taip pat pradinės reakcijos greičio konstantos buvo 3,3 ir 4,2 karto didesnės bandiniais, turinčiais sudėtyje MFC (atitinkamai CuSr/MFC/Po ir CuSw/MFC/Po) nei bandiniais be hidrofiliškumo stipriklio (5.9 pav.). Tai patvirtina, kad MFC buvimas porėtuose bandiniuose skatina greitesnę fotokatalitinę reakciją. Kadangi porėtų bandinių paviršiaus drėkinimo kampas buvo sumažintas, padidėjęs porėtos struktūros drėkinamumas ir pralaidumas TC vandeniniam tirpalui lėmė didesnį aktyvaus paviršiaus plotą, veikiamą organinių molekulių tirpalo.

Kita vertus, MFC įterpimas į kompozito sudėtį turėjo neigiamos įtakos efektyvumui skaidant TC plėvelės formos bandiniais. Pavyzdžiui, visiškas TC suskaidymas taikant kompozitus be hidrofiliškumo stipriklio (CuSw/Fi ir CuSr/Fi bandiniais) buvo pasiektas po 150 min apšvietimo, o sudėtyje esant MFC 100 %, TC skaidymas pasiektas 30 min vėliau (5.9 pav.). Reakcijos greičio konstantos taip pat buvo 12 % ir 24 % mažesnės atitinkamai CuSr/MFC/Fi ir CuSw/MFC/Fi, palyginti su CuSr/Fi ir CuSw/Fi (5.9 pav.). Tikėtina, jog šiuos rezultatus lėmė tai, kad plėvelės struktūros bandiniuose abiejų tipų priedai buvo paskirstyti visame plokščiame pagrinde, pasižyminčiame mažesniu paviršiaus plotu, palyginti su porėtais kompozitais. Vadinasi, fotokatalizatoriaus dalelės plėvelės formos bandiniuose buvo labiau iš dalies pridengtos hidrofiliškumo stiprikliu, lemiant paviršiuje mažesnį galimą paveikti fotokatalizatoriaus aktyvių centrų kiekį, kaip parodė FE-SEM tyrimai

(5.7 pav.). Sumažėjęs elektronų–skylių, dalyvaujančių fotoskaidyme, skaičius kartu su nepakitusiu plėvelės mėginių pralaidumu TC vandeniniam tirpalui lėmė bendrą skaidymo efektyvumo sumažėjimą.

Pažymėtina, jog kompozito struktūra taip pat turėjo įtakos fotoskaidymo greičiui. TC skaidymas plėvelės formos kompozitais buvo daug greitesnis, palyginti su porėtais bandiniais, kadangi pradinė reakcijos greičio konstanta pasiekta CuSw/Po buvo 0,083 min^{-1}, o CuSw/Fi – 0,5203 min^{-1} (5.9 pav.). Paminėtina, jog MFC padidino skaidymo greitį porėtais kompozitais ir pradinės reakcijos greičio konstantos, pasiektos naudojant CuSw/MFC/Fi ir CuSw/MFC/Po, atitinkamai buvo 0,3932 ir 0,3642 min^{-1} (5.9 pav.).

Taigi, TC fotoskaidymo kompozitais su vario sulfidu, pagamintu iš sieros antrinės žaliavos (Sw0.5h180C bandinys), bandymų rezultatai buvo analogiški, kaip ir kompozito su CuS, susintetinto iš etaloninės sieros (Sr0.5h180C bandinys). Paminėtina, jog tolesniems tyrimams buvo pasirinkti tik kompozitai, kuriuose yra Sw0.5h180C. Dėl didžiausių pradinio reakcijos greičio ir skilimo efektyvumo verčių per visą apšvietimo trukmę tolesnei analizei buvo atrinkti tik CuSw/MFC/Po ir CuSw/Fi bandiniai.

Kompozitų pakartotinis panaudojimas

Pakartotinis kompozitų panaudojimas fotodegradacijai yra svarbus aspektas, kurį reikia ištirti. Tyrimo rezultatai parodė, kad tiek CuSw/MFC/Po, tiek CuSw/Fi bandiniai gali būti pakartotinai naudojami mažiausiai penkis kartus, kiekvieno ciklo metu pasiekiant 100 % TC skaidymo efektyvumą (5.10 pav.).

Be to, pastebėta, kad antrojo ciklo metu gautos skaidymo efektyvumo vertės buvo didesnės, palyginti su gautomis per pirmąjį. Pavyzdžiui, po 60 min apšvietimo pirminio ciklo metu CuSw/MFC/Po ir CuSw/Fi bandiniais pasiektas skaidymo efektyvumas yra atitinkamai 33 % ir 37 % (5.10 pav.). O per antrąjį ciklą skaidymo efektyvumas padvigubėjo ir po 60 min reakcijos suskaidė 61 % ir 75 % tetraciklino atitinkamai CuS/MFC/Po ir CuSw/Fi bandiniais (5.10 pav.). Paminėtina, jog antrajame cikle abu mėginiai pasiekė 100 % TC skilimą 30 min greičiau, palyginti su pirmojo ciklo duomenimis (5.10 pav.).

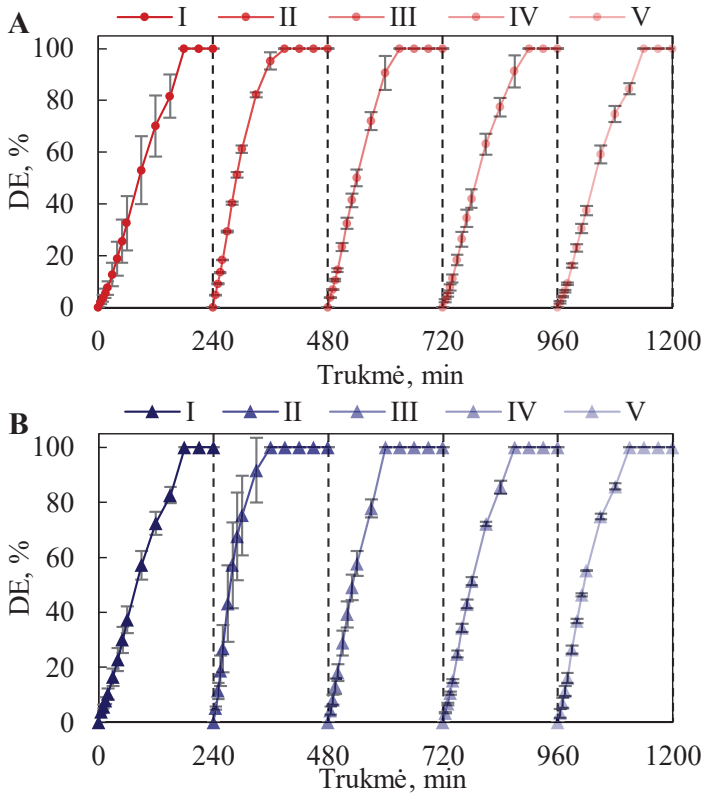

5.10 pav. Skaidymo efektyvumo vertės pakartotinai taikant CuSw/MFC/Po (A) ir CuSw/Fi (B) kompozitus TC skaidyti

Svarbu paminėti, kad buvo pastebėtas neabejotinas organinių molekulių fotoskaidymo efektyvumo padidėjimas abiem tirtais bandiniais. Pavyzdžiui, antrojo ciklo metu pastebėtas spartesnis pradinis skaidymo reakcijos greitis, nes CuSw/MFC/Po bandiniu pasiekta pradinės reakcijos greičio konstanta padidėjo 2,5 karto – nuo 0,3642 min^{-1} iki 0,9036 min^{-1} (5.11 pav.). Analogiškai, CuSw/Fi bandiniu reakcijos greičio konstanta padidėjo 2,3 karto, pasiekdama 1,2051 min^{-1} vertę, palyginti su pirminio ciklo reikšme (0,5203 min^{-1}) (5.11 pav.).

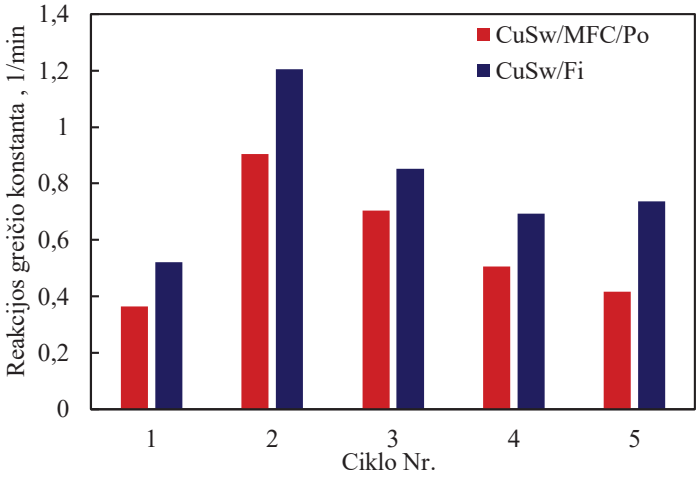

5.11 pav. Pradinės reakcijos greičio konstantos priklausomybė pakartotiniam CuSw/MFC/Po ir CuSw/Fi bandinių panaudojimui

Šis netikėtas reiškinys parodė, kad antrojo ciklo metu fotoskaidymas prasidėjo išnaudojant krūvininkus, kurie jau buvo sugeneruoti per pirmąjį ciklą ir vėliau įstrigo puslaidininkinio junginio paviršiuje [138]. Nepriklausomai nuo taikyto kompozito bandinio, reakcijos greičio konstanta po antrojo ciklo palaipsniui mažėjo didinant pakartotinio panaudojimo kiekį (5.11 pav.). Kaip buvo pastebėta ankstesniuose tyrimuose, šis padarinys buvo priskirtas silpnai fotokatalizatoriaus fotokorozijai, kurios metu susidarę krūvininkai oksidavo sieros jonus, esančius vario sulfide, lemiant fotokatalizatoriaus paviršiuje sumažėjusį aktyvių centrų kiekį [97,139,140].

Toliau tyrimas buvo atliktas siekiant įvertinti paruoštų kompozitų galimybę taikyti vienalaikiam skirtingų organinių molekulių skaidymui. Dėl šios priežasties CuS/MFC/Po ir CuSw/Fi bandiniai buvo naudoti skaidant metileno mėlio ir tetraciklino mišinį apšvietus regimuoju šviesos spektru. Rezultatai parodė, kad CuSw/MFC/Po ir CuSw/Fi kompozitai galėjo tuo pačiu metu skaidyti abi organines molekules pasiekiant 100 % skaidymo efektyvumą abiem molekulėms per 4 h veikimo regimosios šviesos spektru (5.12 pav.). Paminėtina, jog viso proceso metu porėtas bandinys pasižymėjo didesniu TC ir MB skaidymo efektyvumu, palyginti su plėvelėmis pasiektais rezultatais (5.12 pav.). Tiksliau, po 150 min reakcijos CuSw/Fi kompozitas suardo 78,5 % TC ir 89,9 % MB, o CuSw/MFC/Po bandiniu pasiektas skilimo efektyvumas buvo atitinkamai 5,7 % ir 6,3 % didesnis (5.12 pav.).

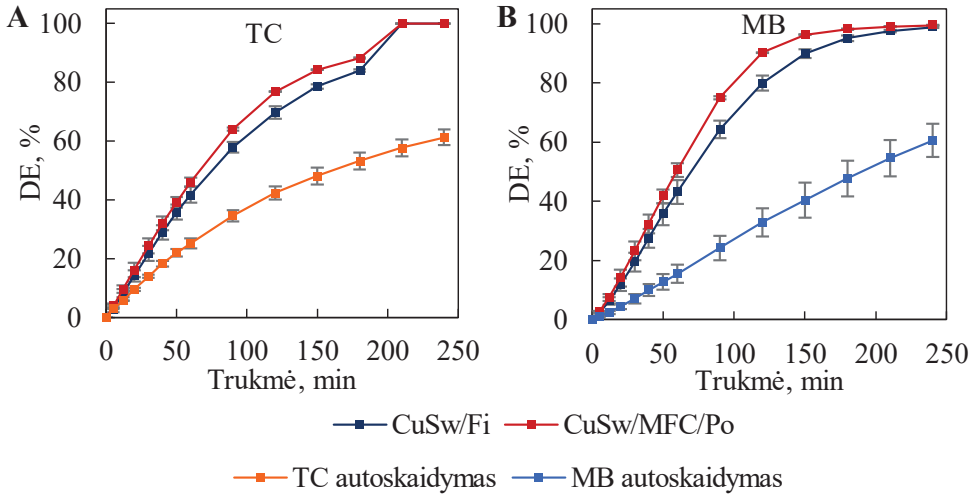

5.12 pav. Skaidymo efektyvumo vertės taikant CuSw/MFC/Po ir CuSsw/Fi kompozitus vienu metu skaidant tetracikliną (A) ir metileno mėlį (B)

Taigi, antrinės žaliavos kilmės vario sulfido bandiniai buvo panaudoti formuojant biopolimerinės matricos kompozitą, kuriuo siekiama didele apimtimi skaidyti organines molekules. Rezultatai atskleidė, kad antrinės žaliavos kilmės CuS–PHBV kompozitiniai bandiniai efektyviai suskaidė tetracikliną iki 100 % per 3 h ir gali būti pakartotinai naudojami bent 5 ciklus. Be to, rezultatai taip pat patvirtino, kad kompozitai gali būti plačiai taikomi, pavyzdžiui, suardant kelias skirtingos kilmės organines molekules vienu metu.

5.4. Išvados

1. Nustatyta, kad hidroterminės sintezės sąlygomis sieros žaliavos kilmė (pramoninė / antrinė žaliava) neturi reikšmingos įtakos vario sulfido susidarymo eigai. Ištirta, kad sieros antrinės žaliavos – vario oksido – vandens mišiniuose 145–180 °C temperatūroje per 0,5–4 h susidarė vyraujantys CuS bandiniai. Palankiausios antrinės žaliavos kilmės CuS kristalizacijos sąlygos yra 0,5 h hidroterminis išlaikymas 180 °C temperatūroje.
2. Ištirta, kad, priklausomai nuo eksperimentinių sąlygų, sintetiniam CuS bandiniui būdingas vidutinis kristalitų dydis kito nuo 27 iki 40 nm, o energetinis draustinės juostos plotis – nuo 1,72 iki 1,81 eV. Didinant sintezės temperatūrą, CuS kristalitų dydis vidutiniškai padidėjo per 6–8 nm abiejuose sieros skirtingos kilmės bandiniuose, o izoterminio išlaikymo trukmė neturėjo įtakos pastarajam parametrui.
3. Sintetiniai CuS bandiniai buvo termiškai patvarūs iki 300 °C. Aukštesnėje terminio apdorojimo temperatūroje nei 450 °C susidaro skirtingos fazinės sudėties bandiniai: $Cu_{1,81}S$, Cu_2S, $CuSO_4$. Izoterminio išlaikymo trukmės padidėjimas nuo 0,5 h iki 4 h (0,5–4 h) lėmė 245–385 °C temperatūroje vykstančio terminio efekto nebuvimą bei mažesnį išsiskiriančios šilumos kiekį terminio apdorojimo metu.

4. Nustatyta, kad, taikant termiškai indukuotos fazės atskyrimo ir liejimo būdus, iš biopolimero poli(3-hidroksibutirat-co-3-hidroksivalerato) ir sintetinių CuS bandinių pagaminti porėtos struktūros (porų dydis <50 μm) ir plėvelės formos (storis 100 μm) biokompozitai. Pagaminti skirtingos struktūros biokompozitai geba skaidyti organines molekules: tetracikliną suskaidė 100 % efektyvumu per 3 h fotokatalitinę reakciją. Didžiausios skaidymo efektyvumo ir greičiausios pradinės fotoskaidymo kinetikos vertės būdingos CuSw/Fi ir CuSw/MFC/Po bandiniams. Nustatyta, kad galimas pakartotinis (ne mažiau nei 5 kartų) biokompozitų panaudojimas, pasiekiant 100 % tetraciklino skaidymo efektyvumą.
5. Nustatyta, kad pagaminti biokompozitai gali būti taikomi vienu metu atliekant skirtingų organinių molekulių (tetraciklino ir metileno mėlio) fotoskaidymą, pasiekiant 100 % skaidymo efektyvumą per 4 h fotokatalitinę reakciją.

REFERENCES

1. EUROPEAN COMMISSION. The European Green Deal. Online. 2023. Available from: https://commission.europa.eu/strategy-and-policy/priorities-2019-2024/european-green-deal_en. [viewed 19 October 2023].

2. GOVERNMENT OF THE REPUBLIC OF LITHUANIA Nutarimas dėl 2021-2030 metų nacionalino pažangos plano patvirtinimo Online. 2020. Available from: https://e-seimas.lrs.lt/portal/legalAct/lt/TAD/c1259440f7dd11eab72ddb4a109da1b5?jfwid=-whxwii77y. [viewed 19 October 2023].

3. UNITED NATIONS. The Sustainable Development Goals Report. Online. 2022. Available from: https://unstats.un.org/sdgs/report/2022/. [viewed 19 October 2023].

4. UNITED NATIONS. Ensure sustainable consumption and production patterns. Online. 2023. Available from: https://sdgs.un.org/goals/goal12. [viewed 11 October 2023].

5. UNITED NATIONS. Sustainable development goals. Online. 2023. Available from: https://www.un.org/sustainabledevelopment/blog/2015/12/sustainable-development-goals-kick-off-with-start-of-new-year/. [viewed 16 November 2023].

6. EUROPEAN COMMISSION. Waste statistics. Online. 2023. Available from: https://ec.europa.eu/eurostat/statistics-explained/index.php?title=Waste_statistics#Hazardous_waste_generation. [viewed 11 October 2023].

7. THE ORGANIZATION FOR ECONOMIC COOPERATION AND DEVELOPMENT (OECD). Towards a more resource-efficient and circular economy. Online. 2021. Available from: https://ec.europa.eu/commission/presscorner/detail/en/ip_23_1661https://ec.europa.eu/commission/presscorner/detail/en/ip_23_1661. [viewed 19 October 2023].

8. EUROPEAN COMMISSION. About sustainable products. Online. 2023. Available from: https://commission.europa.eu/energy-climate-change-environment/standards-tools-and-labels/products-labelling-rules-and-requirements/sustainable-products/about-sustainable-products_en. [viewed 19 October 2023].

9. EUROPEAN COMMISSION. Circular economy. Online. 2023. Available from: https://environment.ec.europa.eu/topics/circular-economy_en. [viewed 19 October 2023].

10. EUROPEAN COMMISSION. SDGs & me: Responsible consumption and production. Online. 2023. Available from: https://ec.europa.eu/eurostat/web/products-eurostat-news/w/ddn-20230830-1. [viewed 19 October 2023].

11. EUROPEAN COMMISION. A secure and sustainable supply of critical raw materials in support of the twin transition . Online. 2023. Available from: https://eur-lex.europa.eu/legal-content/EN/TXT/?uri=COM%3A2023%3A165%3AFIN. [viewed 19 October 2023].

12. EUROPEAN COMMISION. In depth reviews of stategic areas for Europe's interests Online. 2021. Available from: https://ec.europa.eu/info/strategy/priorities-2019-2024/europe-fit-digital-age/european-industrial-strategy/depth-reviews-strategic-areas-europes-interests_lt. [viewed 19 October 2023].

13. THE MINISTRY OF THE ECONOMY AND INNOVATION OF THE REPUBLIC OF LITHUANIA. The Advanced Specialization Online. 2022. Available from: https://eimin.lrv.lt/lt/veiklos-sritys/inovaciju-veiklos-sritis/sumanioji-specializacija. [viewed 19 October 2023].

14. WAGENFELD J-G, AL-ALI K, ALMHEIRI S, Slavens AF, Calvet N. Sustainable applications utilizing sulfur, a by-product from oil and gas industry: A state-of-the-art review. *Waste Management*. 2019, vol. 95, p. 78–89. ISSN 0956053X

15. Rappold TA, Lackner KS. Large scale disposal of waste sulfur: From sulfide fuels to sulfate sequestration. *Energy*. 2010, vol. 35, p. 1368–1380. ISSN 0360-5442

16. Gómez-Ramírez M, Zarco-Tovar K, Aburto J, de León RG, Rojas-Avelizapa NormaG. Microbial treatment of sulfur-contaminated industrial wastes. *Journal of Environmental Science and Health, Part A*. 2014, vol. 49, p. 228–232. ISSN 1093-4529

17. Spatolisano E, de Angelis AR, Pellegrini LA. Middle Scale Hydrogen Sulphide Conversion and Valorisation Technologies: A Review. *ChemBioEng Reviews*. 2022, vol. 9, p. 370–392. ISSN 2196-9744

18. Sunil Dahiya, Andreas Anhäuser, Aidan Farrow, Hubert Thieriot, Avinash Chanchal, Lauri Myllyvirta. Global SO2 emission hotspot database. Online. 2020. Available from: https://www.greenpeace.org/static/planet4-mena-stateless/a372e5fe-so2-report-english.pdf [viewed 19 October 2023].

19. Liu F-J, Wei X-Y, Wang Y-G, Li P, Li Z-K, Zong Z-M. Sulfur-containing species in the extraction residue from Xianfeng lignite characterized by X-ray photoelectron spectrometry and electrospray ionization Fourier transform ion cyclotron resonance mass spectrometry. *RSC Advances*. 2015, vol. 5, p. 7125–7130. ISSN 2046-2069

20. Wang L, Li M, Yu S, Chen X, Li Z, Zhang Y, et al. Unexpected rise of ozone in urban and rural areas, and sulfur dioxide in rural areas during the coronavirus city lockdown in Hangzhou, China: implications for air quality. *Environmental Chemistry Letters*. 2020, vol.18, p. 1713–1723. ISSN 1610-3661

21. Chung WJ, Griebel JJ, Kim ET, Yoon H, Simmonds AG, Ji HJ, et al. The use of elemental sulfur as an alternative feedstock for polymeric materials. *Nature Chemistry*. 2013, vol. 5, p. 518–524. ISSN 1755-4330

22. MOHAMED A-MO and M EL-GAMAL. Sulfur concrete for the construction industry: a sustainable development approach. Fort Lauderdale, FL: J. Ross Publishing; 2010. ISBN 9781604270051

23. Layr K, Hartlieb P. Market Analysis for Urban Mining of Phosphogypsum. *BHM Berg- und Hüttenmännische Monatshefte*. 2019, vol. 164, p. 245–249. ISSN 1613-7531

24. Halfyard JE, Hawboldt K. Separation of elemental sulfur from hydrometallurgical residue: A review. *Hydrometallurgy*. 2011;109:80–9. ISSN 0304-386X

25. Chen L, Xu G, Rui Z, Alshawabkeh AN. Demonstration of a feasible energy-water-environment nexus: Waste sulfur dioxide for water treatment. *Applied Energy*. 2019, vol. 250, p. 1011–1122. ISSN 0306-2619

26. Lin S, Mackey HR, Hao T, Guo G, van Loosdrecht MCM, Chen G. Biological sulfur oxidation in wastewater treatment: A review of emerging opportunities. *Water Research*. 2018, vol. 143, p. 399–415. ISSN 1879-2448

27. Coughlan C, Ibáñez M, Dobrozhan O, Singh A, Cabot A, Ryan KM. Compound Copper Chalcogenide Nanocrystals. *Chemical Reviews*. 2017, vol. 117, p. 5865–6109. ISSN 0009-2665

28. Song Z, Lei H, Li B, Wang H, Wen J, Li S, et al. Enhanced field emission from in situ synthesized 2D copper sulfide nanoflakes at low temperature by using a novel controllable solvothermal preferred edge growth route. *Physical Chemistry Chemical Physics*. 2015, vol. 17, p. 11790–11795. ISSN 1463-9076

29. Kalimuldina G, Nurpeissova A, Adylkhanova A, Adair D, Taniguchi I, Bakenov Z. Morphology and Dimension Variations of Copper Sulfide for High-Performance Electrode in Rechargeable Batteries: A Review. *ACS Applied Energy Materials*. 2020, vol. 3, p. 11480–11499. ISSN 2574-0962

30. Tirado J, Roldán-Carmona C, Muñoz-Guerrero FA, Bonilla-Arboleda G, Ralaiarisoa M, Grancini G, et al. Copper sulfide nanoparticles as hole-transporting-material in a fully-inorganic blocking layers n-i-p perovskite solar cells: Application and working insights. *Applied Surface Science*. 2019, vol. 478, p. 607–14. ISSN 0169-4332

31. Masar M, Urbanek M, Urbanek P, Machovska Z, Maslik J, Yadav RS, et al. Synthesis, characterization and examination of photocatalytic performance of hexagonal covellite CuS nanoplates. *Materials Chemistry and Physics*. 2019, vol. 237, p. 121823. ISSN 0254-0584

32. Wu L, Gao J, Qin Z, Sun Y, Tian R, Zhang Q, et al. Deactivated-desulfurizer-derived hollow copper sulfide as anode materials for advanced sodium ion batteries. J Power Sources. 2020;479:228518.

33. Roy P, Srivastava SK. Nanostructured copper sulfides: Synthesis, properties and applications. *CrystEngComm*. 2015, vol. 17, p. 7801–15. ISSN 1466-8033

34. Majumdar D. Recent progress in copper sulfide based nanomaterials for high energy supercapacitor applications. *Journal of Electroanalytical Chemistry.* 2021, vol. 880, p. 114825. ISSN 1572-6657

35. Sudhaik A, Raizada P, Rangabhashiyam S, Singh A, Nguyen V-H, Van Le Q, et al. Copper sulfides based photocatalysts for degradation of environmental pollution hazards: A review on the recent catalyst design concepts and future perspectives. *Surfaces and Interfaces*. 2022, vol. 33, p. 102182. ISSN 2468-0230

36. ul Ain N, Nasir JA, Khan Z, Butler IS, Rehman Z. Copper sulfide nanostructures: Synthesis and biological applications. *RSC Advances*. 2022, vol. 12, p. 7550–7567. ISSN 2046-2069

37. Chen P, Zhang P, Cui Y, Fu X, Wang Y. Recent progress in copper-based inorganic nanostructure photocatalysts: properties, synthesis and photocatalysis applications. *Materials Today Sustainability*. 2023, vol. 21, p. 100276. ISSN 2589-2347

38. Sun S, Li P, Liang S, Yang Z. Diversified copper sulfide (Cu 2−x S) micro-/nanostructures: a comprehensive review on synthesis, modifications and applications. *Nanoscale*. 2017, vol. 9, p. 11357–11404. ISSN 2040-3364

39. Kim Y, Woo K, Kim I, Cho YS, Jeong S, Moon J. Highly concentrated synthesis of copper-zinc-tin-sulfide nanocrystals with easily decomposable capping molecules for printed photovoltaic applications. *Nanoscale.* 2013, vol. 5, p. 10183–10188. ISSN 2040-3364

40. Wang H, Liu Q, Li W, Wen L, Zheng D, Bo Z, et al. Colloidal Synthesis of Lettuce-like Copper Sulfide for Light-Gating Heterogeneous Nanochannels. *ACS Nano*. 2016, vol. 10, p. 3606–3613. ISSN 1936-0851

41. van Oversteeg CHM, Oropeza FE, Hofmann JP, Hensen EJM, de Jongh PE, de Mello Donega C. Water-Dispersible Copper Sulfide Nanocrystals via Ligand Exchange of 1-Dodecanethiol. *Chemistry of Materials.* 2019, vol. 31, p. 541–552. ISSN 0897-4756

42. Chen K, Zhou J, Chen W, Zhong Q, Yang T, Yang X, et al. Growth kinetics and mechanisms of multinary copper-based metal sulfide nanocrystals. *Nanoscale*. 2017, vol. 9, p. 12470–12478. ISSN 2040-3364

43. Chen Y, Chen K, Fu J, Yamaguchi A, Li H, Pan H, et al. Recent advances in the utilization of copper sulfide compounds for electrochemical CO2 reduction. *Nano Materials Science*. 2020 vol.2:235–47. ISSN 2589-9651

44. THE NOBEL COMMITTEE FOR CHEMISTRY. Quantum dots- seeds of nanoscience. Online. 2023. Available from: https://www.nobelprize.org/uploads/2023/10/advanced-chemistryprize2023.pdf. [viewed 19 December 2023].

45. Tan Q, Li J. Recycling metals from wastes: A novel application of mechanochemistry. *Environmental Science and Technology*. 2015, vol. 49, p. 5849–5861. ISSN 1520-5851

46. Guo X, Xiang D, Duan G, Mou P. A review of mechanochemistry applications in waste management. *Waste management*. 2010, vol. 30, p. 4–10. ISSN 1879-2456

47. Shalabayev Z, Baláž M, Daneu N, Dutková E, Bujňáková Z, Kaňuchová M, et al. Sulfur-Mediated Mechanochemical Synthesis of Spherical and Needle-Like Copper Sulfide Nanocrystals with Antibacterial Activity. *ACS Sustainable Chemistry and Engineering*. 2019, vol. 7, p. 12897–128909. ISSN 2168-0485

48. Achimovičová M, Dutková E, Tóthová E, Bujňáková Z, Briančin J, Kitazono S. Structural and optical properties of nanostructured copper sulfide semiconductor synthesized in an industrial mill. *Frontiers of Chemical Science and Engineering*. 2019, vol. 13, p. 164–170. ISSN 2095-0179

49. Baláž M, Tešinský M, Marquardt J, Škrobian M, Daneu N, Rajňák M, et al. Synthesis of copper nanoparticles from refractory sulfides using a semi-industrial mechanochemical approach. *Advanced Powder Technology*. 2020, vol. 31, p. 782–791. ISSN 0921-8831

50. Song Z, Liu Y, Zhang B, Song S, Zhou Z, Huang Y, et al. Magnetic grinding synthesis of copper sulfide-based photocatalytic composites for the degradation of

organic dyes under visible light. *New Journal of Chemistry*. 2023, vol. 47, p. 2286–95. ISSN 1144-0546

51. Baláž M, Augustyniak A, Tatykayev B, Shalabayev Z, Burashev G, Dutková E, et al. Mechanochemical synthesis of non-stoichiometric copper sulfide Cu1.8S applicable as a photocatalyst and antibacterial agent and synthesis scalability verification. *Faraday Discussions*. 2023, vol. 241, p. 367–386. ISSN 1359-6640

52. Baláž M, Dutková E, Bujňáková Z, Tóthová E, Kostova NG, Karakirova Y, et al. Mechanochemistry of copper sulfides: Characterization, surface oxidation and photocatalytic activity. *Journal of Alloys and Compounds*. 2018, vol.746, p. 576–582. ISSN 0925-8388

53. Hedlund JK, Estrada TG, Walker A V. Mechanism Chemical Bath Deposition of Copper Sulfide on Functionalized SAMs: An Unusual Selectivity. *Langmuir*. 2020, vol. 36, p. 3119–3126. ISSN 0743-7463

54. Justin Raj C, Kim BC, Cho W-J, Lee W-G, Seo Y, Yu K-H. Electrochemical capacitor behavior of copper sulfide (CuS) nanoplatelets. *Journal of Alloys and Compounds*. 2014, vol.586, p. 191–196. ISSN 0925-8388

55. Shaikh S, Rabinal MK. Rapid ambient growth of copper sulfide microstructures: Binder free electrodes for supercapacitor. *Journal of Energy Storage*. 2020, vol. 28, p. 101288. ISSN 2352-152X

56. Lai CH, Lu MY, Chen LJ. Metal sulfide nanostructures: Synthesis, properties and applications in energy conversion and storage. *Journal of Material Chemistry*. 2012, vol. 22, p. 19–30. ISSN 09599428

57. Faraji G, Kim HS, Kashi HT. Introduction. In: Severe Plastic Deformation. Amsterdam: Elsevier, 2018, p. 1–17. ISBN 978-0-12-813518-1

58. Saeed S, Rashid N, Hussain R, Malik MA, O'Brien P, Wong W-T. Semiconducting nanostructured copper sulfide thin films from bidentate copper (ii) complexes of N-(dialkylcarbamothioyl)-nitrosubstituted benzamides by chemical vapour deposition. *New Journal of Chemistry*. 2013, vol. 37, p. 3214–3221. ISSN 1144-0546

59. Khan MD, Malik MA, Akhtar J, Mlowe S, Revaprasadu N. Phase pure deposition of flower-like thin films by aerosol assisted chemical vapor deposition and solvent mediated structural transformation in copper sulfide nanostructures. *Thin Solid Films*. 2017, vol. 638, p. 338–344. ISSN 0040-6090

60. Wang W, Liu Y, Yu S, Wen X, Wu D. Highly efficient solar-light-driven photocatalytic degradation of pollutants in petroleum refinery wastewater on hierarchically-structured copper sulfide (CuS) hollow nanocatalysts. *Separation and Purification Technology*. 2022, vol. 284, p. 120254. ISSN 1383-5866

61. Shahi S, Saeednia S, Iranmanesh P, Hatefi Ardakani M. Influence of synthesis parameters on the optical and photocatalytic properties of solvo/hydrothermal CuS and ZnS nanoparticles. *Luminescence*. 2021, vol. 36, p. 180–191. ISSN 1522-7235

62. Demazeau G. Solvothermal processes: definition, key factors governing the involved chemical reactions and new trends. *Zeitschrift für Naturforschung B*. 2010, vol. 65, p. 999–1006. ISSN 0932-0776

63. Agboola PO, Haider S, Shakir I. Copper sulfide and their hybrids with carbon nanotubes for photocatalysis and antibacterial studies. *Ceramics International*. 2022, vol. 48, p. 10136–10143. ISSN 0272-8842

64. Zhou S, Gong L, Zhao X, Liang Q, Zhang W, Wang L, et al. Synthesis and photocatalytic performance of copper sulfide by a simple solvothermal method. *Chemical Phys Lett*. 2020, vol. 759, p. 138034. ISSN

65. Mousavi-Kamazani M, Zarghami Z, Salavati-Niasari M. Facile and novel chemical synthesis, characterization, and formation mechanism of copper sulfide (Cu2S, Cu2S/CuS, CuS) nanostructures for increasing the efficiency of solar cells. *The Journal of Physical Chemistry C*. 2016, vol. 120, p. 2096–20108. ISSN

66. Hong J, Kim B-S, Yang S, Jang A-R, Lee Y-W, Pak S, et al. Chalcogenide solution-mediated activation protocol for scalable and ultrafast synthesis of single-crystalline 1-D copper sulfide for supercapacitors. *Journal of Materials Chemistry A*. 2019, vol. 7, p. 2529–2535. ISSN 2050-7488

67. Saranya M, Santhosh C, Ramachandran R, Kollu P, Saravanan P, Vinoba M, et al. Hydrothermal growth of CuS nanostructures and its photocatalytic properties. *Powder Technology*. 2014, vol. 252, p. 25–32. ISSN 0032-5910

68. Auyoong YL, Yap PL, Huang X, Abd Hamid SB. Optimization of reaction parameters in hydrothermal synthesis: a strategy towards the formation of CuS hexagonal plates. *Chemistry Central Journal*. 2013, vol. 7, p. 67. ISSN 1752-153X

69. Mulla R, Jones DR, Dunnill CW. Economical and Facile Route to Produce Gram-Scale and Phase-Selective Copper Sulfides for Thermoelectric Applications. *ACS Sustainable Chemistry and Engineering.* 2020, vol. 8, p. 14234–14242. ISSN 2168-0485

70. Cheng Y, Deng L, Wang D, Wang X, Ji C, Zhou Y-H. CuS@ Cu-CD composites as efficient heterogeneous Fenton-like catalysts for the photodegradation of tetracycline. *Environmental Science: Advances.* 2023, vol. 2, p. 495–507.

71. Shamraiz U, Badshah A, Hussain RA, Nadeem MA, Saba S. Surfactant free fabrication of copper sulphide (CuS–Cu 2 S) nanoparticles from single source precursor for photocatalytic applications. *Journal of Saudi Chemical Society*. 2017, vol. 21, p. 390–398. ISSN 1319-6103

72. Yadav S, Shrivas K, Bajpai PK. Role of precursors in controlling the size, shape and morphology in the synthesis of copper sulfide nanoparticles and their application for fluorescence detection. *Journal of Alloys and Compdounds*. 2019, vol. 772, p. 579–592. ISSN 0925-8388

73. Ghosh K, Srivastava SK. Enhanced supercapacitor performance and electromagnetic interference shielding effectiveness of CuS quantum dots grown on reduced graphene oxide sheets. *ACS Omega*. 2021, vol. 6, p. 4582–4596. ISSN 2470-1343

74. Maksoud MIAA, Fahim RA, Shalan AE, Abd Elkodous M, Olojede SO, Osman AI, et al. Advanced materials and technologies for supercapacitors used in energy conversion and storage: a review. *Environmental Chemistry Letters*. 2020, vol. 1–65. ISSN 1610-3661

75. El-Hout SI, Mohamed SG, Gaber A, Attia SY, Shawky A, El-Sheikh SM. High electrochemical performance of rGO anchored CuS nanospheres for

supercapacitor applications. *Journal of Energy Storage*. 2021, vol. 34, p. 102001. ISSN 2352-152X

76. Xu X, Liu W, Kim Y, Cho J. Nanostructured transition metal sulfides for lithium ion batteries: progress and challenges. *Nano Today*. 2014, vol. 9, p. 604–630. ISSN 1748-0132

77. Chen Y, Li J, Lei Z, Huo Y, Yang L, Zeng S, et al. Hollow CuS Nanoboxes as Li-Free Cathode for High-Rate and Long-Life Lithium Metal Batteries. *Advances of Energy Materials*. 2020, vol. 10, p. 1903401. ISSN 1614-6832

78. Feng C, Zhang L, Wang Z, Song X, Sun K, Wu F, et al. Synthesis of copper sulfide nanowire bundles in a mixed solvent as a cathode material for lithium-ion batteries. *Journal of Power Sources*. 2014, vol. 269, p. 550–555. ISSN 0378-7753

79. Kalimuldina G, Taniguchi I. Sulfur-rich CuS1+x cathode for lithium batteries. *Material Letters*. 2021, vol. 282, p. 128705. ISSN 01675-77X

80. Shen Y, Wang Y, Miao Y, Yang M, Zhao X, Shen X. High-energy interlayer-expanded copper sulfide cathode material in non-corrosive electrolyte for rechargeable magnesium batteries. *Advanced Materials*. 2020, vol. 32, p. 1905524. ISSN 0935-9648

81. Tsiba Matondo J, Malouangou Maurice D, Chen Q, Bai L, Guli M. Inorganic copper-based hole transport materials for perovskite photovoltaics: Challenges in normally structured cells, advances in photovoltaic performance and device stability. *Solar Energy Materials and Solar Cells*. 2021, vol. 224, p. 111011. ISSN 0927-0248

82. Wang M, Liu D, Xu Z, Tian Q, Chai W, An L. Photothermally boosted Fenton-like activity of copper sulfide toward the catalytic degradation of 4-chlorophenol. *Journal of Alloys and Compounds*. 2023, vol. 946, p. 169337. ISSN 0925-8388

83. Iqbal S, Bahadur A, Anwer S, Ali S, Saeed A, Muhammad Irfan R, et al. Shape and phase-controlled synthesis of specially designed 2D morphologies of l-cysteine surface capped covellite (CuS) and chalcocite (Cu2S) with excellent photocatalytic properties in the visible spectrum. *Applied Surface Science*. 2020, vol. 526, p. 146691. ISSN 0169-4332

84. Das M, Das D, Sil S, Ray PP. Development of hierarchical copper sulfide–carbon nanotube (CuS–CNT) composites and utilization of their superior carrier mobility in efficient charge transport towards photodegradation of Rhodamine B under visible light. *Nanoscale Advances*. 2023, vol. 5, p. 3655–3663. ISSN 2516-0230

85. Nancucheo I, Segura A, Hernández P, Hernández-Montelongo J, Pesenti H, Arranz A, et al. Covellite nanoparticles with high photocatalytic activity bioproduced by using H2S generated from a sulfidogenic bioreactor. *Journal of Environmental Chemical Engineering*. 2022, vol. 10, p. 107409. ISSN 2213-3437

86. Siddhardhan E V, Surender S, Arumanayagam T. Degradation of tetracycline drug in aquatic environment by visible light active CuS/CdS photocatalyst. *Inorganic Chemistry Communications*. 2023, vol. 147, p. 110244. ISSN 1387-7003

87. Kamranifar M, Allahresani A, Naghizadeh A. Synthesis and characterizations of a novel CoFe2O4@CuS magnetic nanocomposite and investigation of its efficiency for photocatalytic degradation of penicillin G antibiotic

in simulated wastewater. *Journal of Hazardous Material*. 2019, vol. 366, p. 545–555. ISSN 0304-3894

88. Yang J, Fang L, Gan X, Meng G, Li H, Jia Y. Efficient degradation of sulfamethoxazole under visible light irradiation by polyaniline/copper sulfide composite photocatalyst. *Environmental Science and Pollution Research*. 2022 vol. 29, p. 36502–36511. ISSN 1614-7499

89. Bhagat C, Kumar M, Tyagi VK, Mohapatra PK. Proclivities for prevalence and treatment of antibiotics in the ambient water: a review. *NPJ Clean Water*. 2020, vol. 3, p. 42. ISSN 2059-7037

90. Ahmed M, Mavukkandy MO, Giwa A, Elektorowicz M, Katsou E, Khelifi O, et al. Recent developments in hazardous pollutants removal from wastewater and water reuse within a circular economy. *NPJ Clean Water*. 2022, vol. 5, p. 12. ISSN 2059-7037

91. Lin J, Ye W, Xie M, Seo DH, Luo J, Wan Y, et al. Environmental impacts and remediation of dye-containing wastewater. *Nature Reviews Earth & Environment*. 2023, vol. 4, p. 785–803. ISSN 2662-138X

92. WORLD HEALTH ORGANIZATION. Technical brief on water sanitation, hygiene and wastewater management to prevent infections and reduce the spread of antimicrobial resistance. Online. 2020. Available from: https://www.who.int/publications/i/item/9789240006416. [viewed 23 February 2023].

93. Tacconelli E, Sifakis F, Harbarth S, Schrijver R, van Mourik M, Voss A, et al. Surveillance for control of antimicrobial resistance. *Lancet Infectious Disease*. 2018, vol. 18, p. e99–106. ISSN 1473-3099

94. WORLD HEALTH ORGANIZATION. Antibiotics resistance. Online. 2020. Available from: https://www.who.int/news-room/fact-sheets/detail/antibiotic-resistance#:~:text=Antibiotics%20resistance%20occurs%20when%20bacteria,caused%20by%20non%2Dresistant%20bacteria. [viewed 23 February 2023].

95. de Ilurdoz MS, Sadhwani JJ, Reboso JV. Antibiotic removal processes from water & wastewater for the protection of the aquatic environment - a review. *Journal of Water Process Engineering*. 2022, vol. 45, p. 102474. ISSN

96. Parvulescu VI, Epron F, Garcia H, Granger P. Recent Progress and Prospects in Catalytic Water Treatment. *Chemical Reviews*. 2022, vol. 122, p. 2981–3121. ISSN 0009-2665

97. Mohammed R, Ali MEM, Gomaa E, Mohsen M. Copper sulfide and zinc oxide hybrid nanocomposite for wastewater decontamination of pharmaceuticals and pesticides. *Scientific Reports*. 2022, vol. 12, p. 18153. ISSN 2045-2322

98. Guo X, Yang F, Sun X, Han C, Bai Y, Liu G, et al. Fabrication of a novel separation-free heterostructured photocatalyst with enhanced visible light activity in photocatalytic degradation of antibiotics. *Journal of Materials Chemistry A*. 2022, vol. 10, p. 3146–3158. ISSN 2050-7488

99. Xu W, Zhu S, Liang Y, Li Z, Cui Z, Yang X, et al. Nanoporous CuS with excellent photocatalytic property. *Scientific Reports.* 2015, vol. 5, p. 18125. ISSN 2045-2322

100. Calvete MJF, Piccirillo G, Vinagreiro CS, Pereira MM. Hybrid materials for heterogeneous photocatalytic degradation of antibiotics. *Coord Chem Rev*. 2019, vol. 395, p. 63–85. ISSN

101. Zhou Z, Li B, Liu X, Li Z, Zhu S, Liang Y, et al. Recent Progress in Photocatalytic Antibacterial. *ACS Applied Bio Materials*. 2021, vol. 4, p. 3909–3936. ISSN 2576-6422

102. Zhong Y, Zheng XT, Zhao S, Su X, Loh XJ. Stimuli-activable metal-bearing nanomaterials and precise on-demand antibacterial strategies. *ACS Nano*. 2022, vol. 16, p. 19840–19872. ISSN 1936-0851

103. Wang H-Y, Hua X-W, Wu F-G, Li B, Liu P, Gu N, et al. Synthesis of ultrastable copper sulfide nanoclusters via trapping the reaction intermediate: potential anticancer and antibacterial applications. *ACS Applied Material & Interfaces*. 2015, vol. 7, p. 7082–7092. ISSN 1944-8244

104. Mutalik C, Okoro G, Krisnawati DI, Jazidie A, Rahmawati EQ, Rahayu D, et al. Copper sulfide with morphology-dependent photodynamic and photothermal antibacterial activities. *Journal of Colloid and Interface Science*. 2022, vol. 607, p. 1825–1835. ISSN 0021-9797

105. Chandrasekaran S, Yao L, Deng L, Bowen C, Zhang Y, Chen S, et al. Recent advances in metal sulfides: from controlled fabrication to electrocatalytic, photocatalytic and photoelectrochemical water splitting and beyond. *Chemical Society Reviews*. 2019, vol. 48, p. 4178–4280. ISSN 1460-4744

106. Zhang J, Bifulco A, Amato P, Imparato C, Qi K. Copper indium sulfide quantum dots in photocatalysis. *Journal of Colloid and Interface Science*. 2023. ISSN 0021-9797

107. Cavdar O, Malankowska A, Łuczak J, Żak A, Lisowski W, Klimczuk T, et al. Capping ligand initiated CuInS2 quantum dots decoration on, ZnIn2S4 microspheres surface under different alkalinity levels resulting in different hydrogen evolution performance. *Colloids and Surfaces A Physicochemical Engineering Aspects*. 2022, vol. 652, p. 129760. ISSN 0927-7757

108. Saito T, Nishiyama Y, Putaux J-L, Vignon M, Isogai A. Homogeneous Suspensions of Individualized Microfibrils from TEMPO-Catalyzed Oxidation of Native Cellulose. *Biomacromolecules*. 2006, vol. 7:1687–1691. ISSN 1525-7797

109. Morselli D, Campagnolo L, Prato M, Papadopoulou EL, Scarpellini A, Athanassiou A, et al. Ceria/Gold Nanoparticles in Situ Synthesized on Polymeric Membranes with Enhanced Photocatalytic and Radical Scavenging Activity. *ACS Applied Nano Materials.* 2018, vol. 1, p. 5601–5611. ISSN 2574-0970

110. Escobedo-Morales A, Ruiz-López II, Ruiz-Peralta M deL, Tepech-Carrillo L, Sánchez-Cantú M, Moreno-Orea JE. Automated method for the determination of the band gap energy of pure and mixed powder samples using diffuse reflectance spectroscopy. *Heliyon*. 2019, vol. 5, p. e01505. ISSN 2405-8440

111. Dambrauskas T, Baltakys K, Eisinas A. Formation and thermal stability of calcium silicate hydrate substituted with Al3+ ions in the mixtures with CaO/SiO2 = 1.5. *Journal of Thermal Analysis Calorimetry.* 2018, vol. 131, p. 501–512. ISSN 1388-6150

112. Gineika A, Baltakys K, Dambrauskas T. The application of silica gel waste for the two-step synthesis of wollastonite in temperature range of 200–950 °C. *Journal of Thermal Analysis Calorimetry*. 2019, vol. 138, p. 2263–2273. ISSN 1388-6150

113. Jiang R, Jia C-S, Wang Y-Q, Peng X-L, Zhang L-H. Prediction of Gibbs free energy for the gases Cl2, Br2, and HCl. *Chemical Physics Letters*. 2019, vol. 726, p. 83–86. ISSN 0009-2614

114. Lide DR. Standard thermodynamic properties of chemical substances. In: CRC Handbook of Chemistry and Physics. Boca Raton, FL: CRC Press, 2000. ISBN 9780429105456

115. Goldberg RN, Parker VB. Thermodynamics of solution of SO2(g) in water and of aqueous sulfur dioxide solutions. *Journal of Research of the National Bureau of Standards*. 1985 vol. 90, p. 341–358. ISSN 0160-1741

116. Royal Institute of Technology. Thermodynamic data for copper. Implications for the corrosion of copper under repository conditions. Stockholm: CM Digitaltryck AB Bromma. 2000. ISSN 1404-0344

117. Crapanzano L. Polymorphism of sulfur: Structural and Dynamical Aspects. Online. 2008. Université Joseph-Fourier - Grenoble Available from: https://theses.hal.science/tel-00204149v1/document

118. Janickis V. Deguonis, siera, selenas, teluras ir polonis. 1st ed. Kaunas: Technologija, 1994. ISBN 9986-13-149-9

119. Mateti S, Mathesh M, Liu Z, Tao T, Ramireddy T, Glushenkov AM, et al. Mechanochemistry: A force in disguise and conditional effects towards chemical reactions. *Chemical Communications*. 2021, vol.57, p. 1080–1092. ISSN 1359-7345

120. Steudel R. Aqueous Sulfur Sols. In: *Elemental Sulfur and Sulfur-Rich Compounds I*. Berlin: Springer Berlin Heidelberg, 2003. ISBN 978-3-540-44855-6

121. Laperdrix E, Sahibed-dine A, Costentin G, Bensitel M, Lavalley J-C. Evidence of the reverse Claus reaction on metal oxides: Influence of their acid--base properties. *Applied Catalysis B : Environmental.* 2000, vol. 27, p. 137–142. ISSN 0926-3373

122. Li M, Liu Y, Zhang Y, Han X, Zhang T, Zuo Y, et al. Effect of the annealing atmosphere on crystal phase and thermoelectric properties of copper sulfide. *ACS Nano*. 2021, vol. 15, p. 4967–4978. ISSN 1936-0851

123. Sadovnikov SI. Thermal stability and recrystallization of semiconductor nanostructured sulfides and sulfide solid solutions. *Journal of Alloys and Compounds*. 2019, vol. 788, p. 586–599. ISSN 0925-8388

124. Nafees M, Ikram M, Ali S. Thermal behavior and decomposition of copper sulfide nanomaterial synthesized by aqueous sol method. *Digest Journal of Nanomaterials and Biostructures.* 2015, vol. 10, p. 635–641. ISSN 1842-3582

125. Dunn JG, Muzenda C. Thermal oxidation of covellite (CuS). *Thermochimica Acta*. 2001, vol. 369, p. 117–123. ISSN 0040-6031

126. Dexter M, Gao Z, Bansal S, Chang C-H, Malhotra R. Temperature, Crystalline Phase and Influence of Substrate Properties in Intense Pulsed Light Sintering of Copper Sulfide Nanoparticle Thin Films. *Scientific Reports*. 2018, vol. 8, p. 2201. ISSN 2045-2322

127. Mikhlin Y, Nasluzov V, Ivaneeva A, Vorobyev S, Likhatski M, Romanchenko A, et al. Formation, evolution and characteristics of copper sulfide nanoparticles in the reactions of aqueous cupric and sulfide ions. *Materials Chemistry and Physics*. 2020, vol. 255, p. 123600. ISSN 0254-0584

128. Ivanauskas R, Kunciute A, Ancutiene I, Andrulevicius M, Mikolajunas M. Impact of surface morphology and thickness of tin selenide thin films on their optical properties. *Surfaces and Interfaces*. 2022, vol. 28, p. 101675. ISSN 2468-0230

129. Soltani T, Entezari MH. Photolysis and photocatalysis of methylene blue by ferrite bismuth nanoparticles under sunlight irradiation. *Journal of Molecular Catalysis A Chemical*. 2013, vol. 377, p. 197–203. ISSN 1381-1169

130. Al-Nuaim MA, Alwasiti AA, Shnain ZY. The photocatalytic process in the treatment of polluted water. *Chemical Papers*. 2023, vol.77, p. 677–701. ISSN 0366-6352

131. Nandiyanto ABD, Zaen R, Oktiani R. Correlation between crystallite size and photocatalytic performance of micrometer-sized monoclinic WO3 particles. *Arabian Journal of Chemistry*. 2020, vol. 13, p. 1283–96. ISSN 1878-5352

132. Goktas A, Modanlı S, Tumbul A, Kilic A. Facile synthesis and characterization of ZnO, ZnO:Co, and ZnO/ZnO:Co nano rod-like homojunction thin films: Role of crystallite/grain size and microstrain in photocatalytic performance. *Journal of Alloys and Compounds*. 2022, vol. 893, p. 162334. ISSN 0925-8388

133. Nancucheo I, Segura A, Hernández P, Hernández-Montelongo J, Pesenti H, Arranz A, et al. Covellite nanoparticles with high photocatalytic activity bioproduced by using H2S generated from a sulfidogenic bioreactor. *Journal of Environ Chem Eng.* 2022, vol. 10, p. 107409. ISSN 2213-3437

134. Tanveer M, Cao C, Aslam I, Ali Z, Idrees F, Khan WS, et al. Synthesis of CuS flowers exhibiting versatile photo-catalyst response. *New Journal of Chemistry*. 2015, vol. 39, p. 1459–1468. ISSN 1144-0546

135. Xu Y, Zou L, Lu H, Wei Y, Hua J, Chen S. Preparation and characterization of electrospun PHBV/PEO mats: The role of solvent and PEO component. *Journal of Material Science*. 2016, vol. 51, p. 5695–5711. ISSN 1573-4803

136. Sun X, Mei C, French AD, Lee S, Wang Y, Wu Q. Surface wetting behavior of nanocellulose-based composite films. *Cellulose*. 2018, vol. 25, p. 5071–5087. ISSN 1572-882X

137. Sudhaik A, Raizada P, Rangabhashiyam S, Singh A, Nguyen V-H, Van Le Q, et al. Copper sulfides based photocatalysts for degradation of environmental pollution hazards: A review on the recent catalyst design concepts and future perspectives. *Surfaces and Interfaces*. 2022, vol. 33, p. 102182. ISSN 2468-0230

138. Zhang L, Mohamed HH, Dillert R, Bahnemann D. Kinetics and mechanisms of charge transfer processes in photocatalytic systems: A review. *Journal of Photochemistry and Photobiology C: Photochemistry Reviews*. 2012, vol. 13, p. 263–76. ISSN 1389-5567

139. Chen S, Huang D, Xu P, Xue W, Lei L, Cheng M, et al. Semiconductor-based photocatalysts for photocatalytic and photoelectrochemical water splitting: will we stop with photocorrosion? *Journal of Materials Chemistry A.* 2020, vol. 8, p. 2286–2322. ISSN 2050-7488

140. Maleki M, Haghighi M. Sono-dispersion of CuS-CdS over TiO2 in one-pot hydrothermal reactor as visible-light-driven nanostructured photocatalyst. *Journal of Molecular Catalysis A: Chemical*. 2016, vol. 424, p. 283–296. ISSN 1381-1169

141. Siddhardhan E V, Surender S, Arumanayagam T. Degradation of tetracycline drug in aquatic environment by visible light active CuS/CdS photocatalyst. *Inorganic Chemistry Communications*. 2023, vol. 147, p. 110244. ISSN 1387-7003

142. Lai C, Xu F, Zhang M, Li B, Liu S, Yi H, et al. Facile synthesis of CeO2/carbonate doped Bi2O2CO3 Z-scheme heterojunction for improved visible-light photocatalytic performance: Photodegradation of tetracycline and photocatalytic mechanism. *Journal of Colloid Interface Science*. 2021, vol. 588, p. 283–94. ISSN 0021-9797

143. Wang Y, Liu Q, Wong NH, Sunarso J, Huang J, Dai G, et al. Near-infrared (NIR) light responsiveness of CuS/S–C3N4 heterojunction photocatalyst with enhanced tetracycline degradation activity. *Ceramics International*. 2022, vol. 48, p. 2459–69. ISSN 0272-8842

144. Nandi P, Das D. ZnO/CdS/CuS heterostructure: A suitable candidate for applications in visible-light photocatalysis. *Journal of Physics and Chemistry of Solids*. 2022, vol. 160, p. 110344. ISSN 0022-3697

CURRICULUM VITAE

Gabrielė Šarapajevaitė

gabriele.sarapajevaite@ktu.lt

Education:

2002–2014
Panevėžys Gymnasium 5

2014–2018
Bachelor's degree of Chemical Technology and Engineering, Kaunas University of Technology, Lithuania

2018–2020
Master's degree of Chemical Engineering, Kaunas University of Technology, Lithuania

2022–2023
Professional degree in Pedagogy Studies; Kaunas University of Technology, Lithuania

Professional experience:

2018 – present
Department of Silicate Technology, Kaunas University of Technology, laboratory assistant

2021 – present
Department of Silicate Technology, Kaunas University of Technology, lecturer

Scientific interests:

Ms. Gabrielė Šarapajevaitė is interested in waste material valorization, sustainable approaches towards material processing and synthesis aimed at obtaining functional materials.

LIST OF PUBLICATIONS

Articles published in journals indexed in the Clarivate Analytics Web of Science with Impact Factor:

1. Sarapajevaite, Gabriele; Baltakys, Kestutis. Purification of sulfur waste under hydrothermal conditions // *Waste and Biomass Valorization*. Dordrecht: Springer. ISSN 1877-2641. eISSN 1877-265X. 2021, vol. 12, iss. 6, p. 3407–3416. DOI: 10.1007/s12649-020-01206-y
2. Sarapajevaite, Gabriele; Baltakys, Kestutis. Thermal stability and decomposition mechanism of synthetic covellite samples // Journal of thermal analysis and calorimetry. Dordrecht: Springer. ISSN 1388- 6150. eISSN 1588-2926. 2022, vol. 147, iss. 20, p. 10951–10963. DOI: 10.1007/s10973-022-11313-8
3. Sarapajevaite, Gabriele; Morselli, Davide; Baltakys, Kestutis. Aqueous-based synthesis of photocatalytic copper sulfide using sulfur waste as sulfurizing agent // *Materials*. Basel: MDPI. ISSN 1996- 1944. 2022, vol. 15, iss. 15, art. No. 5253, p. 1–15. DOI: 10.3390/ma15155253
4. Sarapajevaite, Gabriele; Baltakys, Kestutis; Degli Esposti, Micaela; Morselli, Davide; Fabbri, Paola. Sustainable PHBV/CuS composite obtained from waste valorization for wastewater purification by visible light-activated photocatalytic activity // *Advanced Sustainable Systems*. Weinheim: John Wiley & Sons. ISSN 2366-7486. 2023, p. 2300112. DOI: 10.1002/adsu.202300112

Articles published in conference proceedings:

1. Sarapajevaite, Gabriele; Baltakys, Kestutis. Thermal stability of hydrothermally synthetic covellite in 0-temperature range // *6th Central and Eastern European Conference on Thermal Analysis and Calorimetry* (CEEC-TAC6) and *15th Mediterranean Conference on Calorimetry and Thermal Analysis* (Medicta2021), 20–24 July 2021, Split, Croatia: book of abstracts / A. Rotaru, M. Erceg (Eds.). București: SITECH, 2021, OP4.09. ISBN 9786061178612. p. 107
2. Sarapajevaite, Gabriele; Baltakys, Kestutis; Morselli, Davide. Synthesis and characterisation of copper sulfide by valorizing sulfur waste // *Chemistry and Chemical Technology*: proceedings of international scientific conference, Kaunas, 2022. Kaunas: Kaunas University of Technology. ISSN 2538-7359. 2022, p. 50.
3. Sarapajevaite, Gabriele; Baltakys, Kestutis; Degli Esposti, Micaela; Fabbri, Paola; Morselli, Davide. Visible light driven photooxidation of tetracycline by sustainable composite for waste water purification // *Merck Young Chemists' Symposium 2022*, XXI edition: Rimini, Italy, 21–23 November 2022: book of

abstracts. Roma: Società Chimica Italiana, 2022, OR14. ISBN 9788894952322. p. 26.
4. Sarapajevaite, Gabriele; Baltakys, Kestutis; Degli Esposti, Micaela; Fabbri, Paola; Morselli, Davide. Visible light-driven degradation of tetracycline by sustainable poly(3-hydroxybutyrate-co-3-hydroxyvalerate) and CuS composite // *Advanced Materials and Technologies*: book of abstracts of 25th international conference-school, 21-25 August 2023, Palanga, Lithuania. Kaunas: Kaunas University of Technology. ISSN 2669-1930. 2023, P73, p. 112.
5. Sarapajevaite, Gabriele; Baltakys, Kestutis; Esposti, Micaela Degli; Fabbri, Paola; Morselli, Davide. Biopolymer based composite application for sustainable photodegradation of antibiotics // *Workshop on Polymers and Biopolymers for Sustainable Life and Applications*, 3–5 September 2023, Sofia, Bulgaria: book of abstracts. 2023, O5, p. 35–36.
6. Sarapajevaite, Gabriele; Baltakys, Kestutis. The valorization of industrial sulfur waste by synthesis of copper sulfide and the application products in waste water treatment // *BUP Symposium 2023*: 7 November 2023: book of abstracts. Uppsala: Uppsala Universitet. 2023, p. 9.

ACKNOWLEDGEMENTS

I would like to express my deepest gratitude to my long-time supervisor Prof. Dr. Kęstutis Baltakys for his invaluable support and continuous encouragement throughout the entire research period. I would also like to thank the supervisors Prof. Dr. Paola Fabbri and Dr. Davide Morselli who were guiding me during the study period at the University of Bologna. The expertise and insightful feedback of all of them has been instrumental in shaping this thesis and my personal growth as a researcher.

I extend my heartfelt thanks to Kaunas University of Technology and to University of Bologna for providing the resources, facilities, and conducive research environment essential for the completion of this study. My sincere gratitude goes to colleagues from the Department of Silicate Technology for their always available guidance and support. I would also like to thank many inspiring and encouraging professors and researchers whom I was lucky enough to meet, to be taught by, or even collaborate.

Special thanks to my peers and colleagues who became my friends throughout this academic journey. Our philosophical discussions and mutual willingness towards the actual change in this world is the aspiration for me not to give up on research.

And, lastly, I am deeply indebted to my closest friends, my family, mom and dad, as well as Kornelija and Izabelė. Your love, encouragement and belief in my abilities has been an invaluable source of strength and a constant motivation.

APPENDICES

Appendix 1. The average, min and max values of crystallite size of covellite in the synthesized samples

Synthesis conditions	d, nm	0.305	0.282	0.273	0.190	0.174	0.305	0.282	0.273	0.190	0.174
		Waste					Reference				
0.5 h 145 °C	Average ± st. dev.	41.7 ±2.0	19.9 ±0.3	42.7 ±0.6	30.4 ±0.2	29.3 ±0.7	34.1 ±1.6	18.3 ±0.6	42.3 ±0.8	21.9 ±0.1	19.4 ±0.1
	min	19.9±0.3					18.3±0.6				
	max	42.7±0.6					2.3±0.8				
0.5 h 180 °C	Average ± st. dev.	49.0 ±1.5	27.3 ±0.2	47.8 ±0.2	35.1 ±0.6	34.1 ±0.7	41.1 ±2.2	25.8 ±1.9	50.3 ±2.1	27.0 ±1.8	29.6 ±2.0
	min	27.3±0.2					25.8±1.9				
	max	49.0±1.5					25.8±1.9				
4 h 180 °C	Average ± st. dev.	47.9 ±2.3	28.7 ±1.9	50.6 ±2.2	36.2 ±2.4	34.3 ±3.5	36.8 ±2.1	27.8 ±1.7	53.0 ±0.2	31.7 ±0.9	34.0 ±2.3
	min	28.7±1.9					27.8±1.7				
	max	50.6±2.2					53.0±0.2				

Appendix 2. Standard deviation values of TC degradation efficiency by composites in porous architecture

Standard deviation, %					
Time, min	**Porous sample**				**TC self-deg**
	CuSr/Po	CuSw/Po	CuSr/MFC/Po	CuSw/MFC/Po	
0	0.00	0.00	0.00	0.00	0.00
5	0.09	0.44	0.24	0.62	0.65
10	0.22	0.78	0.28	1.32	0.63
15	0.38	0.98	0.23	1.84	0.63
20	0.49	1.00	0.45	2.65	0.60
30	1.05	1.56	0.84	4.53	0.50
40	1.69	2.08	1.33	6.66	0.45
50	2.30	1.94	2.10	8.37	0.30
60	2.65	1.71	3.07	10.57	0.48
90	3.67	2.04	5.68	13.17	1.01
120	4.34	2.24	6.62	11.82	1.76
150	4.53	1.87	5.02	8.39	1.98
180	0.00	0.00	0.00	0.00	2.60
210	0.00	0.00	0.00	0.00	2.59
240	0.00	0.00	0.00	0.00	2.49

Appendix 3. Standard deviation values of TC degradation efficiency by composites in film architecture

Standard deviation, %				
Time, min	Film sample			
	CuSr/Fi	CuSw/Fi	CuSr/MFC/Fi	CuSw/MFC/Fi
0	0.00	0.00	0.00	0.00
5	0.70	0.38	0.06	0.59
10	0.70	0.54	0.18	0.75
15	0.84	0.78	0.45	0.79
20	1.44	1.14	0.77	0.78
30	2.21	1.61	1.20	0.83
40	3.15	2.09	1.60	0.75
50	4.41	2.70	2.39	0.42
60	4.59	3.07	2.77	0.91
90	7.65	3.21	2.63	0.78
120	7.12	2.34	2.70	1.31
150	6.45	1.82	2.59	1.62
180	0.00	0.00	2.01	1.54
210	0.00	0.00	0.00	0.00
240	0.00	0.00	0.00	0.00

Appendix 4. Standard deviation values of TC degradation efficiency by CuSw/MFC/Po and CuSw/Fi samples obtained from reusability experiments

Time, min	Standard deviation, %							
	CuSw/MFC/Po				CuSw/Fi			
	2	3	4	5	2	3	4	5
0	0.00	0.00	0.00	0.00	0.00	0.00	0.00	0.00
5	0.19	0.11	0.55	0.39	0.55	1.45	0.30	1.61
10	0.34	0.05	0.81	0.18	2.91	1.88	0.43	1.75
15	0.30	0.38	1.18	0.53	5.56	2.81	0.52	1.79
20	0.06	0.71	1.54	0.52	8.58	3.15	0.69	1.75
30	0.33	1.52	2.08	0.83	13.93	4.48	1.19	1.53
40	0.64	2.19	2.85	1.44	15.64	4.76	1.39	0.78
50	1.14	2.71	3.30	1.86	15.97	4.69	1.64	0.52
60	1.53	3.26	3.60	1.82	14.52	4.53	1.50	0.00
90	0.99	3.43	4.14	3.40	11.81	3.29	0.86	1.02
120	3.37	6.64	3.60	3.08	0.00	0.00	2.31	1.04
150	0.00	0.00	6.20	2.22	0.00	0.00	0.00	0.00
180	0.00	0.00	0.00	0.00	0.00	0.00	0.00	0.00
210	0.00	0.00	0.00	0.00	0.00	0.00	0.00	0.00
240	0.00	0.00	0.00	0.00	0.00	0.00	0.00	0.00

Appendix 5. Standard deviation values of simultaneous degradation experiments of TC and MB using CuSw/MFC/Po and CuSw/Fi samples

Time, min	Standard deviation, %			
	CuSw/MFC/Po		CuSw/Fi	
	TC	MB	TC	MB
0	0.00	0.00	0.00	0.00
5	0.76	0.37	1.27	0.87
12	1.25	1.27	1.43	1.33
20	2.53	2.88	1.95	2.14
30	2.62	3.22	2.57	3.13
40	2.35	3.12	2.50	3.21
50	1.76	2.30	2.65	3.70
60	1.62	2.31	2.69	3.92
90	0.52	0.51	1.82	2.99
120	0.18	0.06	2.03	2.52
150	0.12	0.10	0.73	1.46
180	0.25	0.21	0.36	0.88
210	0.00	0.10	0.00	0.48
240	0.00	0.06	0.00	0.27

Appendix 6. Reaction rate constants of TC photodegradation and correlation coefficients (R^2) of linear pseudo-first order model

Sample	Rate constant, min^{-1}	R^2
CuSr/Po	0.0867	0.9993
CuSw/Po	0.0863	0.9856
CuSr/MFC/Po	0.282	0.9996
CuSw/MFC/Po	0.3642	1.0000
CuSr/Fi	0.3834	0.9802
CuSw/Fi	0.5203	0.9797
CuSr/MFC/Fi	0.3367	0.9985
CuSw/MFC/Fi	0.3932	0.9909
TC	0.0786	0.9924
Po	0.1669	1.0000
Fi	0.2005	1.0000

Appendix 7. Rate constants of pollutant photodegradation during recyclability experiments and the correlation coefficients (R^2) of linear pseudo-first order model

Sample	Cycle	Rate constant, min^{-1}	R^2
CuSw/MFC/Po	II	0.9036	0.9998
	III	0.7046	0.9995
	IV	0.5068	0.999
	V	0.4159	0.9998
CuSw/Fi	II	1.2051	0.9965
	III	0.853	0.9992
	IV	0.6934	0.9992
	V	0.7358	0.9982

Appendix 8. Rate constants of TC and MB pollutant photodegradation and the correlation coefficients (R^2) of linear pseudo-first order model

Experiment	Sample	Rate constant, min^{-1}	R^2
TC simultaneous photodegradation	CuSw/Fi	0.6979	0.9990
	CuSw/MFC/Po	0.8044	1.0000
	TC self deg	0.4823	0.9969
MB simultaneous photodegradation	CuSw/Fi	0.5635	0.9946
	CuSw/MFC/Po	0.6744	09947
	MB self deg	0.2176	0.9975

UDK 549.332.057+546.22+539.216](043.3)

SL344. 2024-05-03, 16,75 leidyb. apsk. l. Tiražas 18 egz. Užsakymas 79.
Išleido Kauno technologijos universitetas, K. Donelaičio g. 73, 44249 Kaunas
Spausdino leidyklos „Technologija“ spaustuvė, Studentų g. 54, 51424 Kaunas